

Numerical model exploration of climate-linked drivers and
pathways driving phytoplankton bloom in Puget Sound

fjord

PhD Thesis

Hoa Thi Thai Nguyen

Population modelling and epidemiology – Marine Population Modelling

Department of Mathematics and Statistics

University of Strathclyde, Glasgow

May 10, 2021

This thesis is the result of the author's original research. It has been composed by the author and has not been previously submitted for examination which has led to the award of a degree.

The copyright of this thesis belongs to the author under the terms of the United Kingdom Copyright Acts as qualified by University of Strathclyde Regulation 3.50. Due acknowledgement must always be made of the use of any material contained in, or derived from, this thesis.

Abstract

Phytoplankton spring blooms fertilize the highly productive Puget Sound fjord. However, the mechanism of phytoplankton spring bloom in Puget Sound is not yet fully understood. The main basin of Puget Sound fjord has been undergoing environmental changes to which climate change is one of the major causes. Climate change has been shown to have a prominent influence on altering the timing and magnitude of phytoplankton blooms. Thus, it is important to understand the response of phytoplankton to changes in climate. The study, first, identifies an adequate biophysical model for the main basin Puget Sound (1-D NPZD model). Then, the study employs the model to explore and classify possible climate-induced drivers and pathways that effect main basin Puget Sound phytoplankton spring blooms. The study investigates phytoplankton spring blooms in metrics of (i) annual primary production, (ii) bloom date. The study also examines (iii) phytoplankton concentration during juvenile salmon (chinook and steelhead) outmigration, and (iv) duration nutrient limitation in summer as part of Puget Sound marine survival rate decline hypotheses.

Previous studies in Puget Sound plankton suggested that phytoplankton spring blooms are controlled by light environment. Thus, to describe underwater light field, the study analyses two light-related data sets: Secchi disk depth and beam transmissometer. The analysis results in similar regressions of light attenuation (k_d) and phytoplankton concentration (Chla). The regression that uses Secchi disk depth yields slightly better model good fit to observations. The regressions obtained from both Secchi disk depth and beam transmissometer could not distinguish effect of river inputs (represented by salinity) and background water on total underwater light attenuation.

This is probably due to rivers run into Puget Sound basin come from diverse watersheds with distinctive sediment properties.

Undefined biological parameters in the Puget Sound biophysical model are identified by using parameterisation and sensitivity approaches. Particle swarm optimizer, an optimisation algorithms, proposes numerous parameter sets that produce equal model goodness-of-fit. Among these parameter sets, there are some with contrasting dynamics. Sensitivity analysis is then carried out to classify parameters into the most, moderate and minor impact on model performance. The sensitivity analysis also compares model good fit produced by optimized parameter sets and existing parameters to conclude the new biological parameter set for Puget Sound plankton.

Once the Puget Sound biophysical model defined, it is used to explore all possible climate-induced drivers-pathways which are selected based on previous studies of Puget Sound plankton. The study's outcomes highlight the predominant role of light limitation over nutrient limitation driving spring bloom timings and magnitude. Cloud cover (via light intensity) and riverflow (via mixing mediated by stratification, and also via light attenuation) are suggested to be the first and second order climate drivers of Puget Sound phytoplankton production and bloom date. Processes influencing duration nutrient limitation in summer, however, are more complex. To this metric, nutrient limitation via mixing caused by stratification and riverflow is the major leading mechanism. Moreover, there is a large number of mechanistic pathways (e.g., light limitation via cloud cover, light intensity, via riverflow, stratification, mixing, via riverflow, light attenuation; nutrient limitation via exchange flow, vertical advection) producing the same scale of variation in number of days nutrient is limited in summer.

Contents

List of Figures	vi
List of Tables	x
1 Introduction	2
1.1 Motivation for Puget Sound phytoplankton study	2
1.2 Plankton related hypotheses about declining marine survival rate of Puget Sound salmon	4
1.3 Puget Sound’s phytoplankton dynamics	7
1.4 Study aims	9
1.5 Thesis structure	11
2 A model of Puget Sound plankton dynamics	13
2.1 Brief description of Puget Sound estuarine circulation	14
2.2 Monitoring programs and observational data	16
2.3 A model of Puget Sound plankton dynamics	20
2.3.1 Physical processes	22
2.3.2 Biogeochemical model	31
2.4 Conclusions	39
3 Exploration of a PS–1D model baseline	41
3.1 Model configuration	41
3.1.1 PS-1D parameters values	41
3.1.2 Initial, boundary conditions and forcings	41

3.1.3	Validation data	47
3.2	Model skill assessment	51
3.3	Results	51
3.4	Discussions and Conclusions	56
4	Underwater light field in Puget Sound	58
4.1	Description of ocean optical measurements	59
4.1.1	Brief overview of ocean optical instruments development	59
4.1.2	Secchi disk and diffuse attenuation coefficient	60
4.1.3	Beam transmissometer and beam attenuation coefficient	61
4.2	Puget Sound optical measurements	63
4.2.1	Secchi depth	63
4.2.2	Beam transissionmeter	67
4.3	Statistical analysis and model examination of light functions	67
4.3.1	Light function obtained from Secchi observations	67
4.3.2	Light function obtained from beam transmissometer's measurements	70
4.3.3	Comparison of light functions	74
4.3.4	Model examination of light functions	75
4.4	Discussion and Conclusion	77
5	The PS-1D model parameterisation and sensitivity analysis	83
5.1	Particle Swarm Optimizer (PSO) and the PS-1D model parameter optimization setup	84
5.1.1	Particle Swarm Optimizer	85
5.1.2	Implement the PSO to the PS-1D model	89
5.2	Parameter optimization results	90
5.3	Sensitivity analysis	99
5.4	Selecting final parameters	102
5.5	Discussions and Conclusions	105

6	Climate-linked drivers and pathways regulate Puget Sound phyto- plankton bloom	111
6.1	Numerical experiments set up	112
6.1.1	Investigated forcing ranges	112
6.1.2	Experimental Interpretation	115
6.2	Results	116
6.3	Discussions and Conclusions	126
6.3.1	Primary production	126
6.3.2	Spring bloom timing	126
6.3.3	Conditions during salmon outmigration	127
6.3.4	Nutrient stress in summer	128
7	Summary and Conclusions	132
7.1	Summary	132
7.2	Conclusions	134
	Bibliography	136

List of Figures

1.1	Marine survival rate of Chinook and Coho over time in Puget Sound fjord	3
1.2	Possible environmental drivers and pathways which regulate phytoplankton bloom dynamics in Puget Sound fjord	10
2.1	Map of Puget Sound estuary	15
2.2	A diagram of Puget Sound estuarine circulation	16
2.3	Sampling stations in Puget Sound	18
2.4	Spatial and temporal data coverage of sampling stations from Puget Sound monitoring programs	19
2.5	Number of samples per sampling station per year/day	21
2.6	Gradient of salinity, nitrate and Chla along main basin Puget Sound channel	25
2.7	z-variation of salinity, nitrate and Chla at each station upper 50 m layer	26
2.8	Yearly average vertical velocity profile calculated (a) and smoothed (b) in the main basin Puget Sound	29
2.9	Diffusive coefficient κ_v (m^2s^{-1}) against depth	30
2.10	A diagram of NPZD model	32
3.1	Initial values of Chla, NO_3 , and NH_4	44
3.2	Photosynthetically active radiation (PAR_0) of a typical year	45
3.3	Salinity from observation and model output against depth and year day	46
3.4	Chla, nitrate, and ammonium observation from DoE cruise at station 5 in main basin Puget Sound	48

List of Figures

3.5	Daily average of integrated Chla over euphotic depth (from surface to 30 m depth)	49
3.6	Daily average of integrated NO_3 over euphotic depth (from surface to 30 m depth)	50
3.7	Daily average of integrated NH_4 over euphotic depth (from surface to 30 m depth)	50
3.8	Observations (left, same as Figure 3.4) and the PS-1D model outputs (right) of Chla, NO_3 and NH_4 against time and depth	53
3.9	Daily average integral of Chla over the upper layer of 30 m depth. The PS-1D model run with <i>Davis et al.</i> (2014) parameters of the outer coast	54
3.10	Daily average integral of NO_3 over the upper layer of 30 m depth. The PS-1D model run with <i>Davis et al.</i> (2014) parameters of the outer coast	54
3.11	Daily average integral of NH_4 over the upper layer of 30 m depth. The PS-1D model run with <i>Davis et al.</i> (2014) parameters of the outer coast	55
4.1	Conceptual beam transmissometer	62
4.2	Euphotic depth data set at station 5 from <i>Newton and Van Voorhis</i> (2002) study	64
4.3	Average of integrated Chla over euphotic depth reported in <i>Newton and Van Voorhis</i> (2002)	65
4.4	Approximate 30-year monthly average of measured Secchi depth and monthly average Secchi disk depth calculated back from euphotic depth	66
4.5	Transmission of light (%) from DoE data set at station 5.	68
4.6	Beam attenuation, λ (m^{-1}) calculated from transmission data.	68
4.7	Regressions of k_d and Chla by using euphotic depth and Chla data taken from <i>Newton and Van Voorhis</i> (2002)'s study	69
4.8	Turbidity over period 2009 - 2017 at station 5 from DoE cruise	72
4.9	Regressions of k_d and/or Chla, turbidity, fresh water by using data from DoE cruise.	73

List of Figures

4.10	Comparison of the PS-1D model outputs and observations against time and depth. The PS-1D is run with new light function	78
4.11	Comparison of the PS-1D model outputs and observations in upper layer of 30 m depth. The PS-1D is run with new light function	79
5.1	Particle swarm optimization algorithm	87
5.2	Model assessment skill WSS_MAE against Particle Swarm Optimizer (PSO) iteration	91
5.3	Velocity of swarm particles against iteration	92
5.4	Moving paths of swarm particles at their personal best cost (gray dots) and global (or swarm's) best cost (black dots) in parameter spaces over searching iterations. Blue lines mark iteration 70, 220, and 300	93
5.5	PS-1D outputs compared to observations	95
5.6	The PS-1D model run with parameters extracted at the PSO iteration of 70 th (the first) and 220 th (the second). Compare to figure 5.5, right-hand panels	96
5.7	Average integral of the PS-1D model state variables over euphotic depth against time	97
5.8	Average integral of state variables over euphotic depth from PS-1D outputs (blue line) in comparison to observations (grey dots)	98
5.9	Parameter sensitivity analysis	100
5.10	Differences in dynamics between the two parameter sets which produce similar model goodness-of-fit	107
6.1	Mixing profile variation (gray) with black profile showing yearly average	113
6.2	Vertical advection profile variation (gray) with black profile showing yearly average	114
6.3	Responses of bloom date (metric (<i>i</i>)) to environmental forcings	119
6.4	Responses of primary production (metric (<i>ii</i>)) to environmental forcings	120
6.5	Responses of phytoplankton concentration at Steelhead outmigration (metric (<i>iii</i>)) to environmental forcings	121

List of Figures

6.6	Responses of phytoplankton concentration at Chinook outmigration (metric (<i>iii</i>)) to environmental forcings	122
6.7	Responses of duration nutrient limitation in summer (metric (<i>iv</i>)) to environmental forcings	123
6.8	Final ranking of pathways of climate influence on four metrics of phytoplankton dynamics	129

List of Tables

2.1	Comparison of horizontal and vertical advection fluxes	24
3.1	The PS-1D parameters values, which are taken from <i>Davis et al.</i> (2014) study of the outer coast (excludes κ_v and w_{adv})	42
3.2	Comparison between <i>WSS_MSE</i> and <i>WSS_MAE</i> in main basin Puget Sound top 20 m depth and whole water column; and comparison between <i>WSS_MSE</i> of main basin Puget Sound and the outer coast at the top 20 m depth.	56
4.1	Diffuse attenuation coefficients (att_P and att_{bg}) derived from Secchi disk measurements (<i>Newton and Van Voorhis</i> (2002)'s data set)	70
4.2	Diffuse attenuation coefficients derived from DoE transmissometer data	71
4.3	Set of potential light attenuation functions for station 5, main basin Puget Sound	74
4.4	Comparison of PS-1D performance on potential light attenuation functions (table 4.3) by Willmott Skill Score mean absolute error (WSS_MAE). Remaining PS-1D parameters are as in table 3.1	76
5.1	WSS_MAE (index of model – observation agreement) difference between model runs with PSO-optimized parameters and parameters from the outer coast model	102
5.2	The PS-1D model performance worsens when PSO-proposed parameters are substituted one at a time with parameters from the outer coast model.	103

5.3	Comparison of PS-1D performance using PSO and sensitivity analysis proposed parameters (or final PS-1D parameters, table 5.4, figure 5.5 and 5.7) to parameters taken from <i>Davis et al.</i> (2014)'s study	103
5.4	The final PS-1D model optimized parameter set of main basin Puget Sound, compared with (<i>Davis et al.</i> , 2014) values for the outer coast . .	104
6.1	Estimates of environmental variability used in the scaling analysis. Scales of variation denoted by Δ are defined throughout as 2 standard deviations	117
6.2	Sensitivity of mixing to stratification and wind stress, and of stratification to riverflow	118
6.3	Response of phytoplankton metrics (PP_{tot} , etc.) to variability in physical drivers (<i>mixing</i> , etc).	124
6.4	Scales of variation in five metrics of phytoplankton production (PP_{tot} , etc.) associated with seven climate-linked drivers (τ , etc.).	125

Acknowledgements

I would like to extend my gratitude first and foremost to my supervisor Neil Banas for his mentoring, encouraging, and support during my PhD. I would additionally like to thank my second supervisor, Mike Heath, for helpful comments and discussions on physical model and at the early writing of my thesis. Thank to MASTS Grad School for annual retreats and activities, from which I gained valuable soft skills.

I would like to recognize the invaluable assistance from Marine Group members for all friendship and help during my study, which here I just can name a few: Soizic for physical model outputs; Aidan for advice on technical aspect of parameterization; Fabian, Agnes, and Ricardo for comments on my thesis writing; special thank to Hazel, my “lunch-buddy” since I arrived the office, for proofreading my thesis; Emma for joyful board game nights; Dougie for organising marine outing excursions which I very much enjoyed; and to all colleagues in my office: Abdulmajeed, Alan, Craig and recently Alex, Ana, who make the office more cheerful.

Outside the University, I would like to thank all instructors and members of Yudan Nashi Kan Aikido club for sharing Aikido spirit, practice and friendship. I would also like to thank Jai and Bryn for taking care of me, especially during the Covid-19 pandemic.

Finally, I would like to extend my deepest gratitude to my family, my parents and my brother, for encouraging and supporting me to follow my dreams even in the middle of the family hard time, when they would prefer to have me by their side.

I was funded by Long Live The Kings (LLTK), University of Strathclyde, and NOAA MERHAB program (Monitoring and Event Response for Harmful Algal Blooms).

Chapter 1

Introduction

1.1 Motivation for Puget Sound phytoplankton study

Humans have relied on the ocean as an important source of proteins throughout the history of humankind. Globally, seafood consumption has continuously increased, and is projected to continue (*Watson et al.*, 2015). In 2010s, marine fisheries were estimated to provide 80Mt of protein and micronutrient rich food for human consumption per year, contributed US\$230 billion to the global economy, and offered livelihood support to 8% of the world's population (*Barange et al.*, 2014). In future, the food security of the majority may depend on the ocean (*Watson et al.*, 2015). However, the production of marine fishes is limited (*Watson et al.*, 2014). The annual harvest from the global marine fishery has been static or in decline since the 1990s (*Ye and Cochrane*, 2011; *Sayer*, 2019).

Puget Sound fjord, U.S, like many coastal ecosystems worldwide, is in serious decline (*Ocean Policy*, 2004; *Ruckelshaus and McClure*, 2007; *Heinz*, 2008). Puget Sound is one of the world's most productive salt water environments (*Strickland*, 1983), and is unique by virtue of both high salmon species richness and high natural salmon productivity (*Lombard*, 2006). Despite once being the most productive salmon areas along the Pacific Coast, marine survival rate of juvenile salmon (especially Chinook salmon) has shown a sharp decline over last 30 years for reasons that are yet unknown (Figure 1.1).

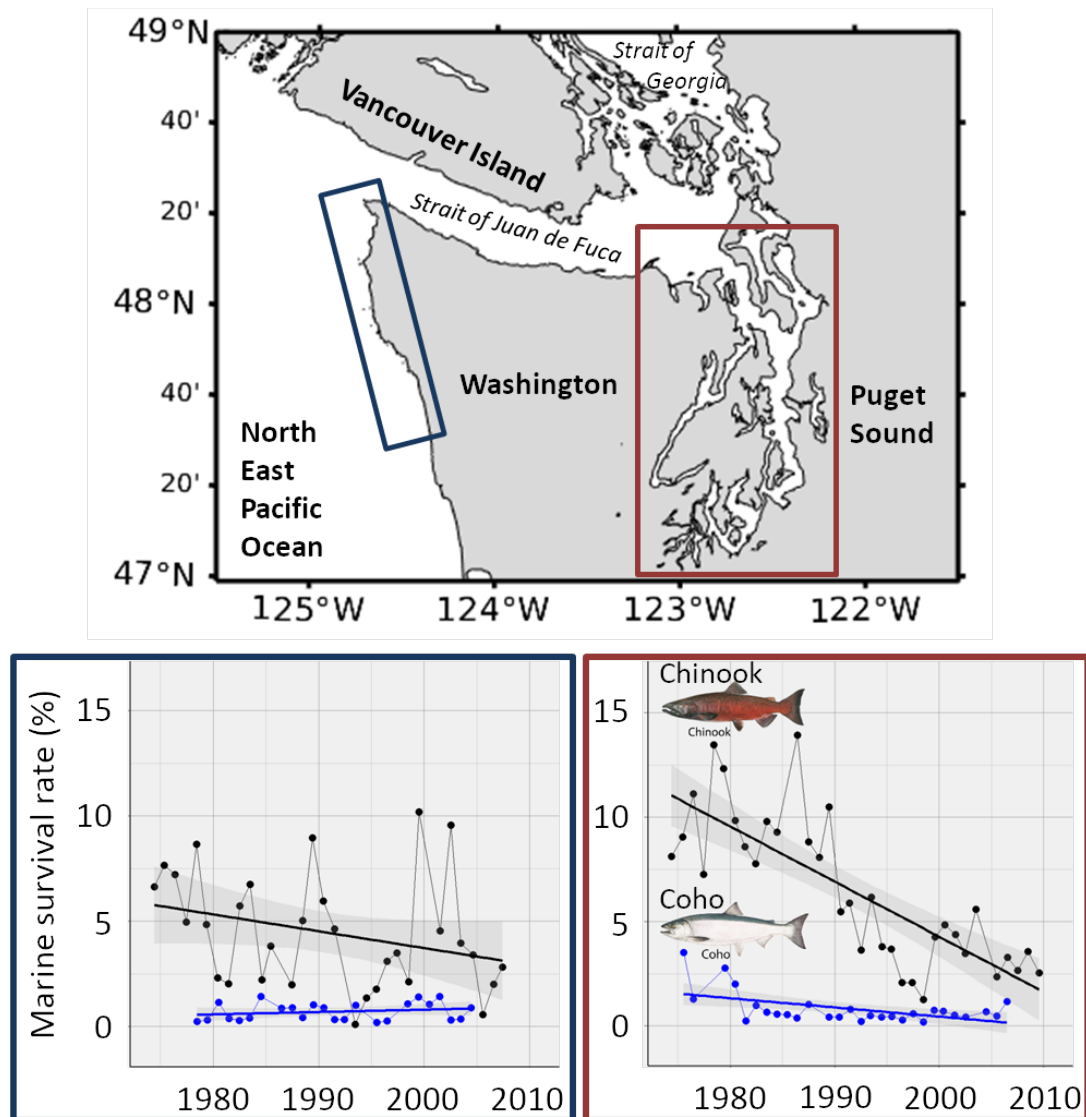


Figure 1.1: Marine survival rate of Chinook and Coho over time in Puget Sound compare to its outer coast [the graphs are reproduced from *The Salish Sea Project*]

Among numerous factors influencing fish production (e.g., over-fishing, environmental or ecological changes, and inadequate fishery management), primary production is arguably the most important and fundamental (Chassot *et al.*, 2010; Pauly and Christensen, 1995; Barange *et al.*, 2014). Evidence has noted a strong link between primary production and fish production (Larkin and Northcote, 1969; Cushing, 1982). The reason is that final production and biomass of many fish with planktonic larvae are

determined by the success of juvenile stages feeding low in the food chain; either on zooplankton or on phytoplankton directly (*Harris, 2012*).

In Puget Sound, although the phytoplankton seasonal cycle is well described (*Winter et al., 1975; Strickland, 1983; Newton and Van Voorhis, 2002*), quantitative estimation of local phytoplankton bloom timing and magnitude (or production) as well as the impact of environmental variation during the year are not. Therefore, this study aims to gain better understanding of what controls the phytoplankton bloom onset and production in the Puget Sound, and how these are likely to be impacted by factors which are driving changes in the Puget Sound.

1.2 Plankton related hypotheses about declining marine survival rate of Puget Sound salmon

The health of the Puget Sound marine ecosystem, same as many coastal ecosystems worldwide, is facing serious decline (*Ocean Policy, 2004; Ruckelshaus and McClure, 2007; Heinz, 2008*). Much of the ecological capital (large salmon runs, mature forests, coastal wetlands, clean water) that supported extractive industries in the late 19th century have been exploited and degraded (*Quinn, 2010*). Water quality is increasingly threatened by non-point sources of contamination. There are increased number of species listed as endangered. Some iconic species such as chinook salmon, and steelhead salmon are among those endangered mostly by human related activities in the region.

In addition, climate changes have occurred in the Puget Sound region in the past century, and the next several decades will likely see even greater changes (*Ruckelshaus and McClure, 2007*). Puget Sound waters warmed substantially, especially in the period since the early 1970s. As a consequence of regional warming in the 20th century, spring time snow pack has decreased markedly at many sites in Puget Sound, the timing of river and stream flow shifted with significant reductions in snowmelt runoff in May-July, thus reduced summer stream flows. These changes are likely to negatively impact

salmon production (*Mote et al.*, 2003). For example, warmer ocean temperatures affect the migration behavior of Fraser River sockeye by diverting them to the northern entrance to the Strait of Georgia rather than by the Juan de Fuca entrance (*Groot and Quinn*, 1987), which dramatically alters commercial fisheries in northern Puget Sound.

Salmon population strongly depend on its living environmental conditions, which is influenced by natural and anthropogenic drivers. Naturally, Puget Sound salmon ecosystems are embedded within a trans-Pacific ocean and climate system which are regulated by oscillations of El Niño-Southern Oscillation (ENSO) and Pacific Decadal Oscillation (PDO). Thus, the ecological conditions that the individuals in a salmon population might encounter in a particular year may vary considerably depending on the climate and its interactions with regional and local scales of variation (*Bottom et al.*, 2008). However, Puget Sound salmon has steadily declined over last thirty years. Hence, direct natural causes are not likely the major declining drivers.

The life cycle of salmon requires specific conditions within the chain of connected environments of rivers, estuaries, and ocean. Salmon in Puget Sound use the estuary to make the transition from rivers to the ocean. Although salmon spend only a part of their life cycle in estuarine environments, these habitats are critical to the survival of salmon populations. There is increasing evidence suggesting the survivability of juvenile salmon, when they first enter marine water, is dependent upon productivity of the sea, and the time spent in these nutrient rich waters (*Thomson et al.*, 2012; *Araujo et al.*, 2013; *Phillips*, 2015). Having abundant, high-quality food resources during the sensitive early marine phase allows for rapid growth and lipid storage, which generally means healthier fish with enhanced predator avoidance, winter survival, and greater reproductive success (*Cushing*, 1990; *Beamish and Mahnken*, 2001). The occurrence of large and productive zooplankton and phytoplankton blooms has been shown to be highly variable in the region, a result of a combination of biophysical factors such as ocean temperature, wind speed, cloud cover, and ocean surface stratification caused by

riverine inputs (*Allen and Wolfe, 2013; Mackas et al., 2013*). This variability creates a large opportunity for a timing mismatch between the spring bloom and early marine entry of juvenile salmon when mortality can be quite high (*Beamish et al., 2012; Preikshot et al., 2012*). During the past 50 years, energy-transfer processes in Puget Sound have gone through major transformations (*Ruckelshaus and McClure, 2007*).

Placed at the base of the marine food web, phytoplankton production is hypothesized to have cascade effects to higher trophic levels (bottom-up control) and may be a possible cause of the observed salmon decline in Puget Sound. The bottom-up hypothesis is stated as:

Circulation and bottom-up processes hypothesis: changes in circulation and water properties have altered phytoplankton and zooplankton production in ways that degraded salmon food-webs in the Salish sea from the 1970s to 2000s (*Beauchamp et al., 2012*).

In addition, increased appearance of harmful algae blooms (HABs) is a possible link to salmon decline. Harmful blooms of dinoflagellates *Alexandrium catenella* have increased in Puget Sound over the last half-century (*Moore et al., 2011*). *Alexandrium catenella* is known to produce powerful neurotoxins that lead to paralytic shellfish poisoning (PSP). Thus, HABs in relation to the salmon decline is hypothesised as:

Harmful algae directly affect salmon survival through acute or chronic mortality and may adversely affect prey availability by food web impoverishment (*Beauchamp et al., 2012*).

Overall, the two hypotheses can be examined through phytoplankton bloom dynamics and species composition.

1.3 Puget Sound’s phytoplankton dynamics

Pelagic phytoplankton in Puget Sound consist of mainly large-sized phytoplankton of two major groups: diatoms and dinoflagellates, with diatoms accounting for most of the biomass (*Ruckelshaus and McClure, 2007*). Phytoplankton abundance and distribution are highly heterogeneous or “patchy,” both spatially and temporally, and are linked to the degree of stratification, light availability, turbidity, and nutrient availability in particular areas (*Ruckelshaus and McClure, 2007*).

Winter et al. (1975) is one of the earliest attempts to quantify the relationship between the growth of phytoplankton and climatic conditions and circulation in Puget Sound. This study, by using approximate circulation analysis and simplified formulation of phytoplankton kinetics, demonstrated that phytoplankton growth in Puget Sound is closely coupled to the seasonal variation and circulation characteristics. According to *Winter et al. (1975)*, the annual cycle of phytoplankton growth was dominated by several intense diatom blooms between early May and September, then shifted to smaller dinoflagellates in late summer and early autumn. *Winter et al. (1975)* noted that during blooming seasons Chla rarely exceeds 15 mg Chla/m^3 despite high nutrient concentrations and photosynthetic rates. Also, *Winter et al. (1975)* suggested phytoplankton seeds supplied from depth is the source of bloom initiation.

On factors controlling bloom formation and disappearance in Puget Sound, *Winter et al. (1975)* highlighted incident light, freshwater runoff, and tidal ranges as the most useful factors. A later study by *Alexander J. Chester et al. (1980)* proposed that wind stress is also a useful predicting variable. *Sinclair (1978)*, who reinterpreted data from (*Winter et al., 1975*), showed a high correlation of primary production and stratification, however biomass itself is not as highly correlated with density stratification. This latter point of *Sinclair (1978)* suggested that the processes influencing the variable density stratification has a strong impact on production processes themselves, the dynamic aspects of phytoplankton growth, rather than being just a physical aggregation effect. This correlation was also observed by *MacCready and Banas (2016)* when analysing

long-term climatological data. *Boss et al.* (1998) confirmed *Winter et al.* (1975) suggestion of large concentration of pigments (not separate Chla and pheopigments) are associated with bottom water renewal processes. However, *Boss et al.* (1998) also observed that more than 80% of the Chla concentration disappeared from the bottom waters within a week, an indication of the rapid consumption and/or sinking of the pigments in the deep-water intrusion. Thus, this finding of *Boss et al.* (1998) did not seem to support *Winter et al.* (1975) conclusion on supply of phytoplankton seeds from depth.

Since then, Puget Sound-wide model development efforts have ranged from simplified box models (*Friebertshauser and Duxbury*, 1972; *Hamilton et al.*, 1985; *Cokelet et al.*, 1990; *Babson et al.*, 2006) to vertical 2-D models (*Lavelle et al.*, 1991) and to fully 3-D baroclinic numerical models (*Khangaonkar et al.*, 2011; *Sutherland et al.*, 2011; *Yang and Khangaonkar*, 2010; *Nairn and Kawase*, 2002). However, these models have mainly focused on hydrodynamics and physical processes (*Khangaonkar et al.*, 2012).

Recent studies on phytoplankton dynamics are often enclosed in this study of water quality. Few efforts from the Washington State Department of Ecology described plankton dynamics as sideline results of water quality studies. For example, *Newton and Van Voorhis* (2002) analysed two years of monthly data which mostly agreed with the dynamics described by *Winter et al.* (1975) and emphasised that primary production in central Puget Sound is predominately controlled by light availability in winter. However, *Newton and Van Voorhis* (2002) observed earlier (and therefore longer) phytoplankton growing season, which was from March to September. The growing season was characterized by a spring bloom, followed by distinct low levels of production, then subsequent summer and autumn blooms. Strong variation between stations in Puget Sound highlighted in *Newton and Van Voorhis* (2002) indicated a very dynamic environment in terms of conditions affecting phytoplankton such as light, nutrient availability, mixing, and grazing pressure. *Roberts et al.* (2008) developed a biogeochemical model of South Puget Sound to simulate dissolved oxygen as a proxy of phytoplankton pri-

mary production. *Khangaonkar et al.* (2012) showed the first offline 3-D water quality model of the entire Salish Sea (which includes Puget Sound, Strait of Juan de Fuca and Strait of Georgia (Figure 2.1)) with a focus on the Puget Sound region. Although, *Khangaonkar et al.* (2012), one year study of dissolved oxygen in Puget Sound, successfully showed phytoplankton growth and die-off, succession between two species of algae, nutrient dynamics, this study was not able to describe forcing drivers, and their variability to regulate plankton dynamics. On going development of LiveOcean, a 3D biogeochemical model, incorporated a biological model of the outer coast (*Davis et al.*, 2014), which covers the entire Salish Sea still need to be improved on Puget Sound phytoplankton dynamics (*McCready, per. comm.*).

Hence, development of quantitative phytoplankton models in Puget Sound have been limited (*Khangaonkar et al.*, 2012). Therefore, development of such a quantitative model is needed.

1.4 Study aims

Figure 1.2 summarizes current understanding of drivers and possible pathways by which regional climate can drive phytoplankton bloom (timing and magnitude) in Puget Sound. The diagram is a pre-selection based on past research in the system (e.g. *Winter et al.* (1975); *Newton and Van Voorhis* (2002); *MacCready and Banas* (2016)). Generally, in addition to temperature, phytoplankton growth is also regulated by light and nutrient availability. Light limitation is determined by incoming radiation, water transparency, vertical mixing and advection. The underwater light attenuation varies strongly with watershed inputs. Vertical mixing and advection contribute to light limitation by controlling the depth range over which phytoplankton cells are exposed to light. Nutrient limitation in the photosynthetic zone is also controlled by vertical mixing and advection, and potentially by changes in the concentration of nutrients in incoming ocean water. In other estuaries, changes in river-derived nutrients would be of first-order importance as well, but nutrients in Puget Sound are overwhelmingly ocean-

derived (*Banas et al.*, 2015). All these drivers are directly influenced by the regional climate, which has seen changing conditions (*Ruckelshaus and McClure*, 2007).

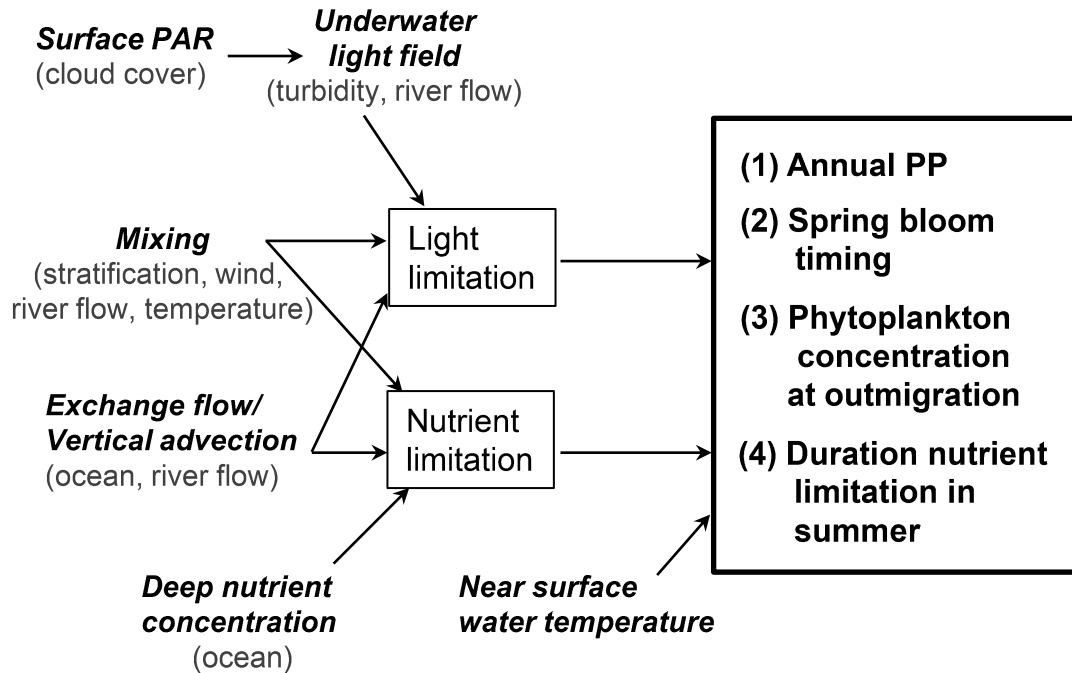


Figure 1.2: Selected possible environmental drivers and pathways regulate phytoplankton bloom dynamics (annual primary production and bloom timing), affect young salmon survival through visual search for food disruption (phytoplankton concentration during outmigration), and enable opportunity of harmful algal blooms (HABs) development through nutrient limitation in summer.

This study investigates Puget Sound phytoplankton blooms through metrics of (1) the annual primary production, (2) timings of spring blooms, (3) spring and summer phytoplankton concentrations, and (4) the occurrence or non-occurrence of strong nutrient limitation in summer. Metrics (1) and (2) are focused on potential bottom-up control effect of phytoplankton to higher trophic levels, which may contribute to the decline of salmon over the past 30 years (the bottom-up hypothesis). Metric (3) aims to analyze patterns of spring and summer phytoplankton concentrations, which is motivated by a non-trophic hypothesis: dense phytoplankton blooms during critical

outmigration times potentially change the underwater light field in a way that disrupts visual search. The non-trophic hypothesis is based on evidence that vision is a dominant modality involved in the formation, maintenance and distribution of visual predators in the water column (*Hunter, 1968; Lehtiniemi et al., 2005; Dupont and Aksnes, 2011*). Finally, metric (4) investigates the occurrence or non-occurrence of strong nutrient limitation in summer as a proxy to examine the occurrence of *Alexandrium* HABs (the HABs hypothesis). The strong nutrient limitation proxy is chosen as nutrient limitation under warm, high light conditions has long been taken to encourage dinoflagellate blooms over diatoms, including toxin-producing taxa like *Alexandrium* (*Kudela et al., 2010; Moore et al., 2011, 2015; Brandenburg et al., 2017*). Moreover, there is no detailed historical record in Puget Sound that directly supports a local link between nutrient limitation and *Alexandrium* HABs.

To identify key drivers and pathways from Figure 1.2, this study will develop a coupled circulation/lower trophic level (NPZD) model to investigate phytoplankton dynamics and its quantitative responses to the listed physical drivers, and finally to answer questions:

1. Which parameter set represents Puget Sound phytoplankton bloom dynamics?
2. What are the most important mediators and pathways between climate and primary production?
3. How do changes in those mediators drive primary production in the region?

1.5 Thesis structure

Examining the drivers and pathways outlined in Figure 1.2 requires the development of a new mathematical model of plankton dynamics for Puget Sound. This is the subject of chapter 2. Chapter 2 describes and examines observations in supporting physical model selection. A biological model is then described following the selection of a suitable physical model. Model configuration, assessment and preliminary exploration are given

in chapter 3. Chapter 4 investigates light limiting factors on phytoplankton growth. This is motivated by suggestions that spring blooms in Puget Sound are predominately controlled by light availability in winter. Since there is not always sufficient data to define or constrain all biological parameters, parameterisation is a necessary step to identify missing parameters values. Chapter 5 will use optimization approach to quantify undefined parameters. After that parameters sensitivity analysis will be also carried out to identify which parameters in the Salish Sea biophysical model (LiveOcean model) really need to change in order to represent Puget Sound plankton. Once the final model is defined in chapter 5, chapter 6 will use the model for numerical experiments (or forcings sensitivity analysis) to define critical drivers and pathways that influence Puget Sound phytoplankton growth (see figure 1.2). Finally, summary and conclusion are given in chapter 7.

Chapter 2

A model of Puget Sound plankton dynamics

This chapter introduces a new model of Puget Sound phytoplankton dynamics. Models of low trophic levels (e.g. phytoplankton) in Puget Sound have been limited (*Khangaonkar et al.*, 2012) despite a number of efforts on model development which range from 2-D box models (*Hamilton et al.*, 1985; *Cokelet et al.*, 1990; *Babson et al.*, 2006) to fully 3-D numerical models (*Sutherland et al.*, 2011; *Khangaonkar et al.*, 2011). LiveOcean, one of the rare 3-D coupled physical-biogeochemical models, has been developed to cover the U.S. Pacific Northwest outer coastal region and Salish Sea which includes Puget Sound, Strait of Juan de Fuca and Strait of Georgia. Although the model adequately simulated total nitrogen distribution and the magnitude and timing of phytoplankton blooms on the outer coast (*Davis et al.*, 2014), its depiction of Puget Sound plankton dynamics still needs to be improved (McCready, University of Washington, *pers. comm.*). To improve the quality of the biogeochemical model in Puget Sound, a 2-D biophysical model was suggested as a first step to systematically explore Puget Sound plankton dynamics (*MacCready and Banas*, 2016). However, *Winter et al.* (1975) demonstrated that a 1-D biophysical model might be applicable when variation of phytoplankton along the Puget Sound channel is negligible.

To decide on suitable model to this study, the chapter starts with a brief description of the Puget Sound estuarine circulation (Section 2.1), and then describes monitoring programs and observations available in Puget Sound (Section 2.2). Section 2.3.1 provides evidence resulted from observations analysis to support selection of an appropriate physical model for the purpose of the study. Section 2.3.2 presents a biological model (or NPZD model) with a focus on phytoplankton dynamics. Conclusions of the new Puget Sound plankton model are given in section 2.4.

2.1 Brief description of Puget Sound estuarine circulation

Puget Sound is a deep, fjord-like estuary carved by retreating glaciers at the end of the last ice age 11000 - 15000 years ago (*Kruckeberg, 1995*). The Puget Sound estuarine system is a complex composite of several basins connected by a system of sills (*Cannon et al., 1983*). The Main Basin of Puget Sound is separated from the others by two sills (Figure 2.1), which strongly influence hydrodynamics of the Main Basin (Figure 2.2) and consequently its biological processes. The first sill located at Admiralty Inlet is around 30 kilometers long and about 64 metres deep. The sill connects Puget Sound to the Pacific Ocean via Strait of Juan de Fuca (*Cannon and Laird, 1978*). The second sill is at Narrows, of 44 meters deep separating main basin Puget Sound from a southern basin (*Cannon and Laird, 1978*). The main basin in between the two sills is approximately 50 km long and 3-5 km wide (*Cannon and Laird, 1980*) with average depth around 62 m and maximum depth at 280 m. There are numerous rivers entering the Puget Sound system. However, the Skagit River entering in the north supplies more than 60% of the freshwater, about half of which flows southward toward the main basin (*Ebbesmeyer et al., 1977; Cannon and Laird, 1980*). Puget Sound's main basin averages approximately 90% oceanic water and 10% fresh-water. Despite the small fresh-water content, the input of the Skagit River and other rivers drive the estuarine circulation of the region. The estuarine circulation is then subject to wind stress and strong tidal mixing (*Sutherland et al., 2011*), which characterize the behaviour of Puget Sound as a partially mixed estuary (*Phillips, 2015*). The estuarine circulation is known to support

high productivity of the region because the deep inflow is enriched by nutrients due to upwelling off the Washington coast (Strickland, 1983). Thus, a close approximation of estuarine circulation is vital to reproduce biological observations in Puget Sound.

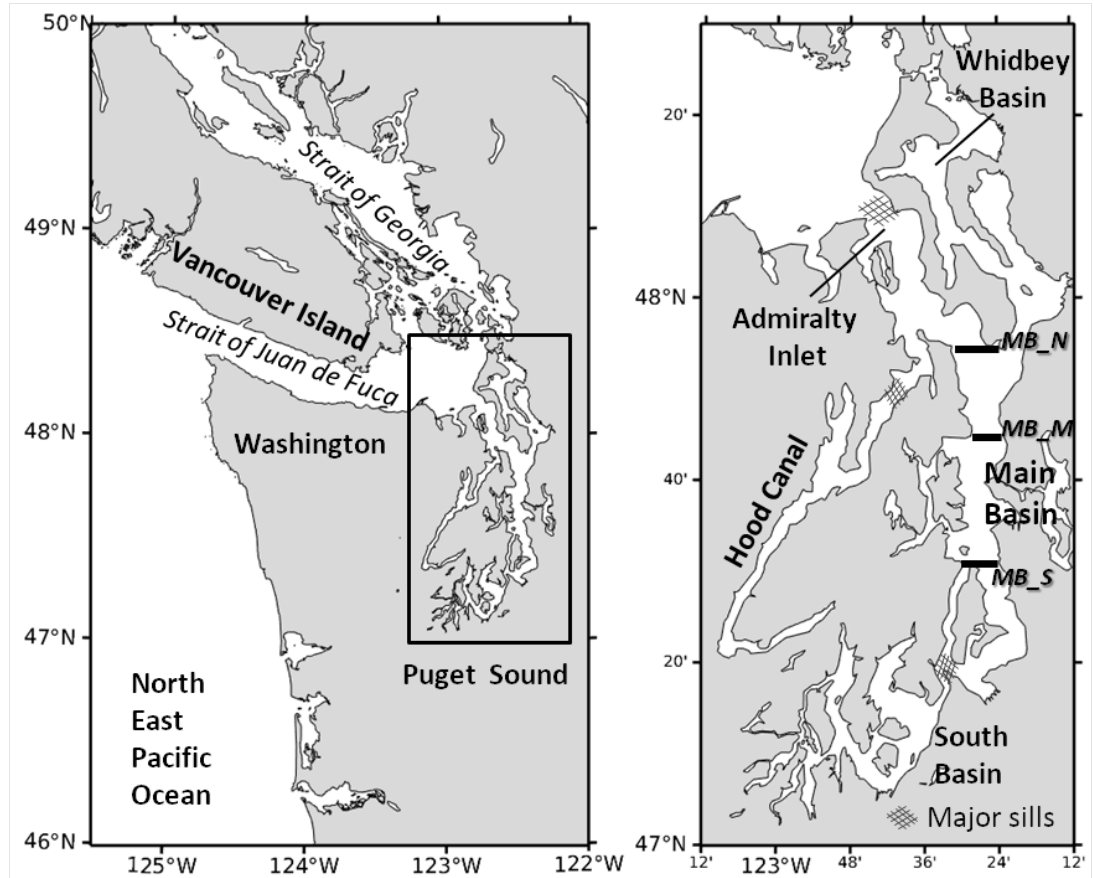


Figure 2.1: Puget Sound estuary includes 5 basins: Main Basin, Admiralty Inlet, South Basin, Whidbey Basin, and Hood Canal

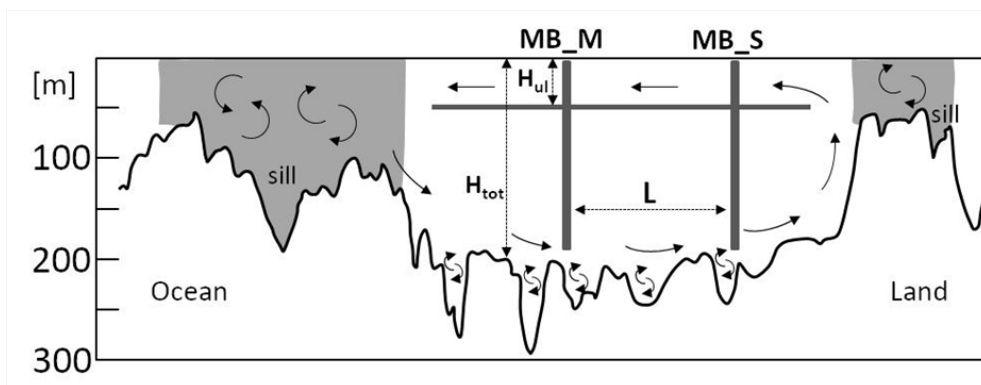


Figure 2.2: A diagram of Puget Sound estuarine circulation

2.2 Monitoring programs and observational data

Currently, there are three major marine monitoring programs and data sets in Puget Sound, namely Department of Ecology (DoE), King County (KC), and Puget Sound Regional Synthesis Model (PRISM). These three programs were set up based on different interests in the Puget Sound marine environment.

The Washington State Department of Ecology (DoE) was first initiated under concerns over dangers of supertankers oil spill to marine life, when Puget Sound was the main route of transporting crude oil from Alaska to the continental U.S. In the 1970s, DoE started an extensive study of shoreline organisms (Marine Waters Monitoring), and then expanded it to a monthly sampling program. However, consistency in measurement systems, and hence good quality *in situ* monthly data, are only available from autumn 1989 onwards (Newton *et al.*, 2003; Moore *et al.*, 2008). During a sampling cruise, a rosette of Niskin bottles was deployed at each station. The Niskin bottles collected water at pre-defined depths (mostly at 0, 10, and 30 m depth), which were analyzed for chemicals (e.g. nitrate, phosphate) and biological variables (e.g. chlorophyll-a (Chla), E. Coli). Physical parameters such as temperature, salinity, dissolved oxygen, pH were measured at the same time by CTD sensors attached to Niskin bottles. The CTD records data throughout the water column, in many cases deeper than 200 m.

In an ongoing effort to maintain and improve Puget Sound’s water quality, the King County’s (KC) routine marine monitoring program focuses primarily on water quality within King County’s borders (<https://green2.kingcounty.gov/marine/>). King County collects monthly *in situ* water column profiles at its offshore monitoring stations (Figure 2.3) using a CTD. A multi-sensor array CTD measures dissolved oxygen, salinity, temperature, density (calculated), transmissivity, photosynthetically active radiation (PAR), and fluorescence (as a measure of Chla). The CTD also triggers the closure of the 5-liter Niskin bottles at pre-programmed depths to collect discrete water-column samples for laboratory analysis of additional parameters (e.g., fecal coliform and enterococcus bacteria, Chla and pheophytin pigments, solids, and nutrients (ammonia, nitrite/nitrate nitrogen, total Kjeldahl nitrogen, total phosphorus, and silica)).

The Puget Sound Regional Synthesis Model Program (PRISM) started in 1998 to better understand the oceanographic conditions of the region. PRISM collected samples twice a year (often in June and December) at around 40 stations within greater Puget Sound, including each of its major sub-regions (Central Basin, South Sound, Hood Canal, Whidbey Basin, Admiralty Inlet, Strait of Juan de Fuca (Figure 2.1)). The PRISM data set is used for research, education, and regional planning regarding Puget Sound by University of Washington. PRISM uses similar sampling methods as in the DoE program (<http://www.prism.washington.edu/story/PRISM+Cruises>).

Figure 2.3 shows all sampling stations from the three monitoring programs.

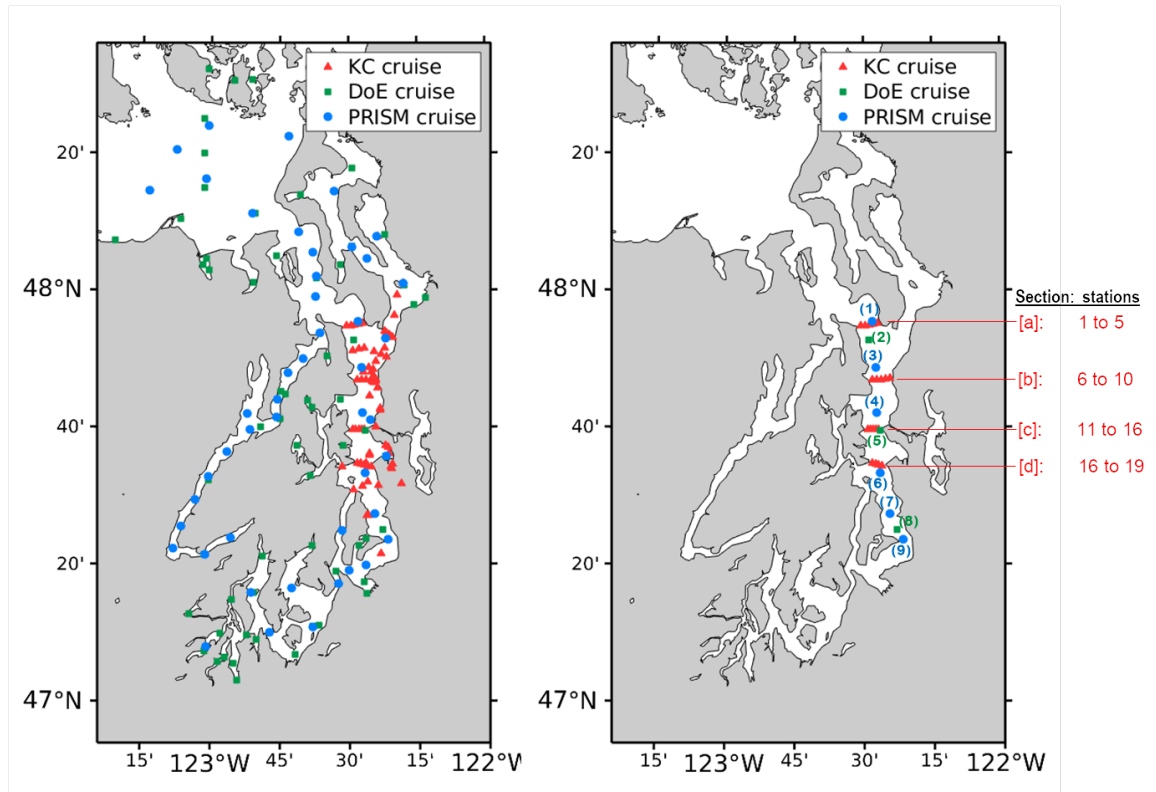


Figure 2.3: Sampling stations of PRISM (blue circle), KC (red triangle), and DoE (green square) programs. (left panel) sampling stations all over Puget Sound. (right panel) selected sampling stations in Main Basin Puget Sound

As three sampling monitoring programs were designed around different interests (marine resources (DoE), water quality (KC), and oceanographic conditions (PRISM)), measured parameters, periods and sampling frequency taken vary between the monitoring programs (Figure 2.4). Among the three, the KC program has the fewest parameters measured and shortest sampling period, while DoE and PRISM have similar monitoring parameters and period of sampling.

Among parameters sampled, ammonium, nitrate, Chla, fluorescence, phaeopigment, transmission, and photosynthetically active radiation (PAR) are often used in studies of patterns and/or interannual variability of the plankton cycle; while density, temperature, and salinity commonly represent the water column properties. Within those

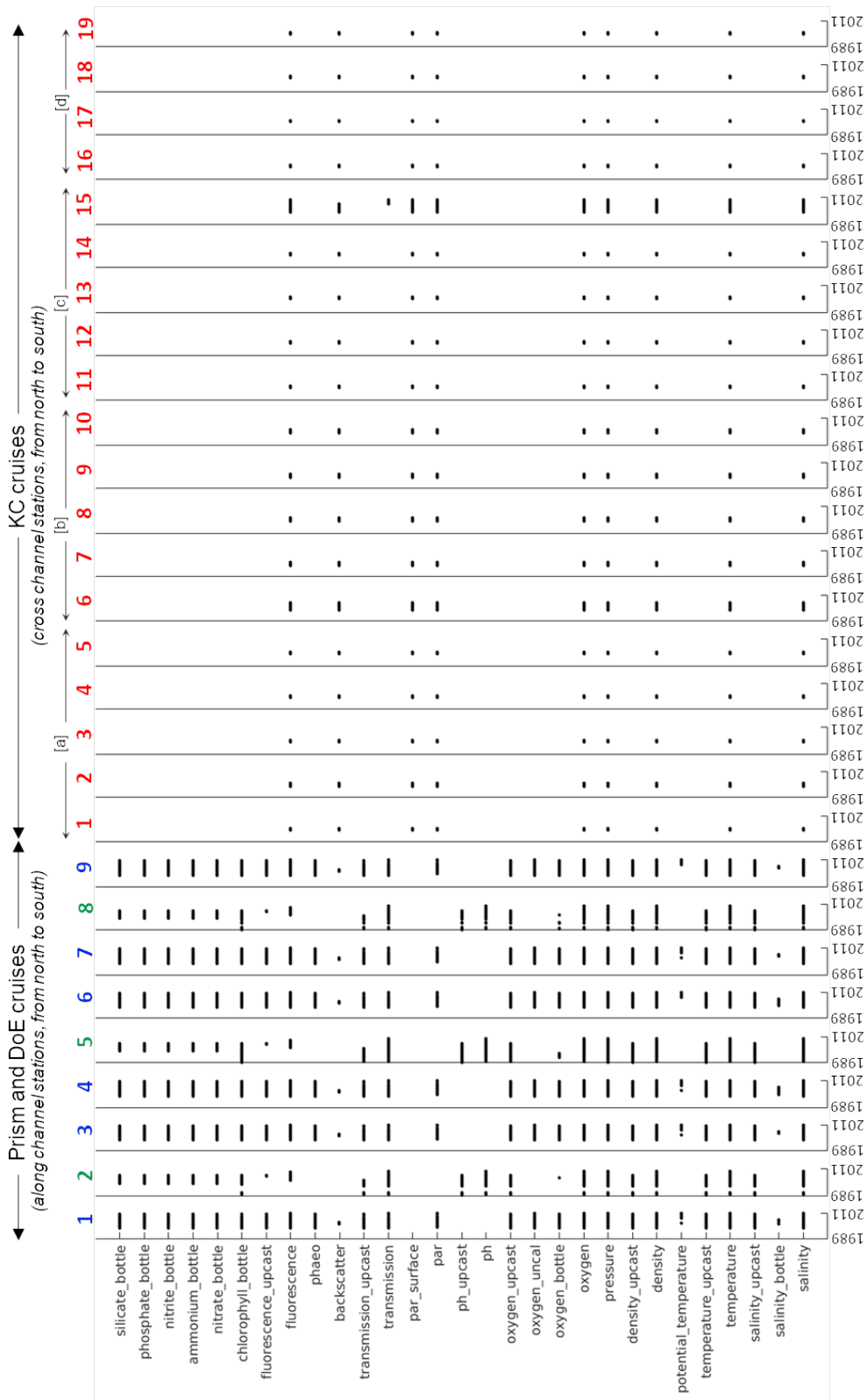


Figure 2.4: Spatial and temporal data coverage from three cruises. All physical and biological parameters measured from the three cruises are on y-axis, while time when samples were taken over period of 1989–2011 are on x-axis. Cruise sampling stations are ordered north to south and are labeled at the top of the figure.

parameters, obviously, KC does not have much data both in number of parameters and sampling periods in comparison to the DoE and PRISM data sets (Figure 2.4).

Figure 2.5 displays the number of samples per station per day of named parameters above. Over 22 years of sampling (1989 – 2011), there are around 150 days with data. KC program again does not show sufficient data that might be useful to this study. Between DoE and PRISM, DoE’s monthly observations are more valuable to explore biological processes, while PRISM’s large number of monitoring stations along Puget Sound channel (Figure 2.3) makes it a useful data source in addition to DoE data set for better picturing Puget Sound physical processes.

2.3 A model of Puget Sound plankton dynamics

The earliest quantitative study on Puget Sound phytoplankton, *Winter et al. (1975)*, and a recent, more sophisticated 3-D biogeochemical model, LiveOcean, are chosen as model references for this study. *Winter et al. (1975)* employed a 1-D biophysical model with biological processes resolving around phytoplankton. Despite the model’s simplicity, *Winter et al. (1975)* adequately reproduced the principal features of phytoplankton concentrations observed during 75 days and 35 days in the springs of 1966 and 1967, respectively. LiveOcean, on the other hand, is a coupling of an NPZD model and a Regional Ocean Modelling System (ROMS) ocean circulation model. LiveOcean works a lot like a weather forecast and predicts currents, salinity, temperature, chemical concentrations of nitrate, oxygen, carbon, and biological fields like phytoplankton, zooplankton, and organic particles (<https://faculty.washington.edu/pmac/LO/LiveOcean.html>).

Although the two referenced studies have different resolution for physical processes (1D and 3D, respectively), their representations of phytoplankton include similar processes such as phytoplankton growth, grazing by zooplankton, mortality, and sinking. Thus, this study uses *Winter et al. (1975)* and *Davis et al. (2014)* as a baseline to build a new biophysical model for Puget Sound. Further model description is given in the following sections.

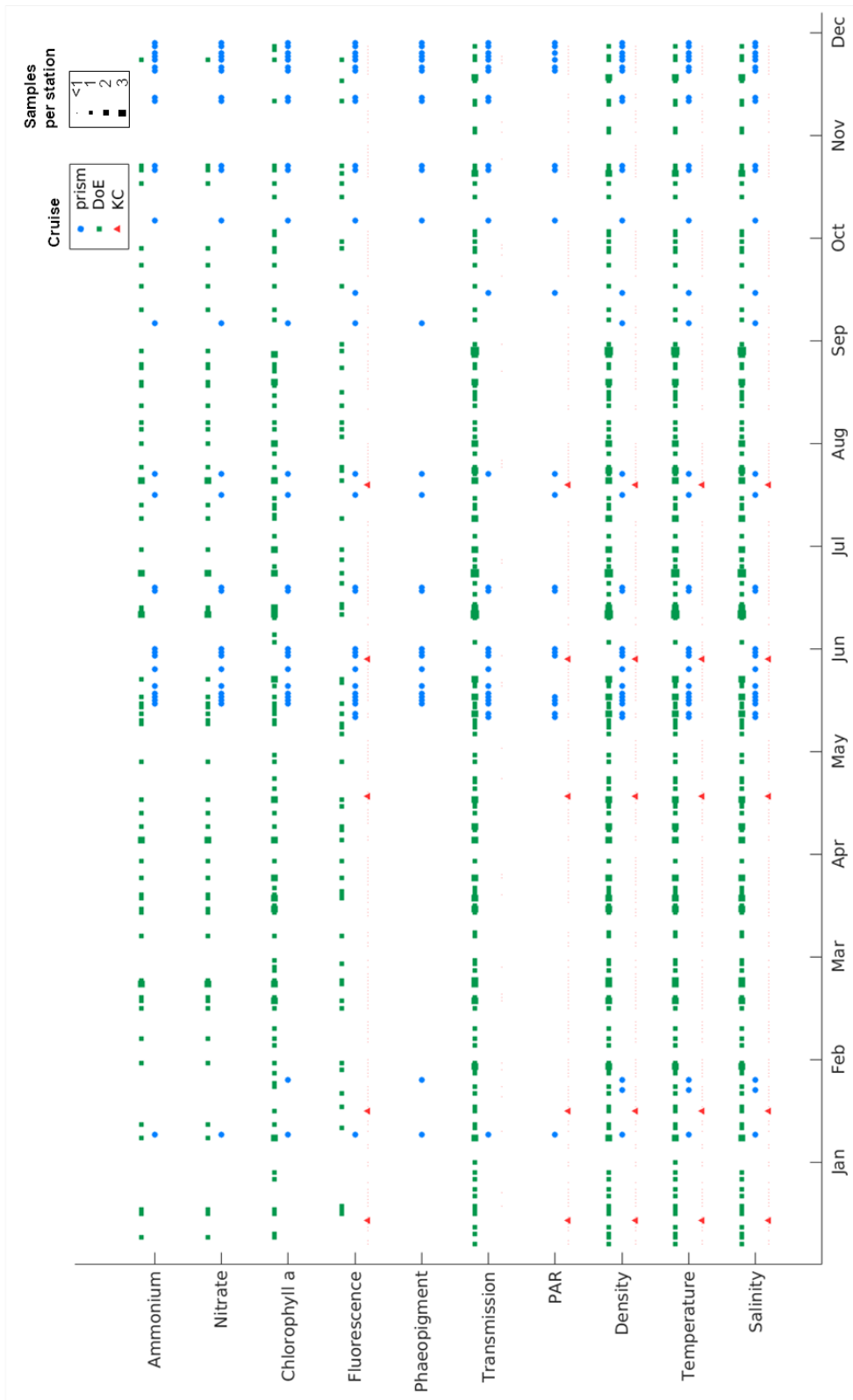


Figure 2.5: Number of samples per station per day. Data sampled over period of 22 years (1989 – 2011). PRISM (blue circle), KC (red triangle), and DoE (green square). Symbols sizes represent number of samples

2.3.1 Physical processes

A laterally-averaged equation for a trace can be written as

$$\frac{\partial C}{\partial t} = [\text{biogeochemical processes}] + u_{adv} \frac{\partial C}{\partial x} + w_{adv} \frac{\partial C}{\partial z} + \frac{\partial}{\partial z} \left(\kappa_v \frac{\partial C}{\partial z} \right) \quad (2.1)$$

By assuming x derivative of phytoplankton concentration is negligible throughout the length of the inlet segment, *Winter et al.* (1975) represented estuarine circulation by vertical advection in his phytoplankton model. The 1-D biophysical model included vertical advection and mixing in *Winter et al.* (1975) was able to reproduce satisfactorily not only the general Chla level but also many of the details of the spring bloom phytoplankton dynamics in both 1966 and 1967 observational periods.

The success of 1-D model in *Winter et al.* (1975) invites this study to examine magnitude of fluxes in equation 2.1 for supporting evidence of 1-D physical processes employment. To compare horizontal and vertical advection fluxes, this study needs to quantify: (i) horizontal and vertical velocity (u_{adv} and w_{adv}); and (ii) derivative of phytoplankton (Chla), nitrate (NO_3) and salinity concentration along the channel ($\frac{\partial C}{\partial x}$) and depth ($\frac{\partial C}{\partial z}$).

Horizontal and vertical velocity. In estuarine circulation, conservation of mass requires water transported to upper layer equal to flow out, hence: $w \cdot B \cdot L = u \cdot B \cdot H$ or $w \cdot L = u \cdot H$ where u , w horizontal and vertical velocity, respectively, B is the channel width, and H is the upper layer thickness. The main basin Puget Sound length is around 26 km (*Winter et al.*, 1975; *Sutherland et al.*, 2011), and the thickness of upper layer is 50 m (*Cannon et al.*, 1983; *Babson et al.*, 2006). Hence, ratio of w and u is

$$\frac{w}{u} = \frac{H}{L} = 2 \times 10^{-3}$$

This ratio is similar to ratio of average upper layer horizontal and vertical advection obtained from *Winter et al.* (1975)'s figure 14.

x-derivative and z-derivative. Secondly, the gradient of phytoplankton, nitrate, and salinity along channel are performed on DoE and PRISM data sets. The gradient, c_{ij} between two adjacent stations of the same monitoring program is calculated as follow:

$$c_{ij} = \frac{|c_j - c_i|}{|x_j - x_i|}$$

where:

c_{ij} is gradient between two adjacent stations in the same monitoring program (e.g. PRISM or DoE). The c_{ij} is placed at position of station j after the calculation.

c_i, c_j monthly average measurements over upper-layer of a parameter at station i, j (e.g. salinity). The upper-layer (H_{ul} in Figure 2.2) is assumed to be 50 m thick (*Cannon et al.*, 1983; *Babson et al.*, 2006).

x_i, x_j : positions of station i, j in the main basin

The z-gradient of phytoplankton, nitrate and salinity at each station is a division of the difference between monthly average at surface and bottom of the upper layer by the upper layer depth (H_{ul}) (Figure 2.7). On average stations and time, x-variation of conservative tracer, salinity, is around 4×10^{-3} ($psu km^{-1}$), while non-conservative tracers, nitrate and Chla, are 5×10^{-2} ($\mu MN m^{-3} km^{-1}$) and 5×10^{-2} ($\mu g m^{-3} km^{-1}$) (Figure 2.6). Similarly, variation in z direction of salinity, nitrate and Chla are 5×10^1 ($psu km^{-1}$), 3×10^2 ($\mu MN m^{-3} km^{-1}$) and 4×10^2 ($\mu g m^{-3} km^{-1}$), respectively. Then, horizontal and vertical advection fluxes present in table 2.1.

	Salinity	Nitrate	Chla
$\frac{w_{adv}}{u_{adv}}$	2×10^{-3}	2×10^{-3}	2×10^{-3}
$\frac{\partial C}{\partial x}$	4×10^{-3}	5×10^{-2}	5×10^{-2}
$\frac{\partial C}{\partial z}$	5×10^1	3×10^2	4×10^2
$\frac{w_{adv} \frac{\partial C}{\partial z}}{u_{adv} \frac{\partial C}{\partial x}}$	25	12	16

Table 2.1: Comparison of horizontal and vertical advection fluxes

Table 2.1 shows that in the main basin Puget Sound vertical variation is more than 10 times larger than along channel variation. Along channel variation is therefore negligible in comparison to vertical variation.

Answering the questions outlined in section 1.4 requires a fast running test-bed, which allows intensive parameter investigation. Extensive searches through parameter spaces are needed for identification of a biological parameter set that is able to reproduce the observations. Several hydrodynamic models have been developed to describe Puget Sound estuarine circulation. However, higher hydrodynamic model resolution often comes with expensive computing cost and time. LiveOcean model, which is based on ROM model for ocean circulation, takes a day for a month simulation when running on a cluster of 196 computers (McCready, University of Washington, *pers. comm.*). Thus, due to the expensive cost of computing and time, fine resolution of existing hydrodynamic model are not suitable for extensive parameter space exploration. Given the success of *Winter et al. (1975)* on capturing phytoplankton dynamics and *Collins et al. (2009)* in defining the role of wind in the timing of the spring bloom in the Strait of Georgia by using 1-D physical model, and given the fact that variation of

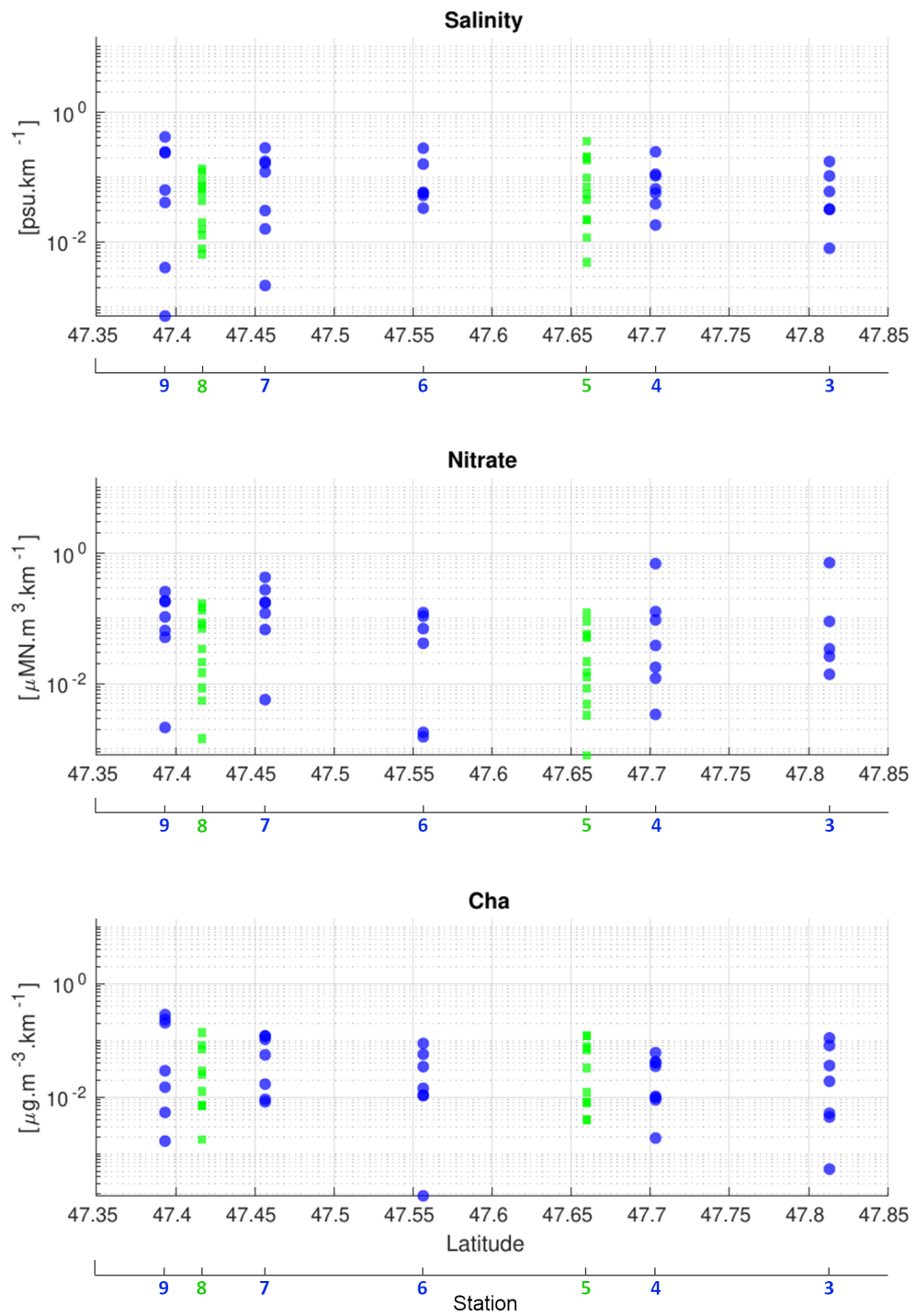


Figure 2.6: Gradient of salinity, nitrate and Chl a along main basin Puget Sound channel (green square: DoE stations, blue circle: PRISM stations)

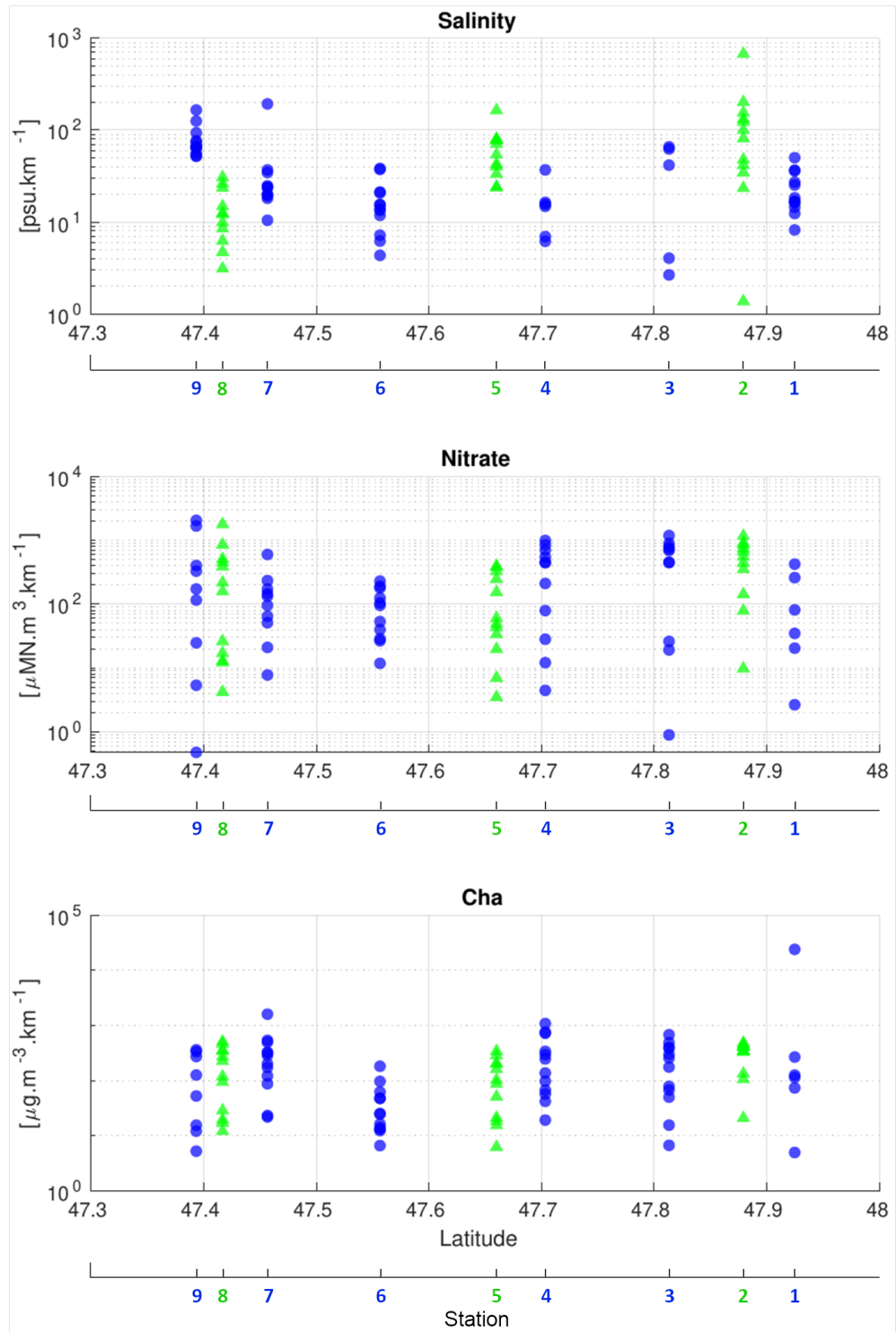


Figure 2.7: z-variation of salinity, nitrate and Chla at each station upper 50 m layer (green square: DoE stations, blue circle: PRISM stations)

phytoplankton, nitrate and salinity are small along the main basin channel, this study follows *Winter et al. (1975)* and *Collins et al. (2009)* to use 1-D physical model as the base for biological processes.

Study site

Although data sets from DoE and PRISM monitoring program have similar variables and sampling periods, PRISM sampled only in June and December, which makes it not suitable to capture bloom timings varying from March to May (*Winter et al., 1975; Newton and Van Voorhis, 2002*). Monthly basic sampling of DoE data set is therefore more appropriate for exploring phytoplankton spring bloom onsets and annual primary production. Among three stations of DoE, station number 2 and 8 (Figure 2.3) are near to sills at both ends, thus they are strongly affected by hydrodynamics caused by sills and can not be used to represent the hydrodynamic properties of the main basin Puget Sound. Hence, station number 5 positioned in middle main basin is most suitable for further investigation. In addition, station number 5 is close to this study site used in *Winter et al. (1975)* and is one of the stations in *Newton and Van Voorhis (2002)* study.

Vertical advection

In general, the vertical velocity associated with the estuarine circulation is zero at the surface, then increases with depth and reach its maximum at mid water column (e.g. the bottom of upper-layer H_{ul} as in figure 2.8a). After this point, vertical velocity decreases with depth until being zero again at the seabed (*Geyer and MacCready, 2014*). The maximum velocity at the mid water column is defined by solving the mass conservation equation.

The conservation of mass in case of incompressibility (i.e. density ρ =constant) is given as $\nabla \cdot \vec{u} = 0$ or

$$\frac{\partial u}{\partial x} + \frac{\partial v}{\partial y} + \frac{\partial w}{\partial z} = 0 \quad (2.2)$$

where u , v , w (ms^{-1}) are velocity in direction of x (along channel), y (cross channel), and z (water depth).

Taking integral both sides of equation 2.2 by variable y , where B is channel width, the equation 2.2 becomes

$$B \frac{\partial u}{\partial x} + [v_{leftshore} - v_{rightshore}] + B \frac{\partial w}{\partial z} = 0 \quad (2.3)$$

and again integral both sides of equation 2.3 with respect to z over H_{ul} depth

$$BH_{ul} \frac{\partial u}{\partial x} + Bw \Big|_{-H_{ul}}^0 = 0 \quad (2.4)$$

The equation 2.4 finally results in

$$\frac{\partial Q}{\partial x} = Bw_{[-H_{ul}]}$$

or

$$w_{[-H_{ul}]} = \frac{1}{B} \frac{\partial Q}{\partial x}$$

In the Main Basin Puget Sound, upper-layer H_{ul} is around 50 m (*Cannon et al.*, 1983; *Babson et al.*, 2006). The channel width B is about 5 km (*Winter et al.*, 1975). The yearly average difference of transported water in upper layer between cross sections MB_M and MB_S (Figure 2.1) was $3500 \text{ m}^3\text{s}^{-1}$ ($\Delta Q = 3500 \text{ m}^3\text{s}^{-1}$), and the distance between the two sections was 26 km ($L = 26 \text{ km}$) (*Sutherland et al.* (2011), figure 12). Hence, the vertical velocity at H_{ul} is $w_{[-H_{ul}]} = \Delta Q L^{-1} B^{-1} = 2.9 \times 10^{-05} \text{ ms}^{-1}$. In summary, the vertical velocity profile at station 5 is now 0 ms^{-1} at the surface and bottom, $2.9 \times 10^{-05} \text{ ms}^{-1}$ at around 50 m depth (Figure 2.8a). Stiff changes in vertical velocity often cause numerical issues (*Burchard et al.*, 2005) which affect model performance. Hence, to avoid model instability due to abrupt changes in vertical velocity, a polynomial fit is applied on the vertical velocity profile (Figure 2.8a) to

smooth the profile. The smoothed velocity profile is shown in figure 2.8b.

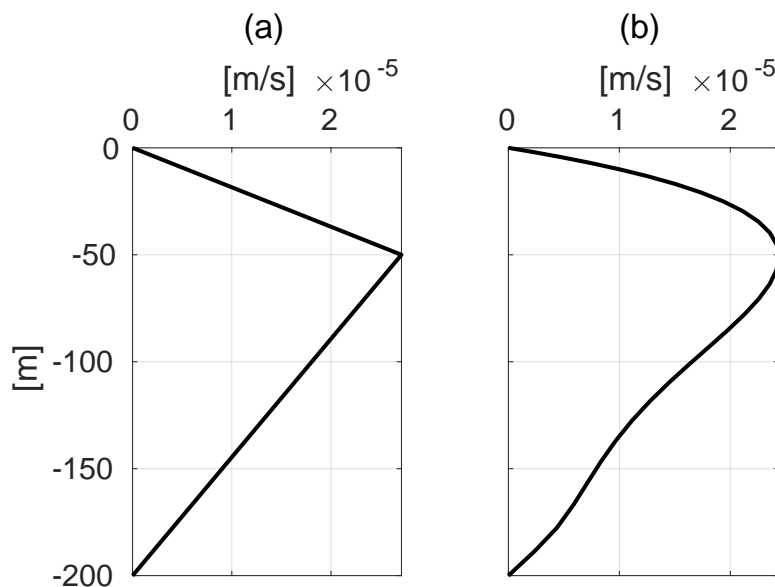


Figure 2.8: Yearly average vertical velocity profile calculated (a) and smoothed (b) in the main basin Puget Sound

Mixing

Next, the model requires a simple but realistic representation of mixing. The mixing process at station 5 is represented by mixing coefficient (or diffusive coefficient – κ_v), and is taken from output of Modeling the Salish Sea model (MoSSea, a predecessor to LiveOcean model). MoSSea created the first ever high-resolution, realistic hindcast simulations of the physical circulation in the entire Salish Sea region, whose details and extensive validation is documented in *Sutherland et al.* (2011) for year 2005 and 2006. For this study, κ_v in year 2006 is extracted hourly from the MoSSea model grid of width, depth and time. The hourly κ_v is tidally averaged by using 24-24-25 Godin filter before being daily averaged (*Garnier (2020), in preparation*). The daily and tidally averaged κ_v is then extracted at station 5 for this study. The κ_v is then organized against depth and days (figure 2.9). The yearly κ_v (blue line) and monthly (black circle) averages are similar during the months preceding spring blooms (February to April). Therefore, to be consistent with our use of yearly vertical advection profiles, this study employs

yearly average mixing profiles in 1-D physical model.

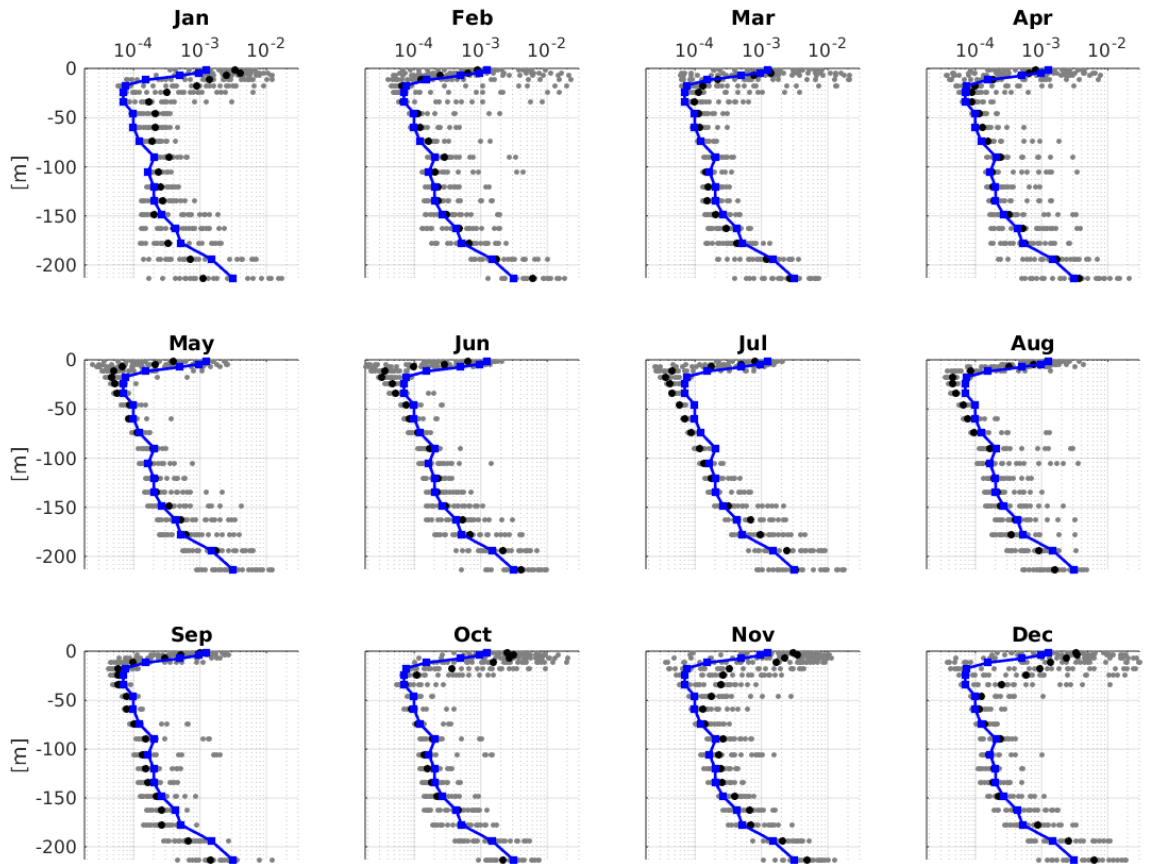


Figure 2.9: Diffusive coefficient κ_v (m^2s^{-1}) against depth [m], with gray circles for all daily data, black circles for monthly average at each depth, and blue square line yearly average at each depth

To implement vertical advection and mixing at station 5, the water column at station number 5 of roughly 200 metre deep is divided into thirty layers, with thinner layers near the surface and thicker layers at the bottom. The thinnest layer at the surface is around 2 metres, and the thickest layer at the bottom is around 11 metres. Vertical advection and mixing (Figure 2.8(b) and 2.9 – blue line) are linearly interpolated to the model grid. Within this grid, the model consists of a set of coupled ordinary differential equations, each one a component of the biological model, which will be shown in the

next section

$$\frac{dC}{dt} = [\text{biogeochemical processes}] + w_{adv} \frac{dC}{dz} + \frac{d}{dz} \left(\kappa_v \frac{dC}{dz} \right) \quad (2.5)$$

2.3.2 Biogeochemical model

To continue previous studies as well as to contribute to ongoing research on Puget Sound plankton, this study adopts *Davis et al.* (2014)'s biogeochemical model, which is currently incorporated in the 3-D model LiveOcean of Salish Sea, with Puget Sound included. The Puget Sound NPZD model (Figure 2.10) is slightly different from *Davis et al.* (2014) model in dividing the dissolved inorganic nutrient pool into nitrate (NO_3) and ammonium (NH_4) fractions (to match available observations) and omitting nutrient exchange flux to the bottom (benthic zone). Thus, the Puget Sound NPZD model includes 6 compartments, namely P (phytoplankton), MZ (microzooplankton), N (nutrient, which is divided in nitrate (NO_3) and ammonium (NH_4)), and detritus (D, includes large (LD) and small (SD)). All six stocks are measured in mmol nitrogen m^{-3} (or μMN). The model is in nitrogen-based unit as phytoplankton growth in Puget Sound is mainly limited by nitrogen compounds (e.g., nitrate, ammonium) and not by other nutrients (such as phosphate, silicate) (*Bernhard and Peele, 1997*). A system of ordinary differential equations (ODEs) for each compartments in the Puget Sound NPZD model is presented as following.

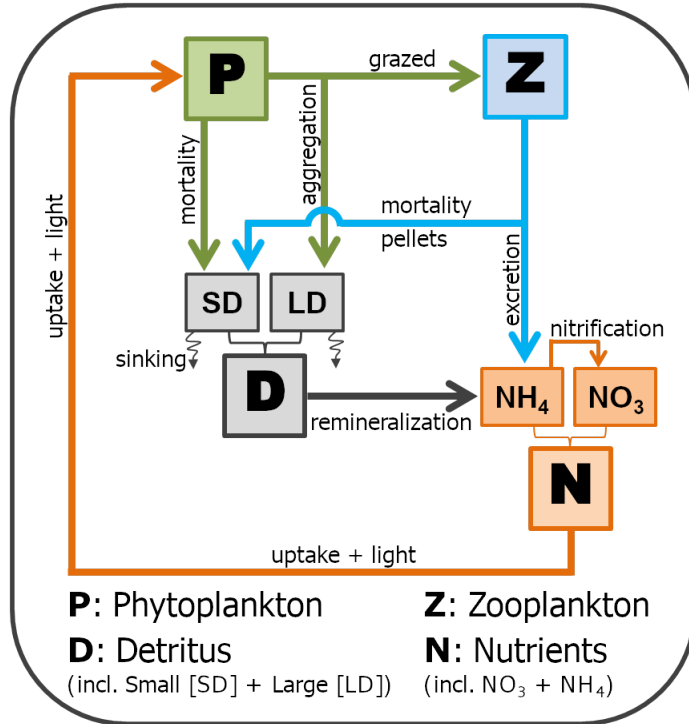


Figure 2.10: A diagram of NPZD model

P - Phytoplankton

Phytoplankton population dynamics are the result of a balance between growth and losses, and is influenced by physical (e.g. turbulence, wind, tide, light), chemical (e.g. nutrient), and biological (e.g. life cycle) variables (Cloern, 1996; Brussaard, 2004). Generally, reproduction strongly ties to irradiance, temperature, nutrient availability, and uptake of nutrient (Dortch, 1982; Dortch et al., 1984; Sommer, 1994; Tilman et al., 1981). Phytoplankton losses are commonly caused by natural mortality (or cell lysis), grazing by zooplankton, and transport (sinking and dispersion).

$$\frac{dP}{dt} = \mu(E, NO_3, NH_4)P - I(P)Z - m_P P - m_{agg} P^2 \quad (2.6)$$

where $\mu(E, NO_3, NH_4)$ [d^{-1}] is phytoplankton growth rate as a function of irradiance E , nitrate and ammonium; $I(P)$ [d^{-1}] is grazing rate by microzooplankton, m_P [d^{-1}] is natural mortality, and m_{agg} [d^{-1}] is aggregation rate.

Phytoplankton growth rate. The dependency of phytoplankton specific growth rate (μ) on different environmental variables (e.g. light (E), NO_3 or NH_4) is complicated and not fully understood. In many marine ecosystem models, phytoplankton growth rate is commonly expressed as function of light and nutrient. The two functions are similar in their characteristics, starting from zero (no light or no nutrients) and approaching saturation at some high light and at replete nutrient concentration. Three approaches are generally found in marine ecosystem models to limit algal growth by photosynthesis and nutrient uptake. The first is to apply Blackman’s law (Blackman, 1905), assuming that growth is reduced by the most limiting factor, either by light or by nutrient availability (e.g., Hurtt and Armstrong (1996); Oschlies and Garçon (1999); Klausmeier and Litchman (2001)). The second is to multiply both limitation functions (e.g., Evans and Parslow (1985); Fasham et al. (1990)). The third approach leads to more complex representations of growth limitation, as they account for interrelations between cellular C:N (or N:C) ratio, N-uptake and the photoacclimation state of the algae (e.g., Geider et al. (1998); Pahlow (2005); Armstrong (2006); Wirtz and Pahlow (2010)). Whether the first, second or third approach is considered, they can be expected to affect estimates of the associated parameter values. Following (Davis et al., 2014), the growth rate function in our model takes the form of multiplying both limitation functions.

$$\mu(E, NO_3, NH_4) = \mu_0 \left(\frac{N_{tot}}{k_{min} + 2\sqrt{k_{min}N_{tot}} + N_{tot}} \right) \left(\frac{\alpha E}{\sqrt{\alpha^2 E^2 + \mu_0^2}} \right) \quad (2.7)$$

where μ_0 [d^{-1}] is maximum growth rate of phytoplankton and is often treated as constant in the model, N_{tot} [μMN] is total effective nutrient, k_{min} [μMN] is minimum half-saturation for nutrient uptake (Optimal uptake model, Smith et al. (2009)). Smith et al. (2009) developed the optimal uptake kinetics to explain variations of half-saturation constant in Michaelis – Menten nutrient uptake equation, which enables models ability to predict the response of marine ecosystems to changes in environmental conditions. Optimal uptake kinetics assumes a physiological trade-off between the efficiency of nutrient encounter at the cell surface, and the maximum rate at which a nutrient can be

assimilated. The key idea is that phytoplankton alter the number of their surface uptake sites, which determine the nutrient encounter time scale, versus internal enzymes, which assimilate the nutrients once encountered (*Smith et al.*, 2009). $\alpha [(Wm^{-2})^{-1}d^{-1}]$ is initial growth-light slope, $E [Wm^{-2}]$ is photosynthetically active radiation (PAR). The first bracket of equation 2.7 express nutrient limitation, while the second represents light limitation.

Total effective nutrient – N_{tot} . The inhibition of nitrate (NO_3) uptake by presence of ammonium (NH_4) is widely known, although the mechanisms behind this $NO_3 - NH_4$ interaction remains still unclear (*Dortch*, 1990). The simplistic view that nitrate uptake is reduced to zero if ammonium exceeds 1 μMN would often result in large underestimates of nitrate uptake and new production (*Dortch*, 1990). Hence, here we do not use threshold on NO_3 uptake in the presence of NH_4 but instead introducing a weight (φ_{NH_4}) on NH_4 to take into account the fact that nitrate is uptaken more slowly in the presence of ammonium (NH_4). Thus, the total effective nutrient is N_{tot} (where $N_{tot} = NO_3 + \varphi_{NH_4}NH_4$). The value of φ_{NH_4} ($\varphi_{NH_4} = 2$) is picked as an analogy with a common formulation of grazing on multiple prey types (*Gentleman et al.*, 2003; *Banas et al.*, 2016).

Minimum half-saturation for nutrient uptake – k_{min} . Recent NO_3 uptake kinetic experiments over the range of ambient NO_3 concentrations showed that half-saturation rate varies with nutrient concentration, for example, half-saturation rate is actually higher in open ocean (poor nutrient), and lower in coastal estuarine water or autotrophic water (rich nutrient) (*Laws*, 2013). Thus, the application of the classical kinetics formula of Michaelis-Menten with half saturation rate independent of environmental nutrient concentration seems to underestimate phytoplankton growth under nutrient transient condition (*Flynn*, 2003; *Smith et al.*, 2009, 2014, 2015; *Franks*, 2009). The use of k_{min} (*Smith et al.*, 2009) is one way to overcome the drawback of the Michaelis-Menten classical kinetics form in nutrient changing conditions. $k_{min} + 2\sqrt{k_{min}N_{tot}}$ in equation 2.7 plays role of half-saturation rate in Michaelis-Menten model, which results

in similar growth rate to Michaelis-Menten model when nutrient is abundant and larger when nutrient is low (*Smith et al.*, 2009; *Bonachela et al.*, 2011). As nutrient levels in surface layer of Puget Sound change during the year (e.g. high in winter and low in summer) the use of k_{min} is more appropriate. Based on experimental data and *Smith et al.* (2009)'s model, *Davis et al.* (2014) found $k_{min} = 0.1$ (μMN).

Light limitation. Light limitation is caused by light level and mixing. Light level directly affects the photosynthesis, while effects of mixing is indirectly affected through controlling light level phytoplankton receive by maintaining depth within or outwith well-lit zone. Effect of mixing on the amount of light that phytoplankton is exposed to is taken into account by vertical mixing when coupled to physical model (Equation 2.5). Following mainly focus on light level in relation to phytoplankton photosynthesis.

Photosynthesis effectiveness is expressed by photosynthetic efficiency, or α ($(Wm^{-2})^{-1}d^{-1}$) which is derived from photosynthesis–irradiance (P-I curve) measurements (*Platt and Jassby*, 1976; *Peterson et al.*, 1987; *Platt et al.*, 1992). Measurements of α are typically normalised to Chla concentrations (*Schartau et al.*, 2017). α is often taken as constant in many nitrogen-based model (e.g., *Fasham et al.* (1990); *Sarmiento et al.* (1993); *Doney et al.* (1996); *Gunson et al.* (1999)), although it is known to be sensitive to species due to difference in phytoplankton's cellular Chla content, as well as intracellular photoacclimation (*Slougher et al.*, 2019). Values of α were found to vary by a factor of three (*Côté and Platt*, 1983) during a three month period, which can be attributed to changes in phytoplankton community structure as well as to photoacclimation. *Platt and Jassby* (1976) reported an even larger range over a one year period, from 0.03 to 0.63 mgC ($mgChla$) $^{-1}h^{-1}W^{-1}m^2$ within the upper ten metres.

E is photosynthetically active radiation (PAR), and is a function of depth z , PAR at water surface (PAR_0), and light attenuation in the water column (Equation 2.8 (*Davis et al.*, 2014)). Light attenuation, in turn, depends on various water optical properties, which are commonly influenced by water molecules (att_{bg}), rivers (att_{fw})

and self-shading by phytoplankton (att_P).

$$E(z) = E_0 \exp\left(-\left(att_{bg}z + att_{fw} \int_z^{surface} (Salinity(z') - 32) dz' + att_P \int_z^{surface} P(z') dz'\right)\right) \quad (2.8)$$

where E_z is PAR at depth z , E_0 is PAR at surface, att_{bg} is light attenuation caused by optical properties of a water column itself which accounts for changes in quantity and quality of light at increasing depth (*Cushing and Walsh, 1976*), att_{fw} presents light attenuation caused by turbidity and CDOM from river inputs. Salinity is also often used as a proxy of turbidity. Here, effects of rivers on optical properties of the water column is quantified by the salinity difference between Puget Sound salinity observations (i.e., $(Salinity(z'))$ and oceanic salinity level (at 32 psu, *Davis et al. (2014)*). Finally, att_P is self-shading by phytoplankton growing in a water column.

Phytoplankton loss. Phytoplankton losses are commonly caused by natural mortality, zooplankton grazing, and aggregation, which later are brought to the bottom of the sea. In most models, natural phytoplankton mortality and aggregation are directly proportional to phytoplankton population. Here, natural mortality loss shows a linear relationship, while aggregation follows a quadratic form. *Sheldon et al. (1972)*, a first approximation of the world's ocean particle size distribution, showed that the distribution were well described by a power law (*Burd and Jackson, 2009*). The factors regulating aggregation are still unclear, however, according to coagulation theory, aggregation of phytoplankton results from the repetitive collision of cells and their subsequent attachment to form larger aggregates (*Ackleh et al., 1994; El Saadi and Arino, 2006*). The quadratic form chosen in this study allows rapid aggregation when a bloom happens. Phytoplankton grazed by microzooplankton depends on the grazing rate, which is represented in a number of functional forms (e.g., *Ivlev (1955); Mayzaud and Poulet (1978); Holling (1959)*). These functional responses have a large influence on modelled dynamics (*Holling, 1965*). Among these forms, the Holling Type 3 lets the

model reach a stable steady state for a wide range of parameter values (*Gentleman and Neuheimer, 2008*) and allows microzooplankton to keep up with increasing of phytoplankton when it blooms. Thus, a sigmoidal Holling type 3 (equation 2.9) was used in the model.

$$I(P) = I_0 \frac{P^2}{K_0^2 + P^2} \quad (2.9)$$

where I_0 (d^{-1}) is microzooplankton maximum ingestion rate, K_0 is microzooplankton grazing half-saturation [μMN].

MZ - Microzooplankton

Microzooplankton population is governed by assimilation rate (ϵ) over food obtained from phytoplankton by grazing (equation 2.9), mortality rate (m_{MZ}) (grazed by other predators or natural mortality).

$$\frac{dMZ}{dt} = \epsilon I(P)MZ - m_{MZ}MZ^2 \quad (2.10)$$

where ϵ is gross growth efficiency, which presents the efficiency of food utilization to growth (after taken out metabolic losses or respiration), and m_{MZ} is mortality rate. The mortality followed a quadratic form, as the damping effect of a quadratic form allows the predators' clearance rates to increase when microzooplankton biomass increases, thereby enabling the predators to rapidly respond to any changes in microzooplankton in an analogous manner to what was mentioned above for microzooplankton feeding on phytoplankton (*Gentleman and Neuheimer, 2008*).

D - Detritus: small (SD) and large (LD)

The detritus compartment is divided into small and large detritus. Small detritus is defined as comprising dead phytoplankton and microzooplankton and fecal materials, while large detritus consists of phytoplankton aggregation. Detritus is then recycled to ammonium through a remineralization process. Detrital sinking is modelled by

specifying simple sinking rates, and is exported to the seabed.

$$\frac{dSD}{dt} = (1 - \epsilon)(1 - f_{ex})I(P)MZ + m_P P + m_{MZ} MZ^2 - r_{remin} SD + w_{sSD} \frac{dSD}{dz} \quad (2.11)$$

$$\frac{dLD}{dt} = m_{agg} P^2 - r_{remin} LD + w_{sLD} \frac{dLD}{dz} \quad (2.12)$$

where f_{ex} fraction of grazing excreted to NH_4 , r_{remin} (d^{-1}) detrital remineralization rate, w_{sSD} (ms^{-1}) and w_{sLD} (ms^{-1}) are small and large detritus sinking rate, respectively.

N - Nutrients: ammonium (NH_4) and nitrate (NO_3)

The nutrient pool includes ammonia and nitrate compartment. Ammonia is built up by excretion from microzooplankton and remineralization of small and large detritus. Ammonium loss happens through two processes, one is nitrification, which transforms ammonium to nitrate; and another is uptake, in which phytoplankton utilize ammonium for photosynthesis. The nitrate gain is mainly through nitrification of ammonium, and loss through uptaken by phytoplankton.

$$\begin{aligned} \frac{dNH_4}{dt} = & (1 - \epsilon)f_{ex}I(P)MZ + r_{remin}(SD + LD) - \frac{\varphi_{NH_4}NH_4}{N_{tot}}\mu(E, NO_3, NH_4)P \\ & - r_{nitr}NH_4 \end{aligned} \quad (2.13)$$

$$\frac{dNO_3}{dt} = r_{nitr}NH_4 - \frac{NO_3}{N_{tot}}\mu(E, NO_3, NH_4)P \quad (2.14)$$

where r_{nitr} (d^{-1}) is nitrification rate.

2.4 Conclusions

This chapter introduced over 20-year data sets from 3 monitoring programs – Department of Ecology (DoE), King County (KC), and Puget Sound Regional Synthesis Model Program (PRISM) (Figure 2.3). From data coverage analysis (Figure 2.4 and 2.5), KC data set is not suitable for the purpose of this study – exploring climate-linked drivers and pathways that drive phytoplankton bloom – due to infrequent sampling, and limited number of variables; PRISM data set might provide useful information on hydrodynamic processes as a result of measuring physical variables along Puget Sound channel; and DoE data set is the most appropriate for this study purposes given its sampling frequency, biological and physical variables measured, even though the monthly sampling might easily miss a bloom. High-resolution Chla observations from an ORCA buoy deployed in the Main Basin Puget Sound (https://nwem.apl.washington.edu/about_proj_ORCA.shtml) would be capable of accurately capturing spring blooms. However, the ORCA Chla time series are only available for few years (e.g., 2011). Thus, the ORCA data is not yet useful to this study.

Further analysis on DoE and PRISM data sets demonstrated that variation of Chla, nitrate and salinity concentration along the main basin channel is insignificant (Figure 2.6). The minor change in tracer (salinity, phytoplankton, nitrate) gradient along the Main Basin Puget Sound channel invited this study approximating tracer budgets as a vertical balance by a yearly average vertical advection and mixing (Figure 2.8 and 2.9). The 1-D physical model of Puget Sound phytoplankton model, PS-1D, forms a base for a fast-running test-bed, which allows extensive exploration of parameter spaces as well as investigation into the climate-linked drivers and pathways which govern the Puget Sound phytoplankton bloom (Chapter 5 – 6).

Biological processes around phytoplankton of the PS-1D is mostly based on *Davis et al.* (2014) biological model with adjustments on benthic fluxes (i.e., omitting nutrient exchange flux to the seabed) and dividing the dissolved inorganic nutrient pool in to nitrate and ammonium. This study follows *Davis et al.* (2014) model as it currently

is incorporated in 3-D LiveOcean model, which predicts biophysical characteristics (e.g., nitrate, phytoplankton, zooplankton concentration) for the entire Salish Sea, which includes Puget Sound. In addition to gaining an understanding of Puget Sound phytoplankton bloom dynamics, this study also expects to improve the performance of the biological part in the LiveOcean model, i.e., by proposing parameters values, and/or biological processes that might need to be adjusted. Thus, a biological model close to the one in 3-D LiveOcean, or *Davis et al.* (2014) model, would be applicable in the context of ongoing Puget Sound phytoplankton study.

In the following chapter, we will examine the performance of *Davis et al.* (2014) parameters in the PS-1D model to diagnose potential parameters and/or processes that would need to change to improve the model goodness-of-fit.

Chapter 3

Exploration of a PS–1D model baseline

This chapter describes configuration on parameter values, initial and boundary conditions, and validation data for the PS-1D model (Section 3.1). The model performance against observations is assessed by index of agreement Willmott Skill Score (WSS), which is detailed in Section 3.2. The model is then executed, and preliminary results of the model are presented in Section 3.3. Finally, discussions and conclusions are given in section 3.4.

3.1 Model configuration

3.1.1 PS-1D parameters values

The PS-1D model uses a parameter set from (*Davis et al.*, 2014) (Table 3.1) as a starting point to examine the PS-1D model performance to identify possible parameters and processes that are likely to improve the model goodness-of-fit.

3.1.2 Initial, boundary conditions and forcings

Observations from Department of Ecology (DoE) (Section 2.2) in December are extracted for the PS-1D initial and boundary conditions. The study takes observations

Parameter	Description	Unit	Values
μ_0	Maximum P growth rate	day^{-1}	1.7
k_{min}	Minimum half-saturation for NO_3	μMN	0.1
α	Initial growth-light slope	$(Wm^{-2})^{-1}d^{-1}$	0.07
φ_{NH_4}	Preference for NH_4		2
att_{bg}	Light attenuation by water column	m^{-1}	0.05
att_{fw}	Light attenuation by fresh water	$m^{-1}psu^{-1}$	-0.0065
att_p	Light attenuation by phytoplankton	$m^{-1}\mu MN^{-1}$	0.03
mp	Phytoplankton mortality	day^{-1}	0.1
m_{agg}	Phytoplankton loss via aggregation	$(\mu MN)^{-1}d^{-1}$	0.05
r_Chla_N	Chla to nitrogen ratio	$mg\ Chla\ (mmolN)^{-1}$	2.5
I_0	Microzooplankton maximum ingestion rate		4.8
K_0	Microzooplankton grazing half-saturation	μMN	3
ϵ	Microzooplankton growth efficiency		0.3
mMZ	Microzooplankton mortality	day^{-1}	2
f_{ex}	Fraction of grazing excreted to NH_4		0.5
r_{remin}	Detrital remineralisation rate	day^{-1}	0.1
w_{sSD}	Small detritus sinking rate	$m\ d^{-1}$	8
w_{sLD}	Large detritus sinking rate	$m\ d^{-1}$	80
r_{nitr}	Nitrification rate		0.1
κ_v	Diffusion coefficient	$m^2\ s^{-1}$	MoSSea model (section 2.3.1)
w_{adv}	Vertical advection velocity maximum at the interface of upper and bottom layer	$m\ s^{-1}$	2.9×10^{-05} (section 2.3.1)

Table 3.1: The PS-1D parameters values, which are taken from *Davis et al. (2014)* study of the outer coast (excludes κ_v and w_{adv}). $\mu MN = mmol\ nitrogen\ m^{-3}$.

in December as the water column is often homogeneous at this time of the year. Field observations of Chla (generally assumed to represent the phytoplankton standing stock and compared to the model phytoplankton), NO_3 , and NH_4 in December are averaged out at each sampling depth to get vertical profiles, and used as initial conditions for the PS-1D model (Figure 3.1). These profiles are then linearly interpolated into the model grid (as in section 2.3.1). Chla observational profile is in $\mu g/L$ which is not in the same unit of phytoplankton compartment (μMN) in the model. Hence, a conversion factor is needed to convert between $\mu g/L$ and μMN . The conversion from Chla ($\mu g/L$) to phytoplankton (μMN) and vice versa is problematic, since the intracellular ratios of Chla to nitrogen are known to vary considerably (*Yentsch and Vaccaro, 1958*). The ratio varies not only for different species but also due to changes in environmental conditions, e.g., differences in the ambient nutrient or light climate (*Yentsch and Vaccaro, 1958*). Thus, many studies rely on a constant average conversion ratio. Here, the PS-1D model adopts `r_Chla_N` value suggested by *Davis et al. (2014)* (table 3.1).

It is a common assumption that the number of microzooplankton is relatively low in winter in Puget Sound, as their preys (phytoplankton) grow marginally. Hence, microzooplankton is set as constant for the whole water column at a value of 0.001 (μMN). Similarly, detritus is considered close to zero in winter, thus the initial condition of both small and large detritus are set at 0 (μMN).

In the Main Basin Puget Sound, nutrient-uptake measurements showed no dependence on nitrate in the observed range 7 – 33 μMN (*Collias and Lincoln, 1977*). Summer surface-layer nitrate concentrations are reported usually $> 10 \mu MN$, but briefly and occasionally dip to 1 – 5 μMN (*Winter et al., 1975; Collias and Lincoln, 1977*), while average nitrate in winter observations, the highest level of the year, is around 27.5 μMN (Figure 3.1). Thus, the nitrate level in the main basin Puget Sound does not seem to affect nutrient-uptake. Therefore, the study sets nitrate boundary condition at its level in winter of 27.5 (μMN).

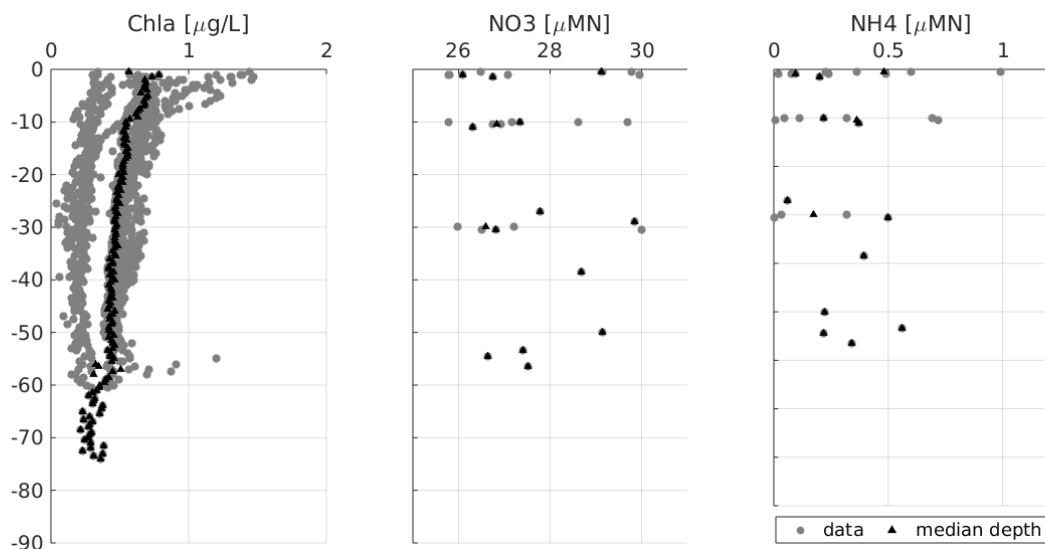


Figure 3.1: Initial values of Chla, NO₃, and NH₄ as median (black triangles) of December observations (gray points) (Data source: DoE)

Apart from external forcings of vertical advection and mixing in 1-D physical model, light and salinity forcings are needed for light function in phytoplankton equation. This study does not have measured data on light, thus this study takes a comparable model output, downward shortwave radiation (SWdown) from MoSSea model in year 2005 – 2006, for light forcings. SWdown time series is extracted hourly from the MoSSea model grid and only at the surface. The SWdown time series is tidally averaged using 24-24-25 Godin filter (*Garnier (2020), in preparation*). The SWdown is then taken around this study site, hours with zeros are subtracted from the rest of the day and remaining hours are averaged out over the day. SWdown at this study site is then converted to photosynthetically active radiation (PAR) using result of *Papaioannou et al. (1993)*, where it approximated that half of the total SWdown is PAR. To convert between energy (Wm^{-2}) and number of photons ($\mu Ein m^{-2} s^{-1}$), a conversion factor for the average energy for PAR wavelengths ($4.6 \mu Ein J^{-1}$) was applied (Equation 3.1). Figure 3.2 shows PAR calculated from SWdown following equation 3.1. The PS-1D models were run with typical year PAR data (Figure 3.2) and climatological year (or an artificially smoothed curve) result in just 3 day difference in bloom date (results

are not shown here), thus the typical year of PAR data is used as light forcing for the PS-1D model.

$$PAR = 0.5 * SW_{down} * 4.6 \quad (3.1)$$

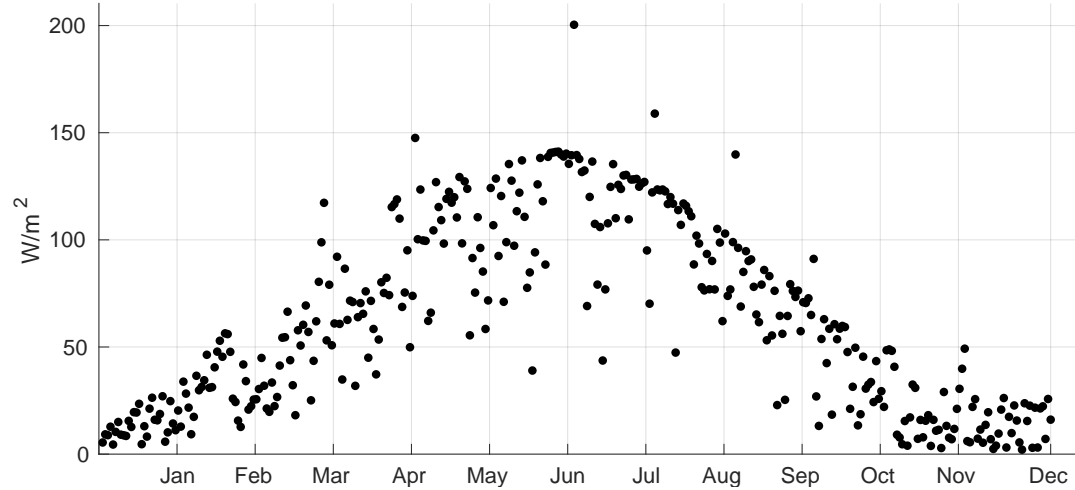


Figure 3.2: Photosynthetically active radiation (PAR_0) of a typical year. PAR_0 is calculated from SW_{down} output of MoSSea model

Although field observations of salinity were available, combining salinity observations over 22 years of sampling does not cover a full year of data (Figure 3.3). High interannual variation in salinity observations makes it not straightforward to use these data as forcing. Here, this study chooses to use salinity from MoSSea model output (Figure 3.3) for the forcing, as modelled salinity considerably reflects its observations over upper 30 m, the layer which comprises most of phytoplankton biomass (see Figure 3.4). There is certain bias in salinity range between model and observations (e.g., cumulative plots of Figure 3.3). However, the bias is mostly due to high values of salinity in bottom layer (e.g., below 50 m depth). In addition, salinity forcing taken from MoSSea model is consistent with vertical mixing and advection, light forcings which are also extracted from MoSSea model.

The model was run with 2 time steps: the physical time step is a day, and the biological time step is around 30 minutes (0.02 d , or 50 biological steps per physical

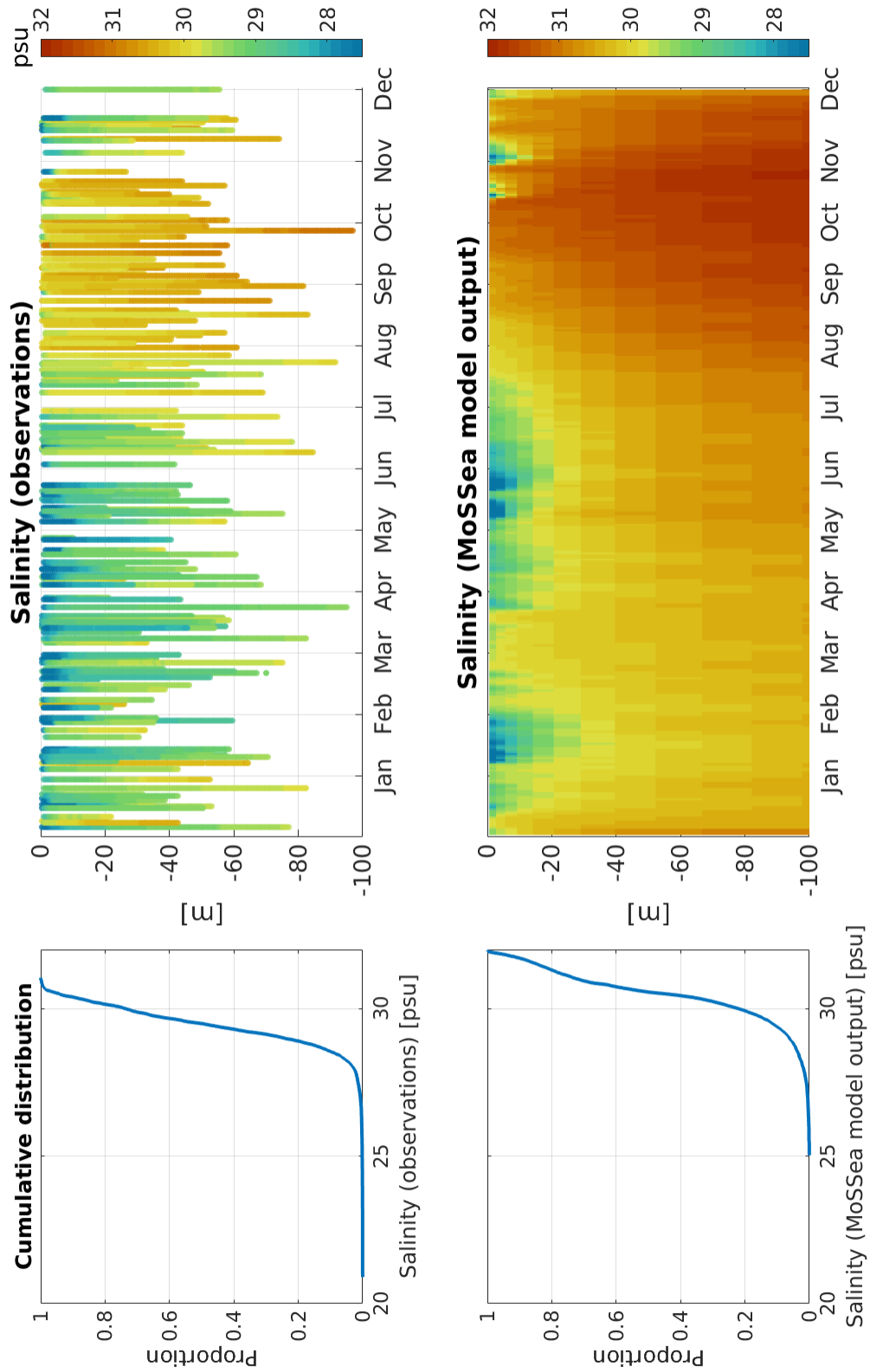


Figure 3.3: Salinity from observation and model output against depth and year day

step). Two different time steps are used as phytoplankton life cycle (days) is shorter than the estuarine circulation cycle (months). The state variables (N, P, Z, D) are saved in day interval.

3.1.3 Validation data

Observations of Chla, NO_3 , and NH_4 (Figure 3.4 to 3.7) from Department of Ecology (DoE) monitoring program at station 5 are used to validate the PS-1D model performance. The 22-year sampling data of DoE are folded on top of each other to yield an annual cycle of Chla, NO_3 , and NH_4 . The Chla annual cycle comprises roughly 160 profiles, while NO_3 and NH_4 have 130 profiles each (Figure 3.4). Figure 3.5 to 3.7 are produced from figure 3.4 by taking the daily average of integrated Chla, NO_3 , and NH_4 over euphotic depth. The euphotic depth, the layer in which photosynthesis is active, at station 5 reported a range from around 8 m to 46 m depth (*Newton and Van Voorhis, 2002*), while *Khangaonkar et al. (2012)* reported photosynthetically active layer varies between 5 – 20 m in thickness. Here, this study defines euphotic depth by taking a value at 90 percentile of euphotic depths given in *Newton and Van Voorhis (2002)*, which is around 30 m depth.

Observational data showed that Chla concentration is rarely over $15 (\mu gL^{-1})$ (Figure 3.4 and 3.5) which was also observed in (*Winter et al., 1975*). Thus, magnitude of spring blooms seem fundamentally unchanged in main basin Puget Sound since *Winter et al. (1975)* study. According to observations, phytoplankton growing season is between the months of April to September. The growing season is characterized by an intensive spring bloom, followed by a distinct low in production, then subsequent summer and fall blooms. The spring bloom often appears in early May and ceases around the end of July although early spring bloom onsets are also noticed in March and April or even in February in several years. However, it is worth noting that monthly sampling might easily miss a bloom. Thus, the picture of phytoplankton bloom dynamics might slightly differ from what is described here. NO_3 data shows a sharp decline from around 30 (μMN) to 10 (μMN) in May, which responds to observed intensive spring blooms of

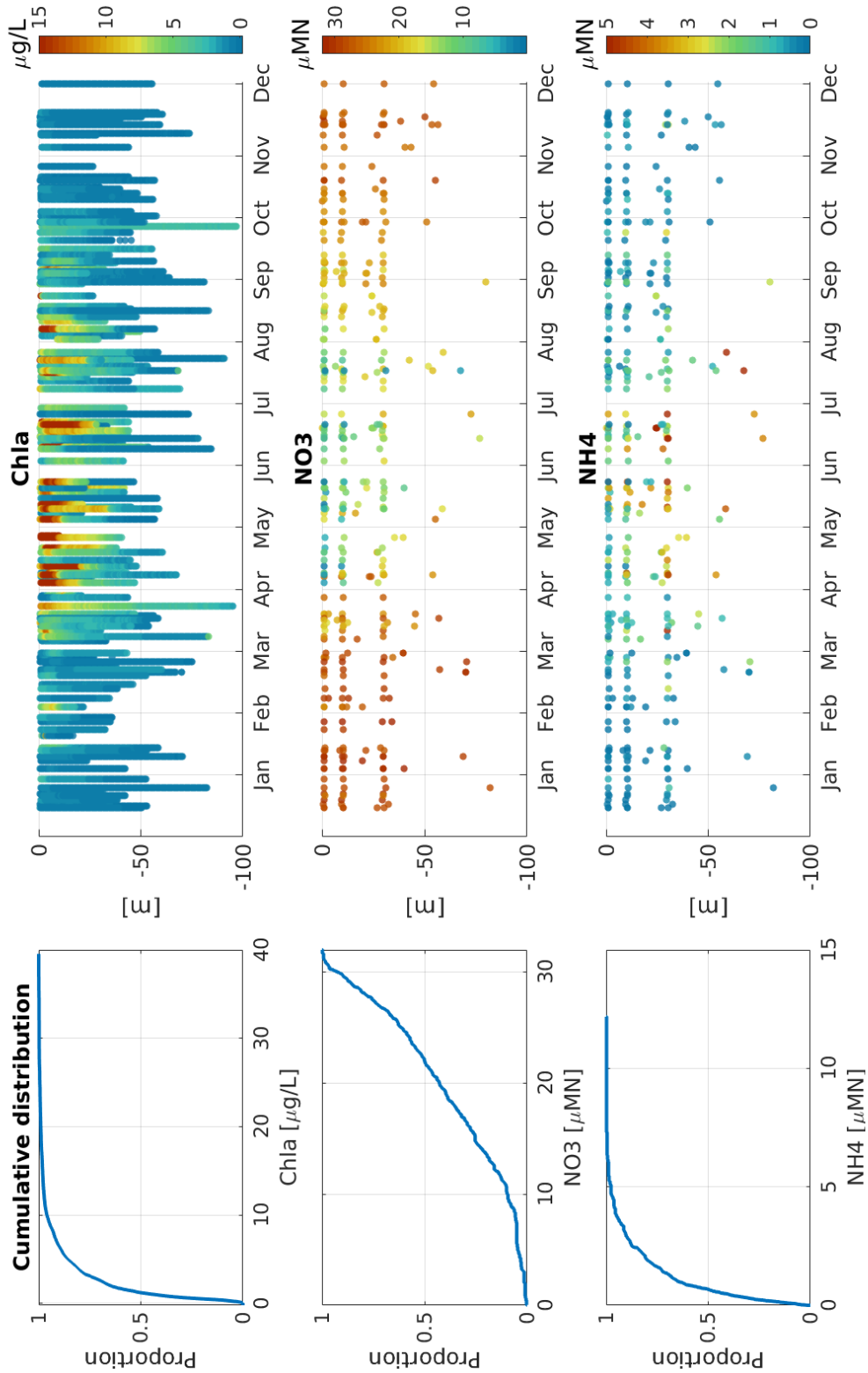


Figure 3.4: Chla, nitrate, and ammonium observation from DoE cruise at station 5 in main basin Puget Sound. Appropriate 160 profiles over 17 years for Chla, and 130 profiles for each nitrate and ammonium

phytoplankton. NO_3 is then kept at this level or below during period of May – July, while NH_4 increase. This reflects the regeneration of nutrient in euphotic zone, and this source of nutrient (NH_4) seems to keep supporting the phytoplankton population during bloom period.

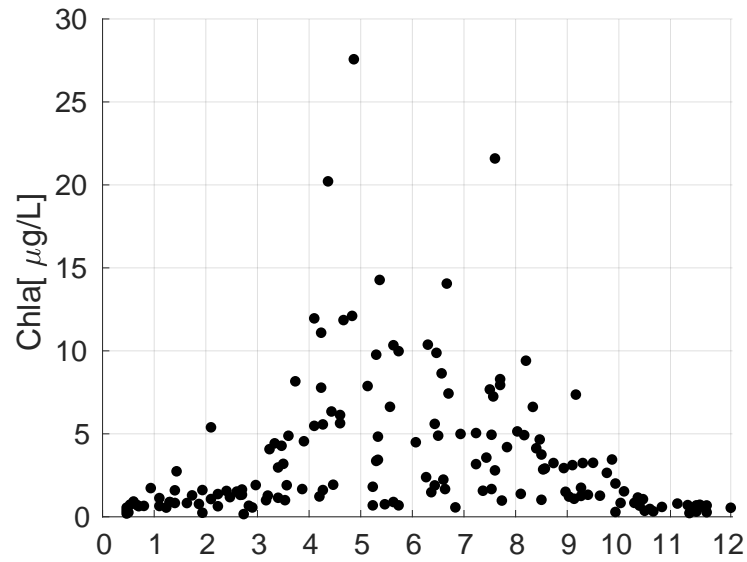


Figure 3.5: Daily average of integrated Chl a over euphotic depth (from surface to 30 m depth)

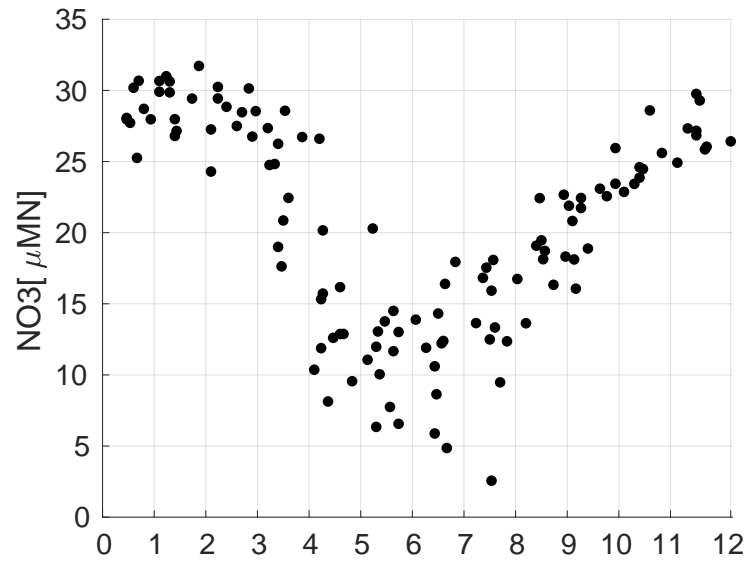


Figure 3.6: Daily average of integrated NO_3 over euphotic depth (from surface to 30 m depth)

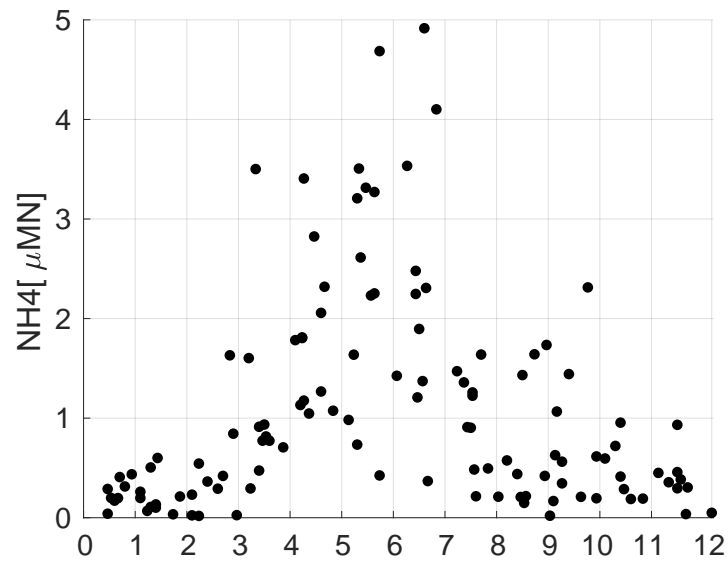


Figure 3.7: Daily average of integrated NH_4 over euphotic depth (from surface to 30 m depth)

3.2 Model skill assessment

Model performance can be qualified in a number of ways such as univariate, multivariate comparison of predictions and observations, multivariate pattern evaluation, and binary discriminator tests (*Stow et al.*, 2009; *Gregg et al.*, 2009). Here, to assess the PS-1D model performance, this study uses Willmott skill score (WSS) (*Willmott*, 1981) as an index of agreement. In addition to WSS mean square error (WSS_MSE , equation 3.2), which was used in *Davis et al.* (2014), this study examines the usage of WSS mean absolute error (WSS_MAE , equation 3.3), a refinement of WSS_MSE (*Willmott et al.*, 2012). Both WSS_MSE and WSS_MAE range from 0 to 1, with values close to 1 indicating a close match between model predictions and observations. *Willmott et al.* (2012) recognized that WSS_MSE can be dominated by a small proportion of extreme values due to squaring the errors, prior to summing. Indeed, larger errors, when squared, over-weighted the influence of those errors on the sum-of-squared error, which resulted in WSS_MSE approaching 1 (good fit) faster. The WSS_MAE was considered to be able to overcome the problem in WSS_MSE (*Willmott et al.*, 2012).

$$WSS_MSE = 1 - \frac{\frac{1}{N} \sum_{i=1}^{i=N} (m_i - o_i)^2}{\frac{1}{N} \sum_{i=1}^{i=N} (|m_i - \bar{o}| + |o_i - \bar{o}|)^2} = 1 - \frac{MSE}{\frac{1}{N} \sum_{i=1}^{i=N} (|m_i - \bar{o}| + |o_i - \bar{o}|)^2} \quad (3.2)$$

$$WSS_MAE = 1 - \frac{\frac{1}{N} \sum_{i=1}^{i=N} |m_i - o_i|}{\frac{1}{N} \sum_{i=1}^{i=N} (|m_i - \bar{o}| + |o_i - \bar{o}|)} = 1 - \frac{MAE}{\frac{1}{N} \sum_{i=1}^{i=N} (|m_i - \bar{o}| + |o_i - \bar{o}|)} \quad (3.3)$$

where m is model output, o is observation, N is number of pair of model–observation, and \bar{o} is observations averaged.

3.3 Results

The PS-1D model with initial, boundary conditions, time step described above and parameters given in table 3.1 (or parameters from *Davis et al.* (2014) study) is run for

a period of 25 months starting in December. The first 13 months (December and the following year) is discarded as spin-up. Trial model runs (not shown here) show that the model is stable and repeats its annual cycle after 3 months. Thus, a model over a period of 25 months with 13 month spin-up is appropriate to obtain an annual cycle of phytoplankton. The model outputs (phytoplankton biomass, NO_3 , and NH_4) of the last year are taken out for validation. Phytoplankton biomass (μMN) is converted to Chla ($\mu g L^{-1}$) by conversion factor `r_Chla_N` before further calculation.

Model outputs of Chla, NO_3 , NH_4 are plotted against depth and time in the same way as observations (figure 3.8). The figure shows model outputs and observation from surface to 50 m depth as most phytoplankton growth happens in the top 30 m layer (see section 3.1.3), and below 50 m depth concentration of Chla, NO_3 , and NH_4 vary insignificantly with depth. The model shows spring bloom onset in late January which lasts until November. This does not agree well with observations. Also, NH_4 does not show an increase in concentration during summer as observed in observations. Although NO_3 from model shows a decline in summer, the period of NO_3 shortage seems longer than observed. Daily average of integrated over euphotic zone (layer of 30 m thickness) of model outputs of Chla, NO_3 , and NH_4 (Figure 3.9 to 3.11) also show a weak agreement between model and observations. For example, timing and magnitude of the bloom are not well captured in the model, also summer NO_3 minimum and NH_4 maximum are not reproduced.

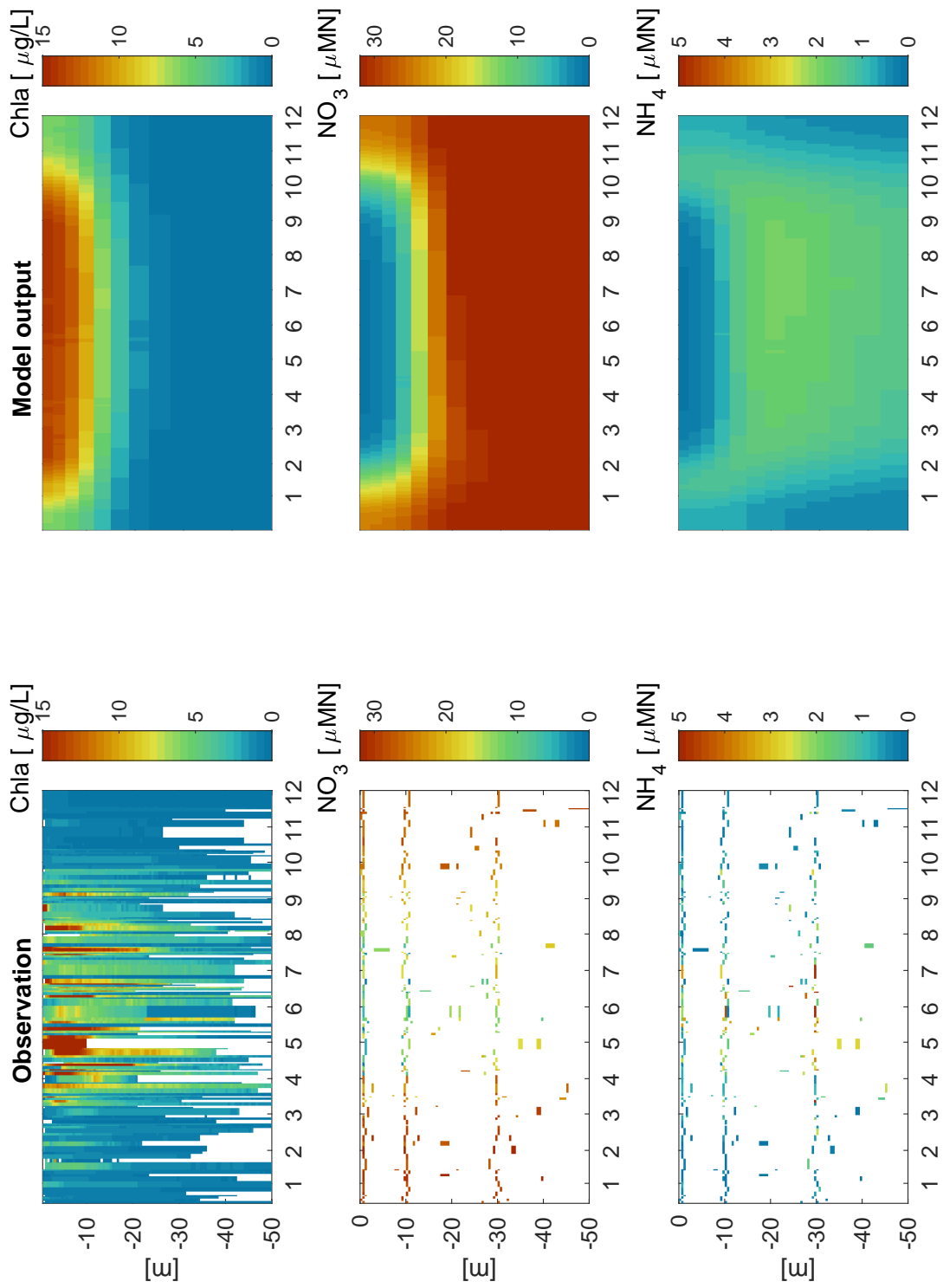


Figure 3.8: Observations (left, same as Figure 3.4) and the PS-1D model outputs (right) of Chla, NO_3 and NH_4 against time and depth

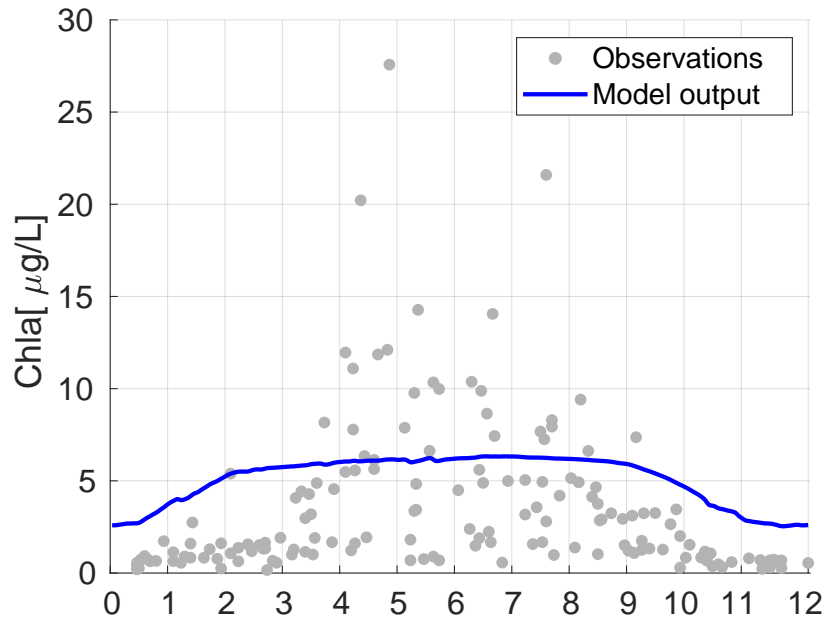


Figure 3.9: Daily average integral of Chl_a over the upper layer of 30 m depth. The PS-1D model run with *Davis et al.* (2014) parameters of the outer coast

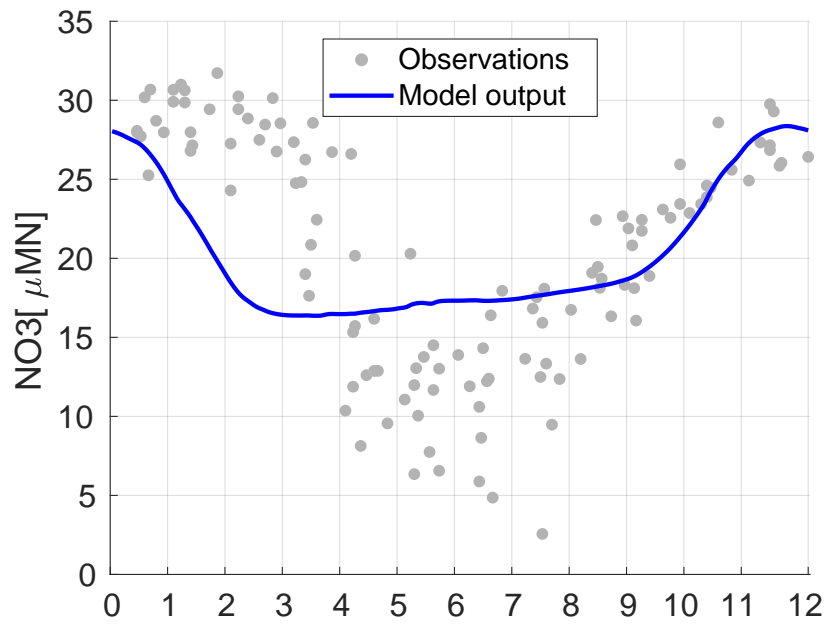


Figure 3.10: Daily average integral of NO_3 over the upper layer of 30 m depth. The PS-1D model run with *Davis et al.* (2014) parameters of the outer coast

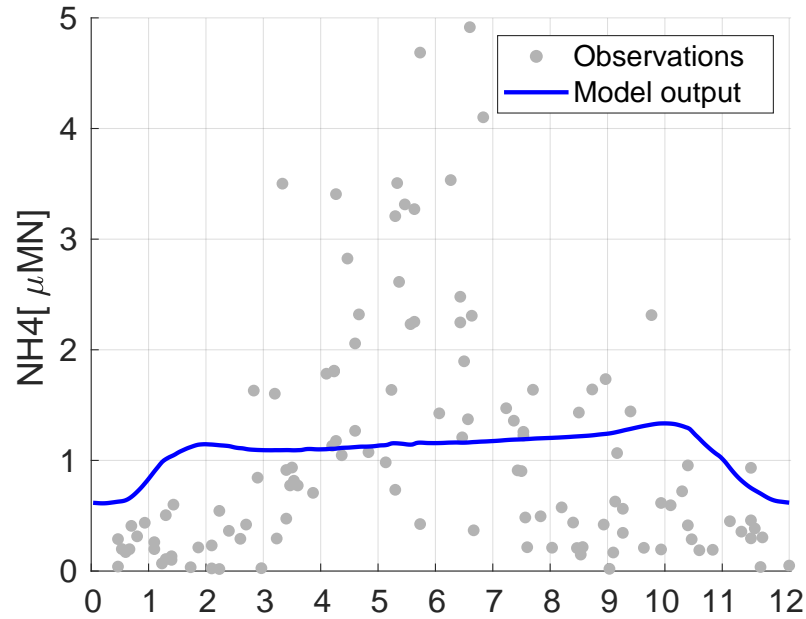


Figure 3.11: Daily average integral of NH_4 over the upper layer of 30 m depth. The PS-1D model run with *Davis et al.* (2014) parameters of the outer coast

Table 3.2 presents WSS_MSE and WSS_MAE of Chla, NO_3 over the top 20 m depth and the whole water column (or all data); and comparison between WSS_MSE of main basin Puget Sound and the outer coast at the top 20 m depth. Between the two regions, the outer coast and main basin Puget Sound, WSS_MSE is similar at the top 20 m. It implies that biological parameters of the outer coast are adequate to use in main basin Puget Sound upper layer. However, this seems not applicable to the whole water column, where WSS_MSE shows a lower value for Chla, and a much lower value for NO_3 . In the main basin Puget Sound, WSS_MAE are quite different from WSS_MSE , with the former being consistently lower. The reason again might lie in the drawback of WSS_MAE which is discussed above. This result suggests that WSS_MSE likely overestimates a model good-fit.

	Top 20 meter		All data	
	Chla	NO_3	Chla	NO_3
Outer coast WSS_MSE (taken from <i>Davis et al. (2014)</i>)	0.58	0.83	0.73	0.93
Puget Sound WSS_MSE	0.52	0.76	0.64	0.56
Puget Sound WSS_MAE	0.32	0.42	0.48	0.41

Table 3.2: Comparison between WSS_MSE and WSS_MAE in main basin Puget Sound top 20 m depth and whole water column; and comparison between WSS_MSE of main basin Puget Sound and the outer coast at the top 20 m depth.

3.4 Discussions and Conclusions

Evidence suggests that parameters taken from *Davis et al. (2014)* study of the outer coast are not capable of capturing both phytoplankton bloom onset and magnitude as well as NO_3 and NH_4 annual patterns (Figure 3.9 to 3.11). This may mean that this study needs to re-parameterise certain biological processes, independent of the physical processes. This study will explore this possibility in chapter 5. But alternatively, it might be explained by the difference in physical forcings between the outer coast and the main basin Puget Sound. The parameters in the outer coast study were tuned based on 3-D hydrodynamics model, which described physical processes in greater details compared to the simplified 1-D physical model of Puget Sound. The yearly profile of mixing in PS-1D results in a constant mixed depth layer and is therefore thought to be the cause of the intensive blooms throughout the year as observed in the model.

Some might argue that salinity bias between model and observations (Figure 3.3) overestimates light level, which leads to the bloom appearing early in the model. This study is well aware of the salinity bias. However, it might not be a problem in the model compared to other issues (i.e., mixing). The largest difference between salinity modelled and observation point-to-point is not over 2 (psu). Given the light attenuation coefficient of freshwater (table 3.1) is around $6 \times 10^{-3} m^{-1} psu^{-1}$, bias in salinity can lead to light level overestimation at order of $0.01 m^{-1}$, which is considerably small compared to light attenuation coefficient of the water column itself ($0.05 m^{-1}$) and

self-shading effect by phytoplankton ($0.03 \text{ m}^{-1}(\mu\text{MN})^{-1}$).

Overall, this chapter has suggested that parameters from *Davis et al.* (2014) study do not capture phytoplankton blooms in the main basin Puget Sound well, and the index of agreement *WSS_MAE* which overcomes drawback of *WSS_MSE* might be a better metric for model assessment. The model results using *Davis et al.* (2014)'s parameters also imply that there might be significant differences in environment conditions and/or biological processes between main basin Puget Sound and the outer coast. Hence, at least one (or more) parameters in the *Davis et al.* (2014) parameter set might need to be changed to allow the parameter set to represent Puget Sound environment.

Puget Sound estuarine circulation brings deep oceanic water from the outer coast into Puget Sound fjord, thus both regions have similar condition on nutrient levels. It is likely that light limitation is the factor that distinguishes phytoplankton growth between the main basin Puget Sound and the outer coast. Therefore, effects of underwater light field on Puget Sound phytoplankton spring bloom will be examined in the next chapter.

Chapter 4

Underwater light field in Puget Sound

Light intensities under water vary depending on the amount of light entering the water column, water transparency, and depth (*Smith and Mobley, 2008*). Solar radiation penetrating the water column depends on position of the sun, cloudiness, and surface conditions (*Kirk, 1994*). If sun rays do not reach water surface at a straight angle, then part of it is reflected to the atmosphere, and the remaining enters the water column (*Kirk, 1994*). Once in the water column, light intensity decreases with depth (i.e., it is attenuated) as it gets absorbed and scattered by suspended matters. Absorbed light is primary source of energy for photosynthesis by phytoplankton and aquatic plants, as well as is being converted to heat when absorbed by water molecules. Scattered light is deflected into new directional paths and moves around in the water column before eventually being either absorbed or directed upward and out of the water. Water molecules, dissolved salts, organic substances, and suspended particles all combine to affect water transparency and cause solar radiation to decrease with depth (*Smith and Mobley, 2008*).

Light intensity, a crucial driver of phytoplankton photosynthesis, is known to decrease with depth. It is therefore vital to accurately represent the light environment in the model of phytoplankton growth. In *Davis et al. (2014)* model, the outer coast light

attenuation was a function of phytoplankton concentration and salinity, where the function coefficients were determined by using observations. Here, this chapter aims to define a light attenuation function in the main basin Puget Sound by using available optical data. This chapter starts by giving a brief overview of methods to observe water optical properties, which are used to estimate light intensity (Section 4.1). Section 4.2 then presents optical data available at the study site, along with empirical formulas to derive light attenuation from the optical data. Afterwards, statistical analysis of light attenuation and its drivers followed by model examination on light functions of phytoplankton growth are given in section 4.3. A discussion and conclusions finally are provided in section 4.4.

4.1 Description of ocean optical measurements

4.1.1 Brief overview of ocean optical instruments development

Moffione (2001) provides a thorough review of measuring ocean optical properties. The earliest quantitative observations of ocean optical properties are believed to have begun in the early 19th century when a Russian naval officer, O.E. Kotzebue, who in 1817 observed the depth at which a piece of cloth attached to a rope disappeared below the surface. This method was later refined by replacing the cloth with a flat back and white disk, and named as Secchi disk (1866) after the Italian astronomer. Recordings of the Secchi depth constitute the longest historical record of water optical properties in existence, which make them scientifically valuable for mainly this reason. Even after the development of opto-electronic light sensors, Secchi depth measurements continued nearly unabated, mainly by biologists, and even continue to this day. The early 20th century marked the development of new instruments, underwater radiometers and opto-electronic sensors. Development of photographic film allowed Murray and Hjort in 1912 and Knudsen in 1922 to build underwater radiometers, the first means for objectively recording spectral irradiance and radiance distributions. At the same time, in 1922, Shelford and Gail introduced application of photoelectric cell to measure underwater light and determine optical properties. It was a then optoelectronic instrumentation,

the first of this genre with internal light sources, developed and introduced by Pettersson during the brief period from 1934 to 1938. The instrument without need of sunlight measured basic optical properties which provided the empirical underpinnings for a theoretical understanding of light and its interaction with ocean water. The 1960s opened the age of laser (Light Amplification by Stimulated Emission Radiation) in measuring light intensities under water. Laser, due to its possibility of projecting controlled and measurable light beams through ocean water, had a profound effect on this study of light and its interaction with ocean water. The laser technique provided a strong boost in the development of instruments and methods for measuring ocean optical properties. Commercial, *in situ* ocean optical instrumentation (e.g., beam transmissometer) began to appear in the late 1970s. The device provided many oceanographers with the first widely available and affordable optical tool for routinely measuring an ocean optical property *in situ*.

In Puget Sound, Secchi disk and beam transmissometer are used to measure the water optical properties. Hence, the following sections further describe Secchi disk and beam transmissometer measuring methods.

4.1.2 Secchi disk and diffuse attenuation coefficient

Secchi disk is a black and white disk of diameter 20 – 30 cm. The depth at which the disk is no longer visually observed as it is lowered into the water is recorded as Secchi depth. Although replaced by modern instruments, Secchi depth measurements are still of interest because of the ease of measurement and the large historical observations going back over a century. A major drawback of Secchi depth is that it cannot measure how the quantity and quality of light change with depths, in other words water optical properties implied from Secchi depth remain constant over the layer of that depth.

Diffuse attenuation coefficient, k_d (m^{-1}), derived from Secchi depth measurements, is commonly used to characterize optical properties of the water. k_d is yielded by the

Secchi depth in metres divided by a constant (Equation 4.1, (*Poole and Atkins*, 1929)).

$$k_d = \frac{c}{Z_{Secchi}} \quad (4.1)$$

The constant c varies by regions, with the range reported in between 1.27 and 1.8 (*Poole and Atkins*, 1929; *Holmes*, 1970; *Idso and Gilbert*, 1974; *Gallegos et al.*, 1990, 2011; *Koenings and Edmundson*, 1991; *Zhang et al.*, 2012; *Lee et al.*, 2018). A constant value of 1.7 was suggested by many authors above, and indeed used by *Winter et al.* (1975) and *Newton and Van Voorhis* (2002) to quantify light attenuation in Puget Sound water.

The light extinction coefficient, k_d , then is applied in Beer-Lambert's law

$$E_z = E_0 e^{-k_d z}$$

to estimate the intensity of light E_z at depth z from the radiation at the ocean surface (E_0). This method gives no indication of the attenuation change with depth or the attenuation of specific wavelengths of light, which is a main disadvantage of the Secchi disk method (*Shannon*, 1975). The magnitude of k_d , in addition to being dependent on the absorption and scattering properties of water, varies with physical and geometrical properties of the disk. For these reasons, k_d is often described as an apparent optical property of water.

4.1.3 Beam transmissometer and beam attenuation coefficient

A detailed description of a general beam transmissometer can be found in *Moore* (2001). A basic transmissiometer (Figure 4.1) consists of a collimated light source projected through an in-water beam path and then refocused on a receiver detector. Typically single-wavelength transmissiometers employ a light-emitting diode coupled with an optical band-pass filter as the source. Source light is often split so that a portion of the beam impinges upon a reference or compensation detector that is either used in numerical processing of the data or integrated into a source stabilization feedback

circuit. The source output is often modulated and the lamp and receiver detector samples are in phase with the source modulation. This greatly reduces ambient light detection by the receiver from the sun or other unwanted sources. Path lengths (r) are fixed with distances typically ranging from 5 cm to 25 cm depending upon the waters in which the sensors are used. The receiver detector converts radiant flux into current and its output is thus proportional to the radiant energy passed through the water. Electronics subsequent to the detector amplify and rectify the signal for digitisation or direct output as a direct current (DC) voltage level. This signal is known as the instrument transmittance (T).

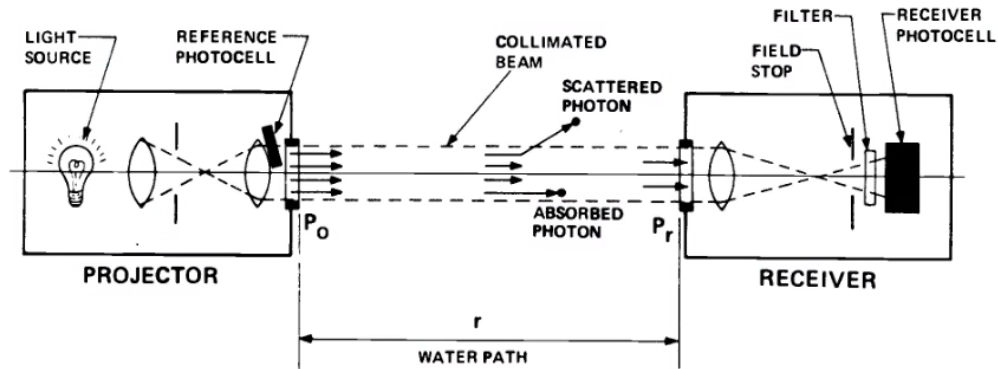


Figure 4.1: Conceptual beam transmissometer (Figure reprinted from *Shannon (1975)*)

Beam attenuation coefficient, commonly called λ (m^{-1}), derived from beam transmissometer measurements, is often used to characterize water optical properties. Beam attenuation coefficients are calculated from transmission following equation 4.2 (*Transmissometer Manual*)

$$\lambda = -\left(\frac{1}{r}\right)\ln\left(\frac{\%Tr}{100}\right) \quad (4.2)$$

where r is beam path length (m), $r = 25(cm) = 0.25(m)$, and $\%Tr$ measured beam transmission of light in percent.

Theoretically, the beam attenuation coefficient λ is related to the absorption and scattering coefficients. Hence, λ is considered to be an inherent optical property of water. It is independent of light beam orientation or the existing light conditions within

the medium. Ideally, the measurement of λ is also independent of such geometric considerations as instrument size, configuration, and receiver acceptance angle. However, the practical measurement of λ is complicated by the problem of distinguishing unscattered light from light which has been scattered into very small angles. This problem is particularly significant because small angle scattering dominates the total scattering phenomenon in natural waters (*Shannon, 1975*). This contamination yields a measured value of transmittance slightly higher than the true value; hence, the value of λ calculated from such a measurement is slightly lower than the true value.

Although measurements from Secchi disk and beam transmissometer yield light attenuation, k_d and λ respectively, they refer to different types of optical properties of water, apparent and inherent, correspondingly. k_d is used directly to calculate light intensity at certain depth (i.e., in Beer-Lambert law equation), whereas λ needs to be converted to k_d before it can be used to estimate light intensity. *Shannon (1975)* while analysing measurements of k_d and λ from wide range of water turbidity suggested an empirical expression of k_d and λ as follows:

$$k_d = 0.2\lambda + 0.04 \quad (4.3)$$

where $0.11 \leq \lambda \leq 1.6$ for empirical relationship exists between these two optical properties.

4.2 Puget Sound optical measurements

4.2.1 Secchi depth

Newton and Van Voorhis (2002) study, which includes roughly 3 year measurements of Secchi observations (Figure 4.2) and Chla concentration (Figure 4.3) might be a satisfactory data source to obtain a light attenuation function that takes into account changes in surrounding water environment.

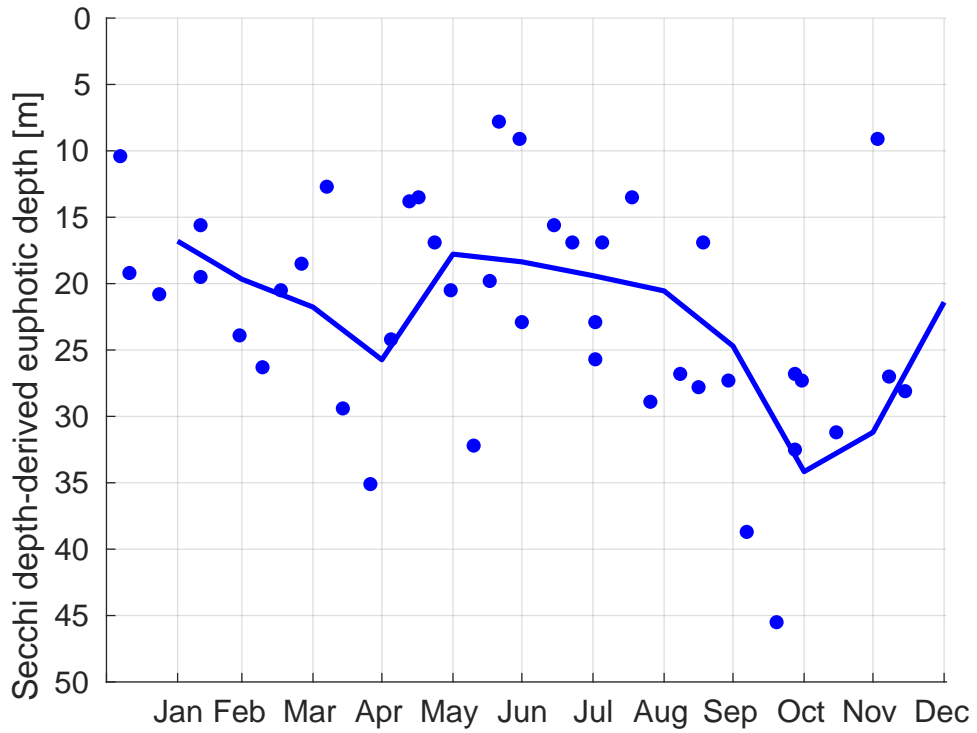


Figure 4.2: Euphotic depth (blue dots) against year day at station 5, reported in *Newton and Van Voorhis* (2002) study over period of 1999 – 2001. The euphotic depth was calculated from Secchi disk depth. Measurements were taken every 2 – 6 weeks, with 42 samples in total. The blue line is the monthly average euphotic depth.

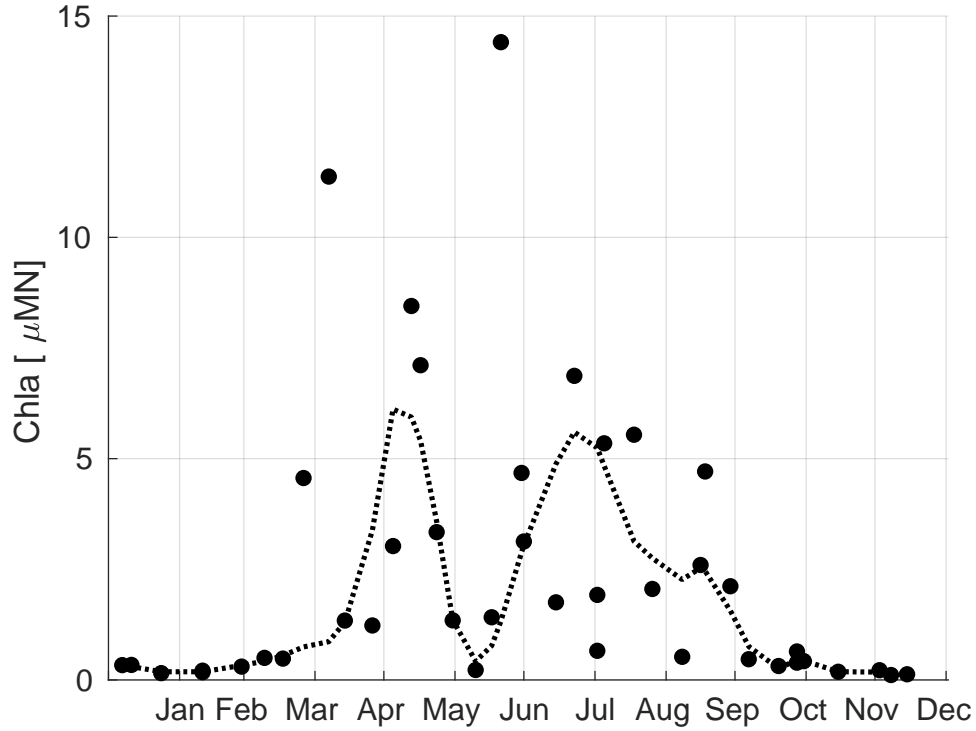


Figure 4.3: Average of integrated Chla over euphotic depth reported in *Newton and Van Voorhis* (2002). Black circles are for observational data, while the dot line is fitting to the circles by using loess filter.

As stated in *Newton and Van Voorhis* (2002), at a sampling cruise, euphotic depth was defined by first measuring Secchi depth. k_d was then derived from measured Secchi depth according to equation 4.1 with $c = 1.7$. Afterwards, k_d was applied into the Beer-Lambert law equation ($E_{(z)} = E_0 e^{-k_d z}$) to define the depth at which light is 1% of the surface irradiance, a conventional definition to define euphotic depth (Z_{eu}). Thus, Z_{eu} in *Newton and Van Voorhis* (2002) was calculated as follow:

$$Z_{eu} = -\frac{\ln(0.01)}{k_d}$$

This procedure is reverted to get Secchi depth from euphotic depth

$$Z_{Secchi} = -\frac{1.7}{\ln(0.01)} Z_{eu}$$

and then reverted Z_{Secchi} are monthly averaged.

Figure 4.4 shows a close agreement between monthly average of 30-year Secchi depth (black line, *provided by Julia Bos, Department of Ecology, Washington*) and monthly average of Secchi depth reverted from 3-year euphotic depth (blue line). This close agreement means that the 3-year Secchi depth adequately represents longer Secchi depth series, and this also means *Newton and Van Voorhis (2002)* data on Secchi depth (figure 4.2) and Chla (figure 4.3) might sufficiently produce light attenuation function as presented in section 4.3.

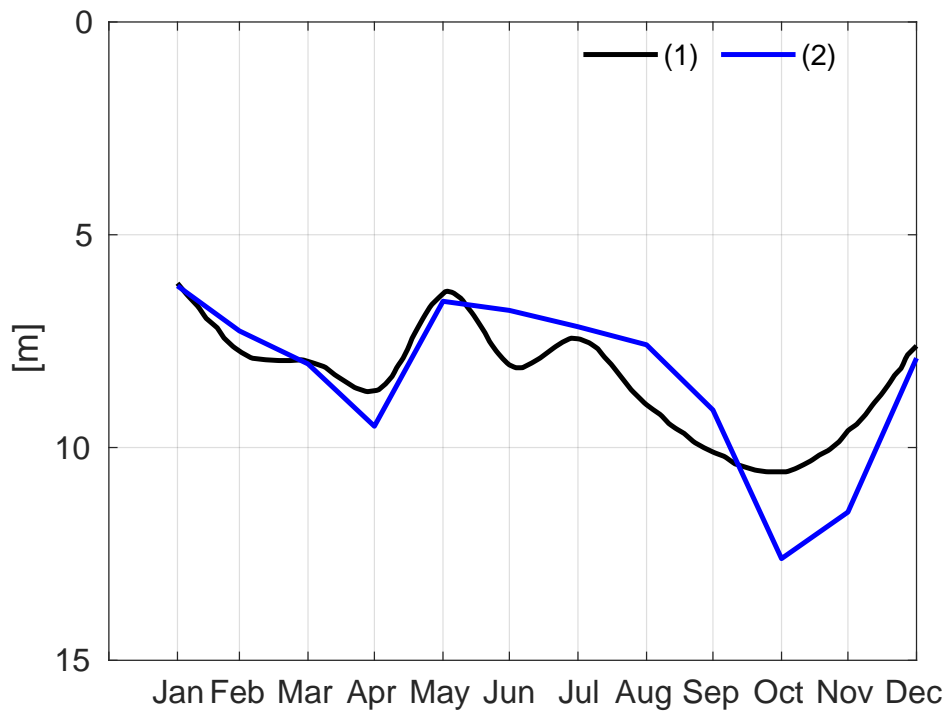


Figure 4.4: (1): approximate 30-year monthly average of measured Secchi disk depth (*provided by Julia Bos, Department of Ecology, Washington*) and (2): monthly average Secchi disk depth calculated back from euphotic depth as in figure 4.2.

4.2.2 Beam transissionmeter

A beam transimissometer (a 25 cm Sea Tech Transmissometer interfaced with CTD) was used to measure transmission of light in main basin Puget Sound (at station 5) since 1999. Over period of 1999 – 2017, in total, there are 191 transmission profiles measured (Figure 4.5), and consequently the same number of beam attenuation profiles obtained by using equation 4.2 (Figure 4.6).

Almost all of the light transmission data fall in the range of 60% to 100%. Transmission data shows strong turbidity which often appears near the water surface, probably due to river influence. The most turbid period is in May, which agrees with Secchi depth measurements (figure 4.4). Subsequently, almost all beam attenuation coefficients fall in the range of [0 – 2].

4.3 Statistical analysis and model examination of light functions

4.3.1 Light function obtained from Secchi observations

Secchi observations (Figure 4.2) and Chla data (Figure 4.3) from *Newton and Van Voorhis* (2002) presented in section 4.2.1 allows this study to derive light attenuation (k_d) as a linear relationship with Chla (i.e., $k_d = att_P Chla + att_{bg}$, where att_P is light attenuation caused by phytoplankton (or self-shading effect) obtained from the regression's slope, and att_{bg} is the regression intercept accounting for light attenuated with depth). The regressions are performed on seasonal data (i.e., spring, summer, autumn, and winter), and on all data that excludes the winter season (Figure 4.7). The regression coefficients and R^2 for each case are given in table 4.1.

It can be seen that regressions in spring, summer, autumn and in all three season combined are fairly well agreed with each other. The regression in winter presents a completely different relationship. Very low Chla concentration, and high turbidity due

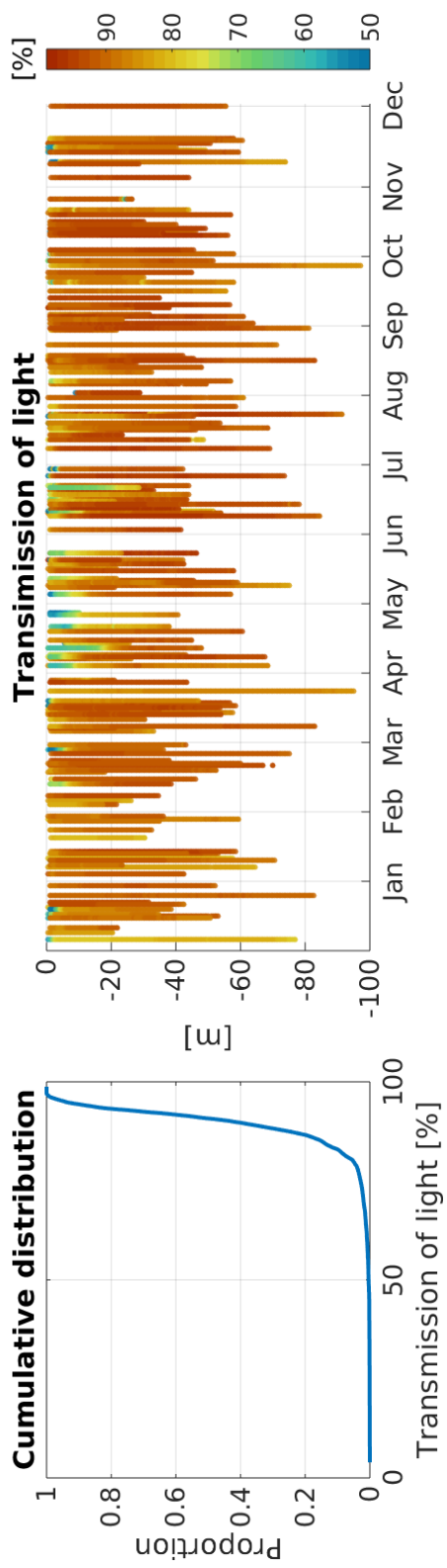


Figure 4.5: Transmission of light (%) from DoE data set at station 5.

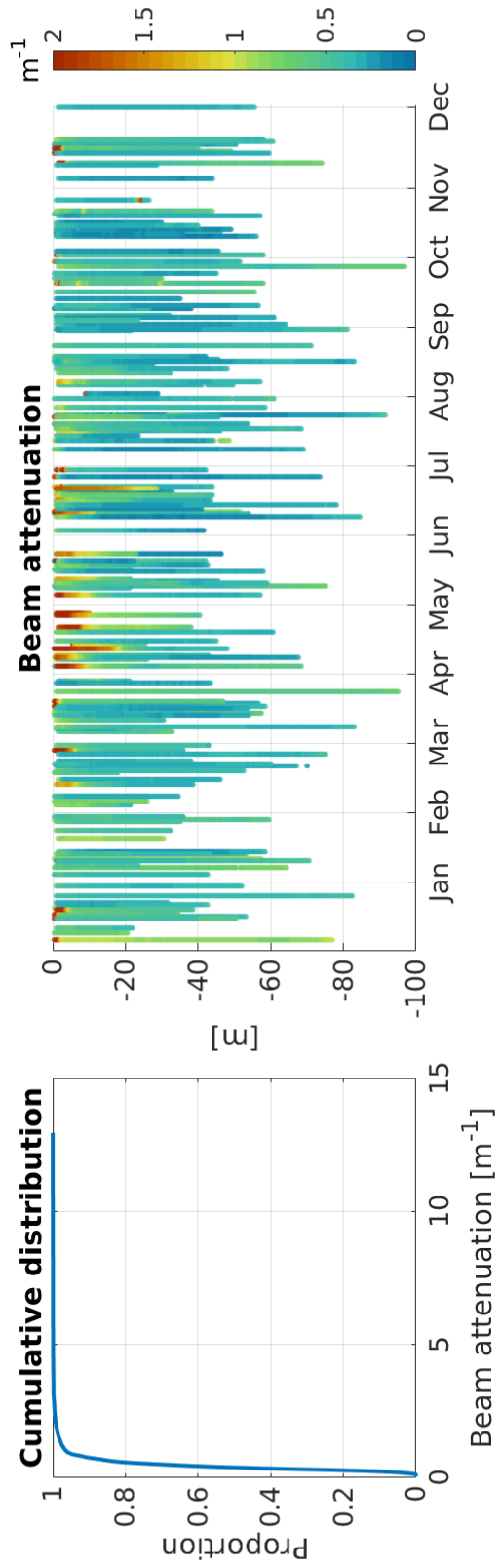


Figure 4.6: Beam attenuation, λ (m^{-1}) calculated from transmission data.

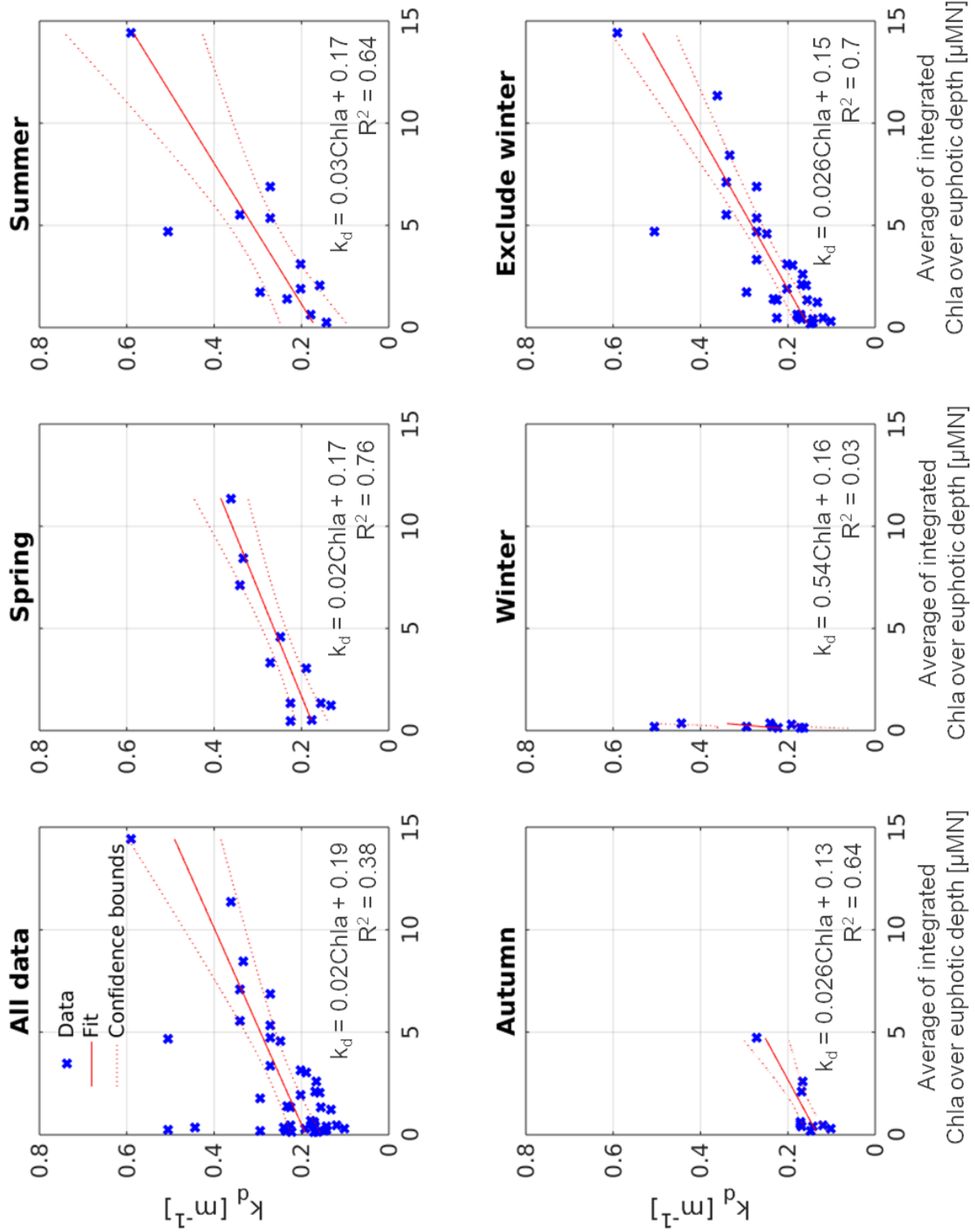


Figure 4.7: Regressions of k_d and Chla by using euphotic depth and Chla data taken from *Newton and Van Voorhis (2002)*'s study. The regressions were performed on all data, seasonal data, and data that excluded data in winter.

	All data	Spring	Summer	Autumn	Winter	Exclude winter
att_P	0.02	0.02	0.03	0.026	0.54	0.026
att_{bg}	0.19	0.17	0.17	0.13	0.16	0.15
R^2	0.38	0.76	0.64	0.64	0.03	0.7
p-value	1.6e-05	3e-04	1e-03	3e-03	0.3	1e-09
Number of observations	42	11	12	10	9	33

Table 4.1: Diffuse attenuation coefficients derived from Secchi disk measurements (*Newton and Van Voorhis (2002)*'s data set), which are outcomes of regressions showed in figure 4.7. att_P corresponds to the regression slope, while att_{bg} is the regression intercept. The coefficients are referred as coefficients derived from euphotic depth.

to storms in winter might be the reason for the different trend observed. However, winter is not considered active growing season of phytoplankton in Puget Sound (i.e., Chla concentration is considerably minor in winter, Figure 4.3). Hence, the use of light attenuation function that excludes the winter data would not noticeably affect modelling of phytoplankton spring bloom. Thus, the regression on seasons that exclude the winter appears to be applicable to present light attenuation (k_d) in Puget Sound.

4.3.2 Light function obtained from beam transmissometer's measurements

Beam attenuation λ (Figure 4.6) calculated from transmission data (Figure 4.5) is used to calculate k_d according to empirical $k_d - \lambda$ relationship (Equation 4.3, *Shannon (1975)*). Together with transmission data, there are observations of Chla (Figure 3.4), turbidity (Figure 4.8), and salinity (Figure 3.3), all of which are sampled by Department of Ecology (DoE). Turbidity commonly represents water transparency under influence of suspended matters, which mainly come from freshwater. Thus, salinity is also often used as a proxy for turbidity. Here, freshwater is expressed as the difference between salinity measured in main basin Puget Sound and salinity of oceanic water from the outer coast (also water at the bottom layer of Puget Sound). Average salinity of the

outer coast oceanic water is reported at 32 psu (*Davis et al.*, 2014). Following, this study explores light attenuation as function of Chla and turbidity ($k_d = att_P Chla + att_{tur} Turbidity + att_{bg}$) or freshwater ($k_d = att_P Chla + att_{fw} FW + att_{bg}$) to examine contribution of Chla concentration (or self-shading effect), freshwater and turbidity to total light attenuation. In addition, this study inspects light attenuation as a function of Chla only ($k_d = att_P Chla + att_{bg}$), which is suggested by the relationship of k_d and Chla obtained in the section 4.3.1 above. Figure 4.9 presents all the regressions with coefficients given in table 4.2.

	$k_d \sim$ <i>Chla + Turbidity</i>	$k_d \sim$ <i>Chla + Freshwater</i>	$k_d \sim$ <i>Chla</i>
$att_P (m^{-1}(\mu MN)^{-1})$	0.024	0.023	0.0243
$att_{tur} (m^{-1} NTU^{-1})$	0.014	-	-
$att_{fw} (m^{-1} psu^{-1})$	-	-0.01	-
$att_{bg} (m^{-1})$	0.09	0.07	0.093
R^2	0.64	0.64	0.61

Table 4.2: Diffuse attenuation coefficients derived from DoE transmissometer data, which were outcomes of regressions performed in figure 4.9. The coefficients are referred as coefficient derived from transmission

It can be seen that k_d regressions that contain turbidity and k_d freshwater yield comparable att_P coefficient and the same level of correlation (R^2). The similarity between k_d regression involving turbidity and freshwater means that freshwater (expressed through salinity) can be interchangeable with turbidity to account for the influence of rivers on underwater light. Given freshwater is a common variable in biogeochemical models, following, the regression of k_d with freshwater will be further examined instead of the regression with turbidity. The k_d regression included freshwater results in negative attenuation coefficient of freshwater ($att_{fw} = -0.01$). This is within this study expectation. As freshwater is formulated as the difference between observed salinity and saltier oceanic water, freshwater results in negative number of psu. Thus, a negative value of att_{fw} is expected to elevate total attenuation under influence of rivers

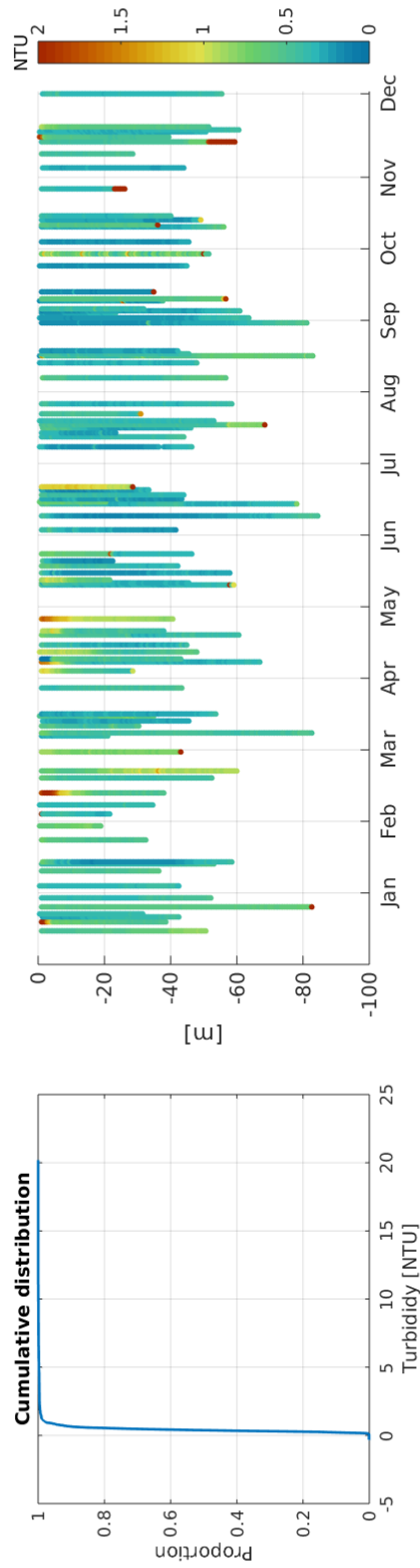


Figure 4.8: Turbidity over period 2009 - 2017 at station 5 from DoE cruise. There are 99 profiles of turbidity over the sampling period.

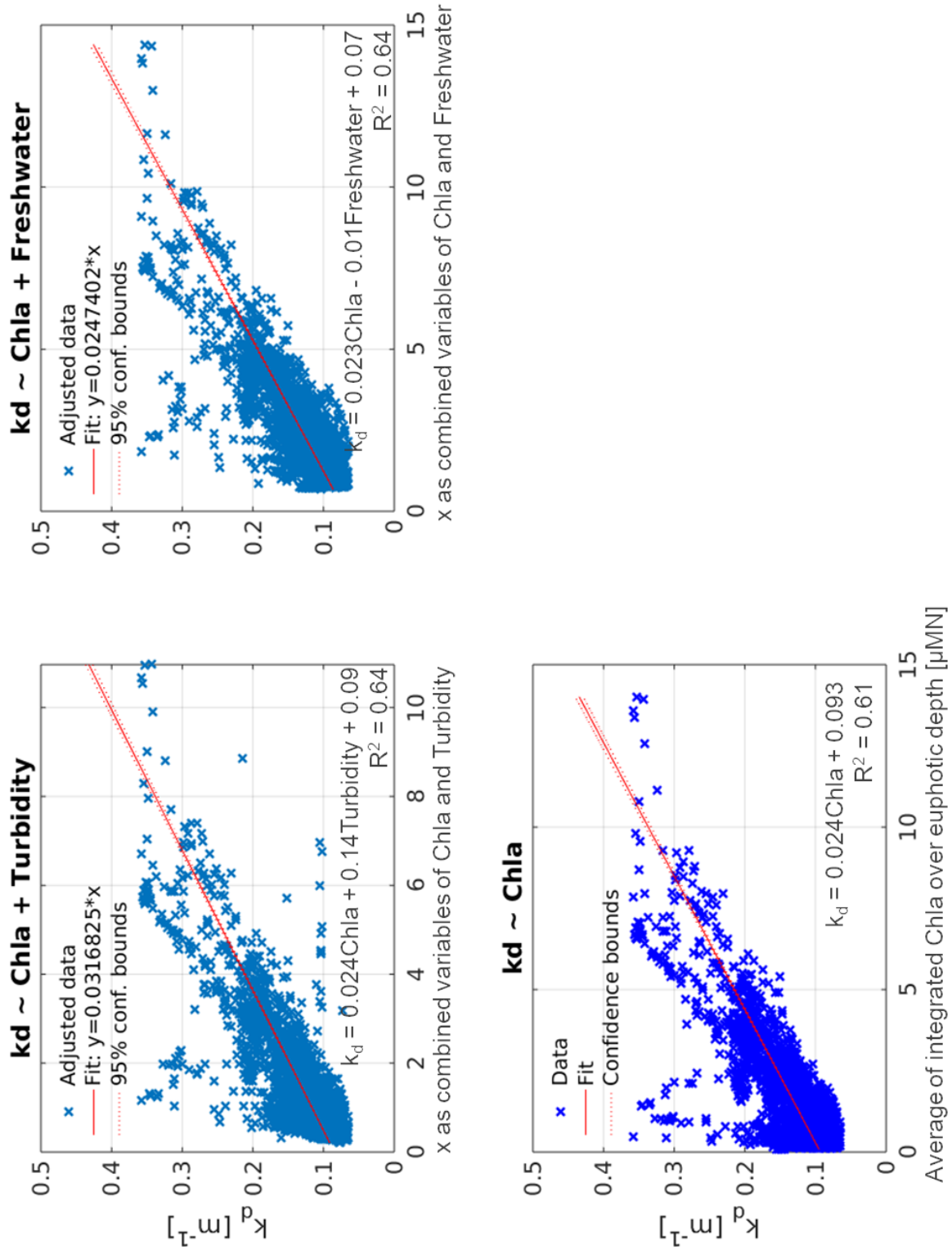


Figure 4.9: Regressions of k_d and/or Chla, turbidity, fresh water by using data from DoE cruise. k_d were calculated from beam transmission measurements.

suspended matters. The regression of k_d without freshwater ($k_d \sim Chla$) is akin to it with freshwater ($k_d \sim Chla + Freshwater$), which implies that self-shading effect (att_P) plays dominant role on k_d in comparison to attenuation caused by river inputs (att_{fw}). Thus, for simplicity, k_d as a function of Chla ($k_d \sim Chla$) is referred to represent light extinction in the main basin Puget Sound water.

4.3.3 Comparison of light functions

This section presents three light attenuation functions ($k_d = att_P Chla + att_{fw} Freshwater + att_{bg}$) that possibly represent Puget Sound underwater light. The first is from *Davis et al.* (2014), the second and third are regressions obtained from (Secchi-derived) euphotic depth (Figure 4.7) and beam attenuation data set (Figure 4.9), respectively. Coefficients (att_P , att_{fw} , and att_{bg}) of the three functions are summarized as in table 4.3.

	(<i>Davis et al.</i> , 2014)	Secchi observations	Beam transmissometer observations
att_P	0.03	0.026 [0.02 – 0.033]	0.0243 [0.0239 – 0.0248]
att_{fw}	-0.0065	NA	0
att_{bg}	0.05	0.15 [0.12 – 0.18]	0.093 [0.092 – 0.094]
R^2	-	0.7	0.61

Table 4.3: Set of potential light attenuation functions for station 5, main basin Puget Sound. [a – b] is 95% confidence levels.

It can be seen that light attenuation caused by phytoplankton (att_P) is similar in function derived from Secchi observations and beam transmission (i.e., att_P is $0.026 \text{ m}^{-1}(\mu MN)^{-1}$ and $0.024 \text{ m}^{-1}(\mu MN)^{-1}$, respectively), while light attenuation caused by phytoplankton at the outer coast is not significantly different ($att_P = 0.03 \text{ m}^{-1}(\mu MN)^{-1}$). Light attenuation caused by freshwater at the outer coast is rather low ($att_{fw} = -0.0065 \text{ m}^{-1} psu^{-1}$), which could be considered equally to transmission-derived att_{fw} . The most difference between the three function lies in light attenuation of water background (att_{bg}), with att_{bg} from *Davis et al.* (2014) is a third or a half

of Secchi or transmission derived. This suggests *Davis et al.* (2014) att_{bg} is underestimating the underwater light field in Puget Sound, and it might be a reason for early observed bloom in chapter 3. att_{bg} derived from transmission is lower than that of Secchi, which might be due to technical problem of beam transmissometer. Difficulties in distinguishing unscattered light from light which has been scattered into very small angles might result in a value of beam attenuation that is slightly lower than the true value (see section 4.1.3), which subsequently produces lower light attenuation. In general, light attenuation functions derived from (Secchi-derived) euphotic depth and transmission are seemingly agreeance with each other. Between the two functions, while the transmission-derived has tighter confidence bounds on coefficients and more data, the euphotic depth-derived has stronger correlation (i.e., higher R^2).

4.3.4 Model examination of light functions

To decide on the most applicable light attenuation function to incorporate in to the PS-1D model, this study set up 2 runs of PS-1D model with light attenuation coefficients (att_P , att_{fw} , and att_{bg}) derived from Secchi observations and transmission (beam transmissometer measurement) (Table 4.3). The setup of PS-1D model is similar to the setup in the chapter 3 except coefficients in the light function of *Davis et al.* (2014) (Equation 2.8) are correspondingly replaced with coefficients derived from Secchi depth and beam transmissometer, respectively. Model skill assessment, WSS_MAE on Chla, NO_3 , and NH_4 are calculated for each run in the upper layer of 30 m depth and the whole water column (Table 4.4).

PS-1D runs with potential light attenuation functions	Top 20 meter			All data		
	Chla	NO_3	NH_4	Chla	NO_3	NH_4
- taken from (<i>Davis et al.</i> , 2014)	0.32	0.42	0.21	0.48	0.41	0.37
- derived from transmissometer	0.36	0.5	0.28	0.51	0.46	0.42
- derived from Secchi observation	0.41	0.58	0.35	0.53	0.5	0.44

Table 4.4: Comparison of PS-1D performance on potential light attenuation functions (table 4.3) by Willmott Skill Score mean absolute error (WSS_MAE). Remaining PS-1D parameters are as in table 3.1

Table 4.4 shows that light attenuation coefficients derived from Secchi depth and beam transmissometer present better model performance than the outer coast coefficients of *Davis et al.* (2014). This suggests a difference in underwater light field between the outer coast and Puget Sound fjord. Thus, light attenuation coefficients probably are the first and foremost parameters that need to be changed in outer coast parameter set so that it can better reproduce Puget Sound phytoplankton bloom. As a consequence of change in the amount of light available for photosynthesis, parameters closely related to photosynthesis such as the slope of phytoplankton growth and irradiance curve (P-I curve) or λ , are also likely to be different. Between attenuation coefficients derived from Secchi depth and beam transmissometer, the former yields slightly higher model-observation agreement score, even though the latter contains higher data resolution. In comparison to the run with *Davis et al.* (2014) attenuation coefficients, Secchi observations coefficients considerably improve model goodness-of-fit of Chla and NO_3 on the top 20 metre layer to 22% and 28% and to whole water column are 9.4% and 18% respectively.

Figure 4.10 and 4.11 illustrate the PS-1D model outputs running with Secchi depth derived light attenuation coefficients. In figure 4.10, Chla model output does not show high concentration (or bloom) around the end of January as observed in the model run with *Davis et al.* (2014) coefficients (Figure 3.8) although an intensive bloom is still observed throughout spring to autumn. Similarly, NO_3 does not show intensive shortage

in comparison to figure 3.8. Figure 4.11 restates the model improvement by showing average of integrated of Chla over 30 m depth approximately inline with observations comparing to the run with *Davis et al.* (2014) parameter set (Figure 3.9) although it still cannot capture the bloom magnitude. The Chla graph shows a potential bloom onset around mid-February, and consistent high phytoplankton concentration appears around mid-March and lasts until September. The bloom timing seems to closely agree with what is reported on Puget Sound blooms (Section 1.3). The improvement can also be seen in NO_3 graph, where modelled NO_3 is getting closer to observations.

Thus, from evidence of the data analysis and model experiments, light attenuation in main basin Puget Sound is satisfactorily expressed as a simple function of Chla:

$$k_d = att_P Chla + att_{bg} \quad (4.4)$$

where $att_P = 0.026 (m^{-1}(\mu MN)^{-1})$ and $att_{bg} = 0.15 (m^{-1})$. The effect of high turbidity in Puget Sound is expressed through a high value for att_{bg} , rather than through an explicit, additional term. Subsequently, light function (Equation 2.8) in phytoplankton growth equation now becomes:

$$E(z) = E_o \exp(- (att_{bg} z + att_P \int_z^{surface} P(z') dz')) \quad (4.5)$$

4.4 Discussion and Conclusion

Analysis on available measurements of underwater light in main basin Puget Sound show evidence that light attenuation coefficients from the outer coast parameter set (*Davis et al.* (2014) coefficients) likely underestimate light attenuation in Puget Sound water (i.e., the outer coast light attenuation coefficients yielded lower attenuation than coefficients derived from Puget Sound water optical measurements). Given primary production in main basin Puget Sound are predominately controlled by light availability in winter (*Newton and Van Voorhis*, 2002), this underestimation of light attenuation of *Davis et al.* (2014) coefficients might respond to the early bloom observed around

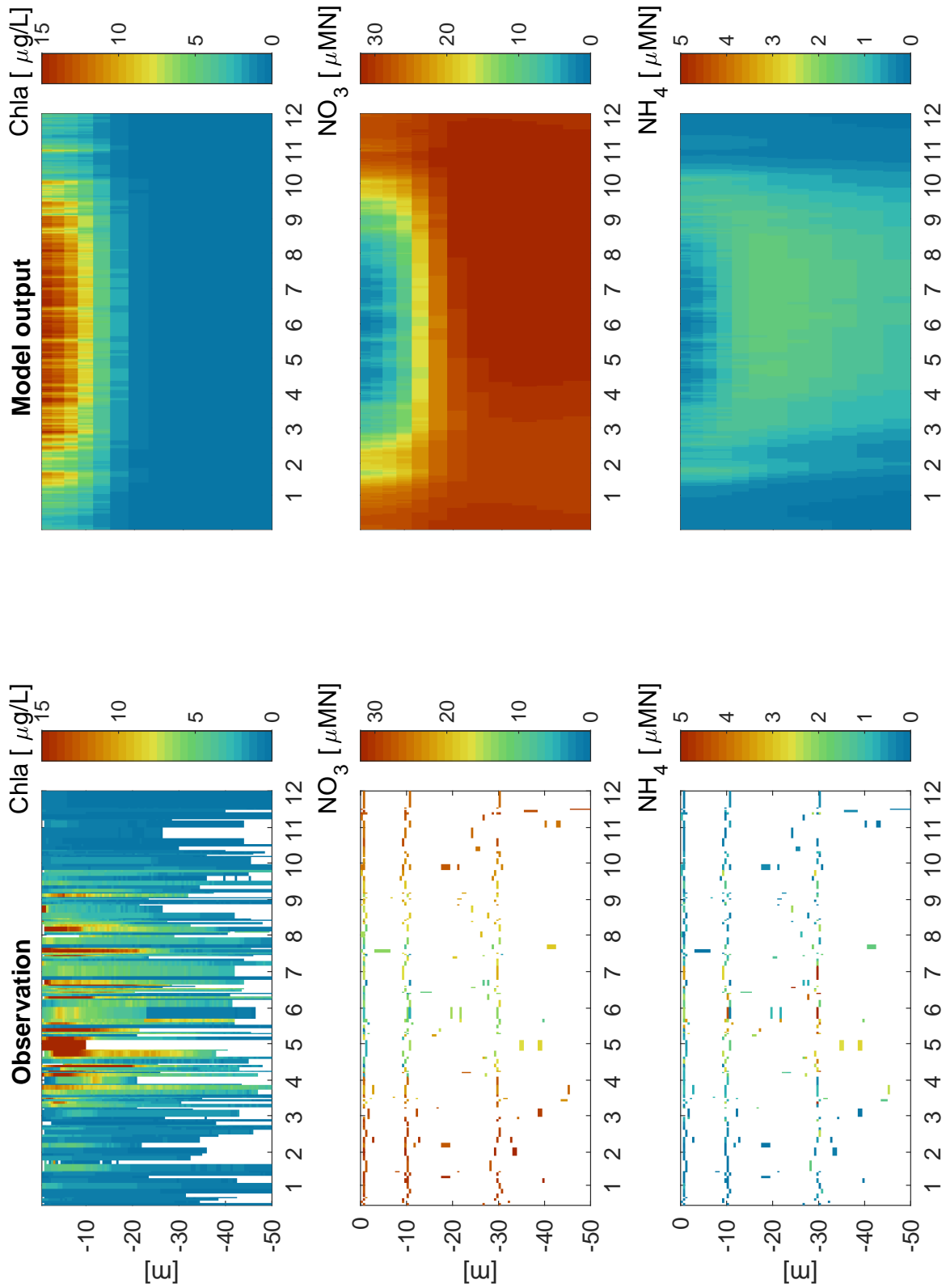


Figure 4.10: Observations (left, same as Figure 3.4) and the PS-1D model outputs (right) of Chla, NO_3 and NH_4 against time and depth. The PS-1D is run with the same setup as in chapter 3 except light function as defined in equation 4.5.

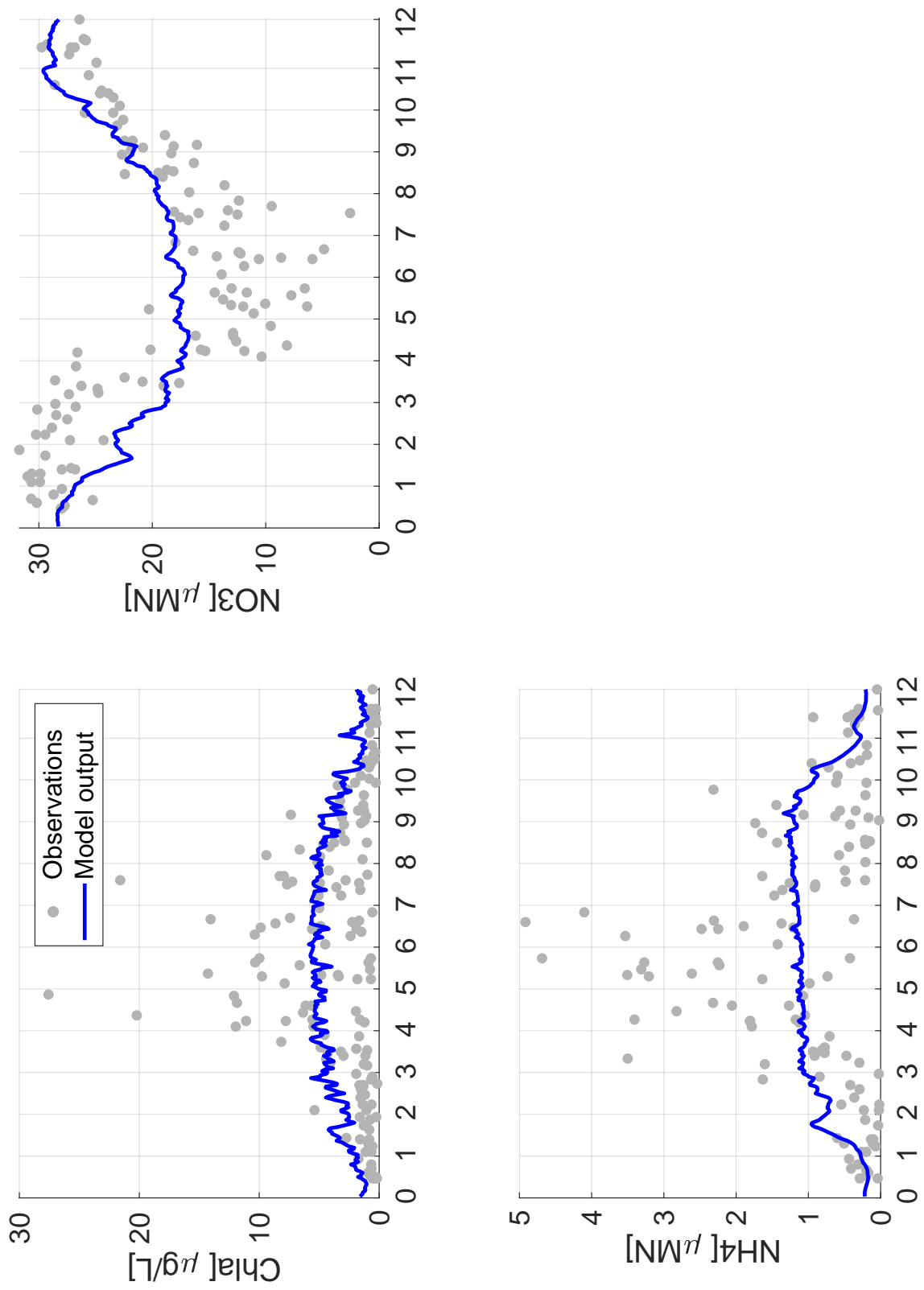


Figure 4.11: Daily average of integrated of Chla, NO_3 and NH_4 over the upper layer of 30 m. The PS-1D is run with the same setup as in chapter 3 except light function as defined in equation 4.5. Compare to Figure 3.9

the end of January in chapter 3. Thus, it is probably that these *Davis et al.* (2014) attenuation coefficients are most likely to need changed to improve the performance of the outer coast model in Puget Sound water.

Strikingly, the analysis on optical measurements yields relatively simple light attenuation function of Chla variable (Equation 4.4). The linear regression is not able to differentiate effects of freshwater from the water background in the Puget Sound underwater light (Figure 4.9). Nevertheless, there is evidence to support contribution of rivers to Puget Sound water transparency (e.g., air photos of river plumes in Puget Sound water from Eyes over Puget Sound program (*Eyes over Puget Sound*)). Puget Sound fjord receives freshwater inputs from around 15 local rivers, however, total freshwater content in Puget Sound are highly non-local in spring and summer, with distant, large rivers (the Fraser and Skagit) accounting for a large fraction of total freshwater (*Banas et al.*, 2015). *Loos et al.* (2017) showed optical properties of Fraser river rapidly attenuated (high k_d) mostly due to suspended inorganic particles (through back-scattering) and colored dissolved organic matter (CDOM, through absorption). The diversity of freshwater inputs suggests that a salinity indicator alone might not be a sufficient proxy to evaluate the contribution of rivers to optical properties of Puget Sound water. A recent study in the North Sea showed that reduced water transparency might have caused up to 3 weeks delay in the spring bloom (*Opdal et al.*, 2019). Given the complexity of river inputs and potential delay in spring blooms due to reduced water transparency, future study of Puget Sound water hydrological structure might be needed to fully quantify the influence of river on Puget Sound water transparency.

Interestingly, light attenuation coefficients (att_P , attenuation caused by self-shading effect of phytoplankton, and att_{bg} , attenuation caused by water column itself) derived from a simple method of Secchi disk (*Newton and Van Voorhis* (2002) data set) and modern laser technique (beam transmissometer) agree well with each other, with Secchi observations coefficients resulting in slightly better model (PS-1D) performance (Table 4.4). This highlights that despite the simplicity of Secchi disk measurement, Secchi

depth might remain a satisfactory approach to define light attenuation.

It is arguable that the attenuation coefficient varies with depth as a result of the changing properties of the irradiance field (*Anderson et al.*, 2015). Indeed, based on a complex treatment of submarine light of *Morel* (1988), *Anderson* (1993) suggested an approach to take into account the depth-variation of attenuation coefficient for Case 1 water (or open ocean water) and general circulation models. However, this approach was not examined in this study as Puget Sound is Case 2 water (*Matsushita et al.*, 2012) and 1-D physical model was used. Nevertheless, consistent attenuation coefficients obtained from different data sources (Secchi disk depth and beam transmissometer) would ensure the optical properties of Puget Sound water accurately represented.

Overall, this chapter proposes a simple light attenuation function of $Chla$ (Equation 4.4), and accordingly alters light function in the phytoplankton growth equation (Equation 4.5). Although the influence of rivers on total light attenuation is dismissed in equation 4.4 and consequently equation 4.5, there is evidence supporting the potential contribution of river input to underwater light. Thus, it is worth noting that att_{bg} in equation 4.4, which was resulted from a regression (Figure 4.7), indeed accounts for the effect of both water column and river inputs. During a phytoplankton spring bloom (e.g., phytoplankton concentration around $15 \mu gL^{-1}$ (*Winter et al.*, 1975; *Newton and Van Voorhis*, 2002)), phytoplankton self-shading effect might account for up to 55% of total light attenuation, which implies that self-shading effect potentially suppresses the bloom.

Changes in Puget Sound underwater light, as a consequence, likely lead to a change in other biological parameters, especially those related to photosynthesis (e.g., initial growth-light slope, α). There is no further data to allow the determination of values for the remaining parameters. The next chapter therefore employs a parameterisation approach to explore the parameter space in order to identify a parameter set that adequately reproduces Puget Sound phytoplankton blooms under the constraint of

data availability.

Chapter 5

The PS-1D model parameterisation and sensitivity analysis

Unlike atmospheric and hydrodynamic models, which are based on sound physical laws such as the Navier-Stokes equations, the ultimate governing equations for marine biogeochemical models have not been devised (*Fennel et al.*, 2001; *Jones et al.*, 2010). Consequently, processes in marine biogeochemical models are highly parameterised and often based on empirical studies (*Miller*, 2009). However, laboratory experiments to define parameters are mostly conducted on a single species under controlled conditions which makes its application to *in situ* conditions questionable (*Fennel et al.*, 2001). An alternative is to use parameter optimisation (*Fennel et al.*, 2001; *Dowd*, 2011).

Given the lack of relevant observations to define remaining parameters in the PS-1D, this chapter thus opts for a parameter optimisation approach accompanied by sensitivity analysis to estimate the undefined parameters. The chapter is organized as follows. Section 5.1 introduces the parameter optimization technique - Particle Swarm Optimizer (PSO) algorithm, and the way the PSO algorithm is incorporated into the PS-1D model. The PS-1D parameter set obtained from the PSO execution is

then presented in section 5.2. Sensitivity analysis follows afterwards to examine the sensitivity of the parameter set (Section 5.3). Finally, discussions and conclusions are drawn in section 5.5.

5.1 Particle Swarm Optimizer (PSO) and the PS-1D model parameter optimization setup

Among the 18 biological parameters of the PS-1D model (Table 3.1), 3 parameters associated to light intensity (att_P , att_{fw} , and att_{bg}) have been defined from observations (Chapter 3). Out of the 15 remaining parameters, microzooplankton growth efficiency (ϵ) and fraction of grazing excreted to ammonium (f_{ex}) are assigned common values of 0.3 (d^{-1}) and 0.5 (dimensionless) respectively. This is because at early trial and error of tuning parameters, varying ϵ and f_{ex} did not show influence on the PS-1D performance (WSS.MAE remained unchanged). As a result of the optimal uptake model (*Smith et al.*, 2009) and observations at the outer coast of Puget Sound (*Davis et al.*, 2014), minimum half-saturation for nitrate (k_{min}) is fixed at value of 0.1 (μMN). Preference for ammonium (φ_{NH_4}) is placed at 2 (dimensionless) as an analogy with a common formulation of grazing on multiple prey types (*Banas et al.*, 2016; *Gentleman et al.*, 2003). Afterwards, there are 11 parameters left to be defined.

Parameter optimization has widely been used in marine ecosystem modelling to optimize poorly known model parameters. Essentially, the optimization is done by fitting the model output to observed data by subjective tuning of the parameters. The parameters are varied until the misfit between the dynamical model and the observed data, often termed the cost function, is minimized, with the model equations fulfilled exactly (*Fennel et al.*, 2001). However, due to the strong nonlinearity of marine ecosystem models, it is likely that a cost function has multiple minima (*Kawamiya*, 2002). Thus, the search for a minimized cost function might easily be trapped in a local mimima, which is a common drawback to the above techniques. Hence, it is obviously more desirable to have techniques that are able to identify the global minimum. Global opti-

misation can be achieved using a number of techniques including simulated annealing, genetic algorithms and particle swarm optimisation. A direct advantage in using formal optimization techniques is that it can be fairly sure that it is the model structure itself that should be improved when a model does not yield a satisfactory result (*Kawamiya, 2002*).

5.1.1 Particle Swarm Optimizer

A variety of optimization methods used in marine ecosystem modeling (e.g., Generalized Likelihood Uncertainty Estimation (GLUE, *Beven and Binley (1992)*), Simulated Annealing (SA, *Kirkpatrick et al. (1983)*), Markov Chain Monte Carlo *Metropolis et al. (1953)*) have been summarized in *Houska (2017)*. Particle Swarm Optimizer (PSO) is such a technique which has now attracted the interest of researchers around the globe (*Poli et al., 2007*). The PSO was first introduced in 1995 by Kennedy (a social psychologist) and Eberhart (an electrical engineer) when they explored analogues of bird flocks searching for corn. Since then, the PSO technique has been continually modified, improved and developed into a powerful optimization method. A thorough history on development, deployment and improvement as well as variants of the PSO can be found in *Poli et al. (2007)*; *Garcia-Gonzalo and Fernandez-Martinez (2012)*; *Sengupta et al. (2019)*.

The PSO algorithm can simply be explained through an analogy of a process using boats to measure the deepest part of a lake. To start, imagine a large lake whose depth needs to be recorded. It is nearly impossible to complete this task with one boat. A more reasonable approach is to use multiple boats, and importantly these boats need to communicate to each other on their measurements. To tackle the given task above, at the first step, for example, two boats A and B are positioned randomly at opposite edges of the lake. They both then measure depths at their first placements, record them as personal (A's and B's) deepest, and inform each other about their measurements. Supposing at the first measurement, A is deeper than B, then A's measurement is recorded as the global deepest. Next to the second step, A stays where it is as A

possesses the global deepest, while B moves toward A by a predefined distance to a new position in the lake. B again measures the new position depth. B then compares the new depth with its personal deepest, and updates the personal deepest if the new depth appears to be deeper. Afterwards, B exchanges its updated personal deepest with A, and updates the global deepest if B's personal deepest is now deeper. Then, the one with the deepest stays and the other moves. This process is repeated until A and B meet (converge) at the same place (the deepest point in the lake). Boats assemble a swarm, in which each boat is a particle of the swarm. The deepest position represents cost function. Clearly, it takes less iterations (time) to find the deepest when there are more boats used.

As the PSO is well reviewed by *Poli et al. (2007)*; *Garcia-Gonzalo and Fernandez-Martinez (2012)*; *Sengupta et al. (2019)*, the algorithm given below is followed *Poli et al. (2007)* with an adjustment on bound condition which was suggested by *A. Hunter (pers. comm.)*

Algorithm. Mathematically, the algorithm is presented as in figure 5.1. A particle i of the swarm at time t is characterized by vector position $\vec{X}_i(t)$, vector velocity $\vec{v}_i(t)$, and its personal cost $\vec{P}_i(t)$. The swarm at time t records its best (global) cost $\vec{G}(t)$. Movement of particle i from time t to time $(t+1)$ at velocity $\vec{V}_i(t+1)$ needs to take into account its current vector velocity, personal cost and the global (swarm) cost to reach position $\vec{X}_i(t+1)$ that is closer to the swarm best position. Thus, the particle i first moves parallel to its current velocity vector ($\vec{v}_i(t)$), then parallel to vector connecting current position ($\vec{X}_i(t)$) to personal best ($\vec{P}_i(t)$), and finally parallel to vector connecting current position ($\vec{X}_i(t)$) to the global best ($\vec{G}(t)$). The addition of these three vectors from the beginning of first vector to the end of third vector is its new velocity ($\vec{V}_i(t+1)$). As the particle i new position is decided by using the previous experience of the particle itself and of the whole swarm, the new position is considered the better location for the particle i to be. When every particle in the swarm follows these rules, they will cooperate to find the best location in the search space, hence the

best solution possible. The algorithm is implemented as follows.

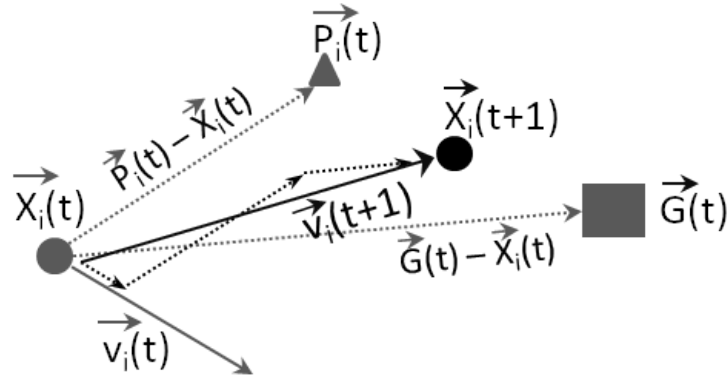


Figure 5.1: Particle swarm optimization algorithm. A particle i of the swarm at time t is characterized by vector position $\vec{X}_i(t)$, vector velocity $\vec{v}_i(t)$, and its personal cost $\vec{P}_i(t)$. The swarm at time t records its best (global) cost $\vec{G}(t)$. The particle i approaches to the global best by first moving parallel to its current velocity vector ($\vec{v}_i(t)$), then parallel to vector connecting current position ($\vec{X}_i(t)$) to personal best ($\vec{P}_i(t)$), and finally parallel to vector connecting current position ($\vec{X}_i(t)$) to the global best ($\vec{G}(t)$). The addition of these three vectors from the beginning of first vector to the end of third vector is its new velocity ($\vec{V}_i(t+1)$).

1. Initialize a population array of particles with random positions and velocities on D dimensions in the search space rescaled to the $(0, 1)$ interval. Particles' personal costs calculated from initialized positions and velocities are assigned to their *pbest*.
2. **loop**
3. For each particle, evaluate the desired optimization fitness function in D variables.
4. Compare particle's fitness evaluation with its $pbest_i$. If current value is better than $pbest_i$, then set $pbest_i$ equal to the current value, and \vec{p}_i equal to the current location \vec{x}_i in D -dimensional space.
5. Identify the particle in the neighborhood with the best success so far, and assign its index to the global variable p_g .

6. Change the velocity and position of the particle according to the following equation (see notes below)

$$\begin{cases} \vec{v}_i \leftarrow \chi \left(\vec{v}_i + \vec{U}(0, \phi_1) \otimes (\vec{p}_i - \vec{x}_i) + \vec{U}(0, \phi_2) \otimes (\vec{p}_g - \vec{x}_i) \right), \\ \vec{x}_i \leftarrow \vec{x}_i + \vec{v}_i \end{cases} \quad (5.1)$$

where

- χ is “constriction coefficients” to control the convergence of the particle

$$\chi = \frac{2}{\phi - 2 + \sqrt{\phi^2 - 4\phi}} \quad (5.2)$$

where $\phi = \phi_1 + \phi_2 > 4$. ϕ is commonly set to 4.1, and $\phi_1 = \phi_2$. ϕ_1 and ϕ_2 are often called acceleration coefficients, which determine the magnitude of the random forces in the direction of personal best (*pbest*) and global best (*g*).

- $\vec{U}(0, \phi_i)$ represents a vector of random numbers uniformly distributed in $[0, \phi_i]$, which is randomly generated at each iteration and for each particle.
 - \otimes is component-wise multiplication.
 - each component of \vec{v}_i is kept within the range $[-V_{max}, +V_{max}]$ so that particles will not go out of searching spaces. The optimal value of V_{max} is problem-specific, but no reasonable rule of thumb is known. For this study, V_{max} is half of max of the search space or 0.5.
7. When the $v(x + 1)$ potentially places $x(t + 1)$ out of its defined search space, the out-of-bounds particle needs to be carefully repositioned. Imagine a ball (a particle) moving between 2 walls (search space) with velocity v . When the ball hits one of the walls, it bounces back to a position between the 2 walls. To present this, choose the “damping” value that controls energy loss of the bouncing ball, to be something like $0 < \beta = 0.8 < 1$ (fairly close to 1). When the particle crosses the lower bound, then reposition the particle as $x(t + 1) = r \cdot \beta \cdot x(t)$, where r is a random number uniformly distributed between 0 and 1. So the particle has

been randomly relocated somewhere between its original position and the lower bound (but damping ensures it's not too close to its original position). If the particle crosses the upper bound then the same bouncing ball analogy applies, but reposition as $x(t + 1) = 1 + r \cdot \beta \cdot (x(t) - 1)$. (Note that, this assumes that parameter search space has been rescaled to the (0, 1) interval). The velocity of an out-of-bounds particle should also be reset. The reset velocity vector should point away from the boundary, towards the original position $x(t)$. Sticking with the bouncing ball analogy: velocity decreases with distance bounced away from the floor. So if the new position $x(t+1)$ is far from the boundary then the velocity is small. Thus, velocities can be reset as: $v(t + 1) = (r \cdot \beta - 1) \cdot v(t)$, which works for particles crossing either the upper or lower bounds.

8. If a criterion is met (usually a sufficiently good fitness or a maximum number of iterations), exit loop.

9. **end**

5.1.2 Implement the PSO to the PS-1D model

The remaining undefined 11 parameters of the PS-1D model form the PSO algorithm dimensions (D). The parameter search spaces are practically defined by halving and doubling values of *Davis et al. (2014)* parameter values (μ_0 , α , K_0 , I_0 , and m_{MZ}). When there is no associated PS-1D parameters in *Davis et al. (2014)*'s model (e.g., m_{aggr}), or parameter ranges produced by halving and doubling *Davis et al. (2014)*'s values are too large or small, this study uses plankton model literature to define the search spaces (m_P , m_{aggr} , w_{sinkLD} , w_{sinkSD} , r_{remin} , and r_{nitr}). The search spaces are then rescaled to the (0, 1) interval. The swarm population consists of 30 particles, which lies in the common empirical range of 20 – 50 for the population size (*Poli et al., 2007*). The cost function is to maximize the total index of model – observation agreement (WSS_MAE , section 3.2) on Chla, nitrate and ammonium combined. The PSO algorithm stops after 300 iterations. The number of iteration is decided based on try and error given constraint on convergence and time.

At the initial step, each particle is positioned randomly in the search space. The random position is sampled in its uniformly distributed space. Each particle attributed by a parameter set is then passed into the PS-1D model to compute Chla, nitrate, and ammonium concentration in time and depth, and to evaluate the cost function WSS_MAE . The WSS_MAE is recorded as the particle best cost. Comparison between particles' best costs result in the global best cost. After the initiation, the PSO algorithm enters the loop of 300 iterations to explore the search space in a manner described in the algorithm section (Section 5.1.1). As stated in the previous section, a common drawback of the technique is to be trapped at a local minima, to avoid this, the swarm is periodically disturbed after each 50 iterations (except at the 250th iteration to ensure the algorithm converges) to allow particle to move out of the current local minima. The disturbance is done through resetting swarm particles to high velocities which allow particles to jump far way from their current position. Accordingly, the position recorded as global best at the last PSO iteration is assumed to be the parameter set (the best PSO parameter set) that give model – observation best fit given the available data and chosen model functions.

5.2 Parameter optimization results

Figure 5.2 presents index of model – observations agreement (WSS_MAE) against the PSO iteration. On the left are the indices for each fitting variable stacked upon each other with the total model index placed at the top. On the right, the figure provides greater details of the model fitness variation throughout iterations. The left axis is WSS_MAE of each variable (Chla, nitrate and ammonium) and the right axis denotes the whole model WSS_MAE . It can be seen that the model shows a better fits to nitrate and chlorophyll, with nitrate WSS_MAE slightly higher. The right figure suggests the PSO converged after roughly 50 iterations, although small variation is still observed on the left figure. This means that parameter sets recorded as PSO global best at 50th iteration onwards can equally yield a similar model goodness-of-fit. The co-existence of many equally good parameter sets is possible and has been recognized as an

expected outcome when simultaneously optimizing too many unconstrained parameters given limited available data, which is the classical problem in marine biogeochemical model parameter fittings (Anderson, 2010).

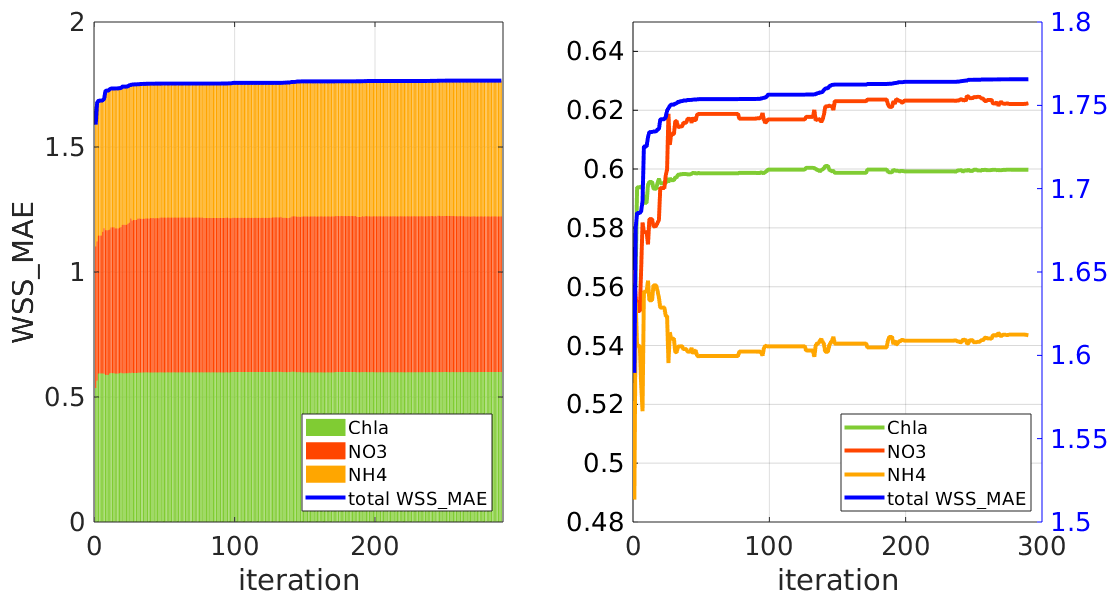


Figure 5.2: Model assessment skill WSS_MAE against Particle Swarm Optimizer (PSO) iteration. The bar stacked graph denoted WSS_MAE contribution of each variable (Chla, NO_3 , and NH_4) on the model total WSS_MAE (blue line). The line graph denoted WSS_MAE variation of each variable as well as the whole model, the left y-axis is WSS_MAE for Chla, NO_3 , and NH_4 , while the right is of the whole model (is sum of WSS_MAE of Chla, NO_3 , and NH_4).

Regarding the PSO convergence, figure 5.3 shows that almost all particle velocities approach zero, which is evidence that almost all particles ultimately reach the same solution. The convergence is clearly observed in the particle velocities of α , m_P , m_{aggr} , R_{remin} , and R_{nitr} . Fluctuation during convergence is largely seen in μ_0 , I_0 , and m_{MZ} . This is because there are many possible combinations of these parameters that yield similar model goodness-of-fit, which is also recognized in figure 5.2. Similarly, figure 5.4 illustrates the paths that parameters move along in each parameter space search. Again, prominent fluctuation is observed in μ_0 , I_0 , and m_{MZ} .

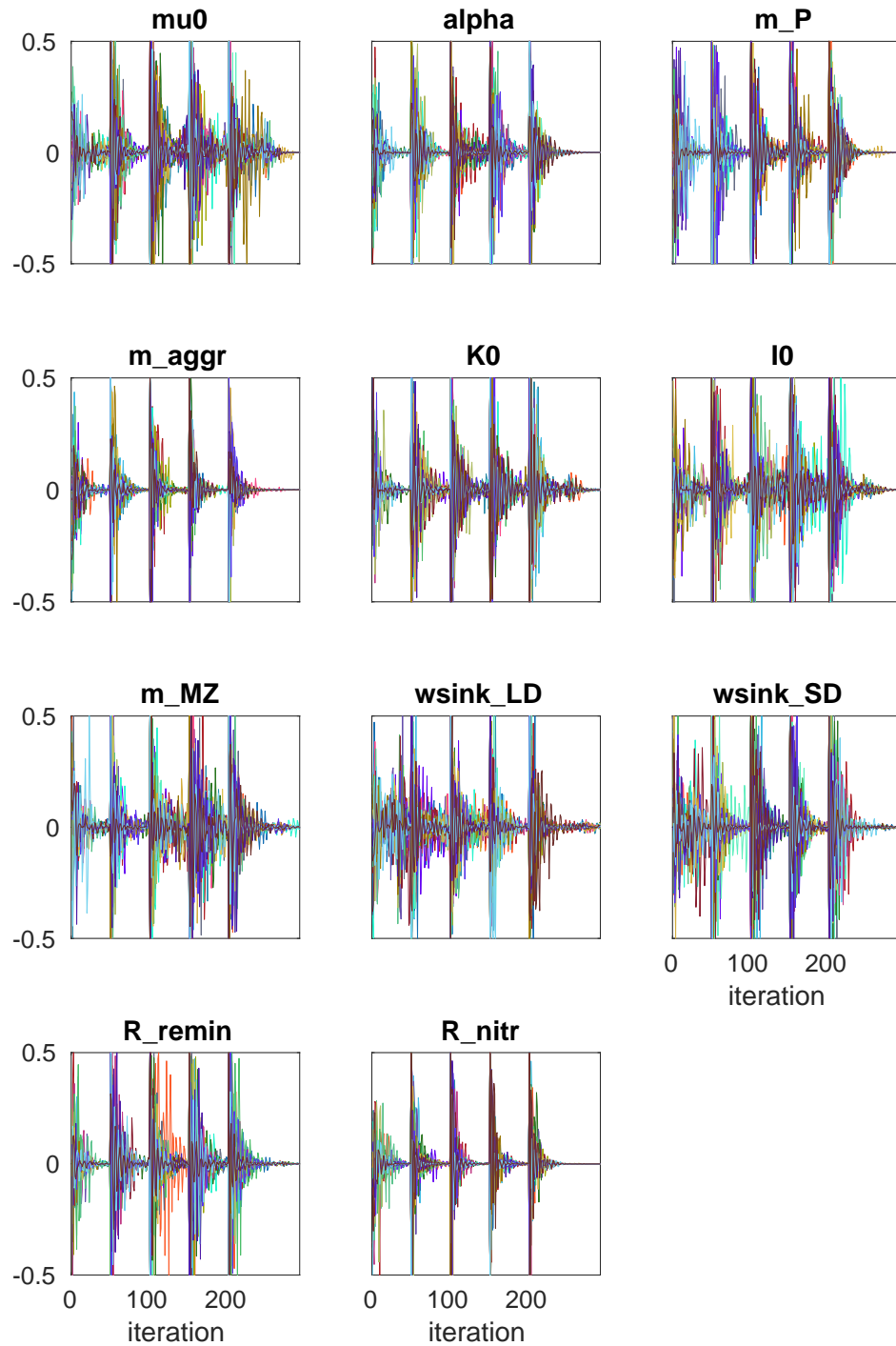


Figure 5.3: Velocity of swarm particles against iteration. The velocity is reduced after each iteration to ensure the algorithm converges. To prevent the algorithm from being trapped in local minima, swarm particles velocities are disturbed periodically after each 50 iterations (except at the iteration of 250). The disturbance repositions particles away from local minima and allow broad searching for the global minimum.

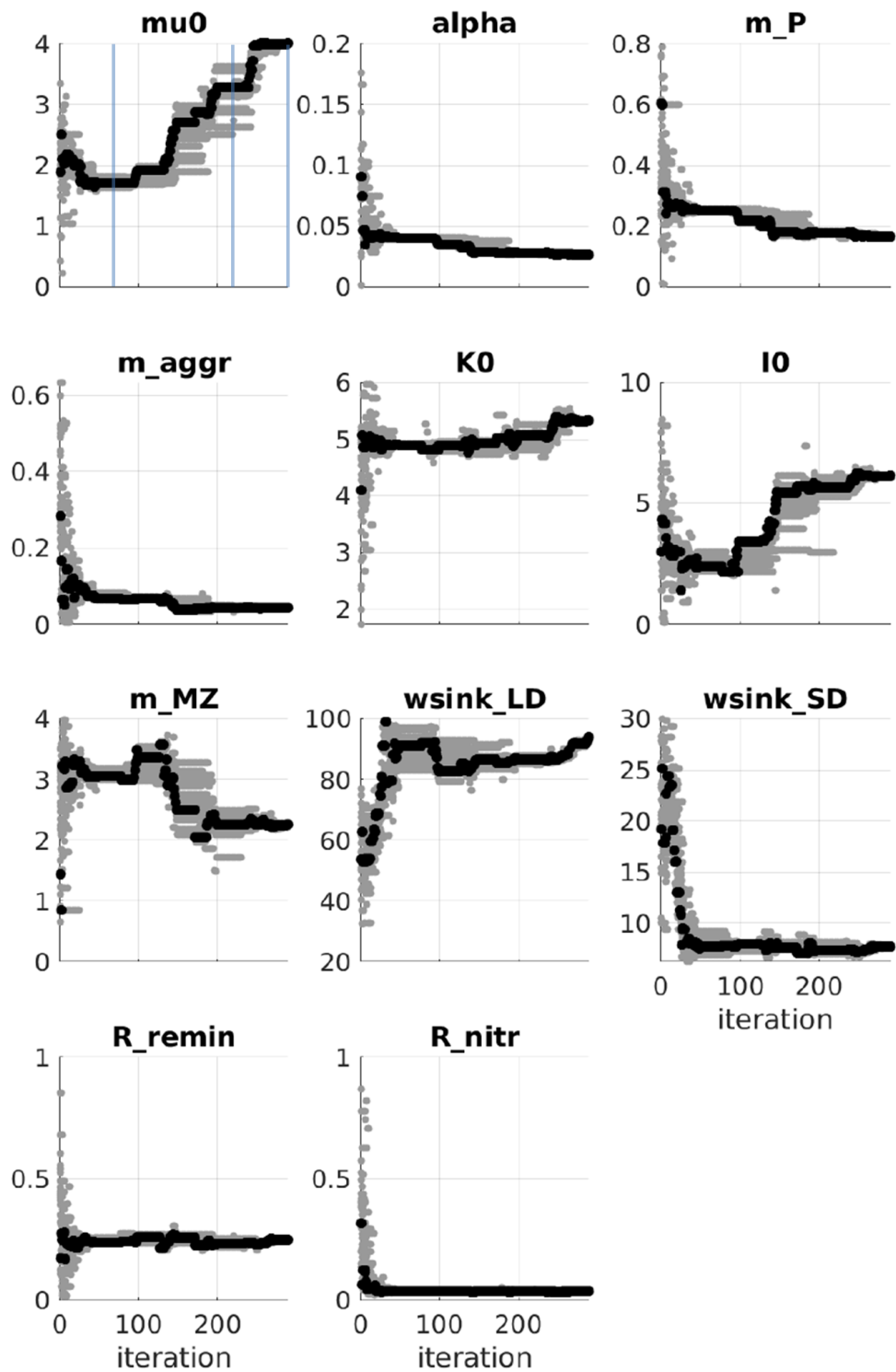


Figure 5.4: Moving paths of swarm particles at their personal best cost (gray dots) and global (or swarm's) best cost (black dots) in parameter spaces over searching iterations. Blue lines mark iteration 70, 220, and 300

Among many equally good parameter sets, this study focuses specifically on 3 parameter sets. The first is extracted at the 70th iteration, which is the start of the PSO convergence. The second is at the 220th iteration, where the total model *WSS_MAE* variation is unnoticeable. Finally the third is the global best parameter set at the last iteration (the PSO best parameter set). Regarding *WSS_MAE*, the second and the third are almost akin, and they are just slightly higher than the first one. However, the first parameter set presents a highly contrasting dynamic system in comparison the second and the third. The first parameter set indicates low turnover production rate (i.e., low in μ_0 , I_0), while the second and the third demonstrate high turnover rate (i.e., high in μ_0 , I_0) (Figure 5.4).

Figure 5.5 to 5.8 depict the PS-1D model outputs of Chla, nitrate and ammonium of the three parameter sets outlined above. The second (at 220th iteration) and third (at the last iteration) parameter sets expectedly result in almost identical distributions of Chla, nitrate, and ammonium in depth and time (Figure 5.5 and 5.6), which consequently yield similar average of integrated variables over euphotic depth (Figure 5.7 and 5.8). Despite distinguishing system dynamics (e.g. low – high turnover production rate), the first parameter set (at 70th iteration) paints rather similar patterns to the second and third, with variable concentrations just slightly lower (Figure 5.6 and 5.8). Noticeably, all three parameter sets capture the same bloom timing and sharp decline and rise in nitrate and ammonium, respectively. This means that the large difference in the system dynamics does not influence the ability to capture bloom onset of the PS-1D model, which is a major metric this study chooses to describe phytoplankton bloom (Section 1.4). Also, none of the three parameter sets adequately produces bloom magnitude (Figure 5.7 and 5.8).

Finally, it is obvious that parameter sets proposed by the PSO indicates considerable improvement of the model – observation agreement in comparison to *Davis et al.* (2014)'s parameter set (Figure 3.8 to 3.11) or *Davis et al.* (2014)'s parameter set replaced with observation-derived light attenuation (Figure 4.10 and 4.11).

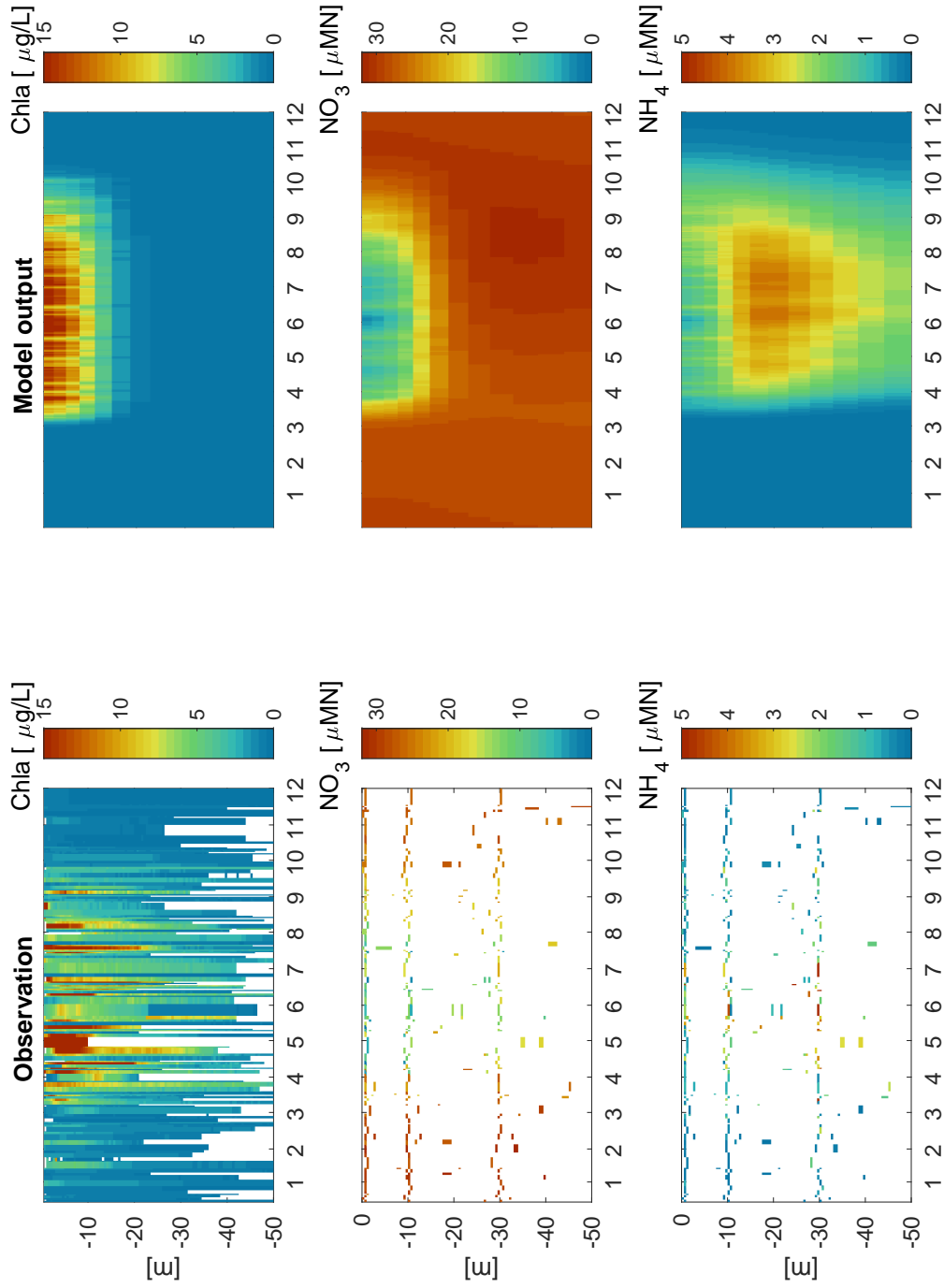


Figure 5.5: PS-1D outputs compared to observations. PS-1D is run with the PSO best parameter set. Model outputs and observations were plotted against depth and year day (labelled in month), with variables magnitude was color coded.

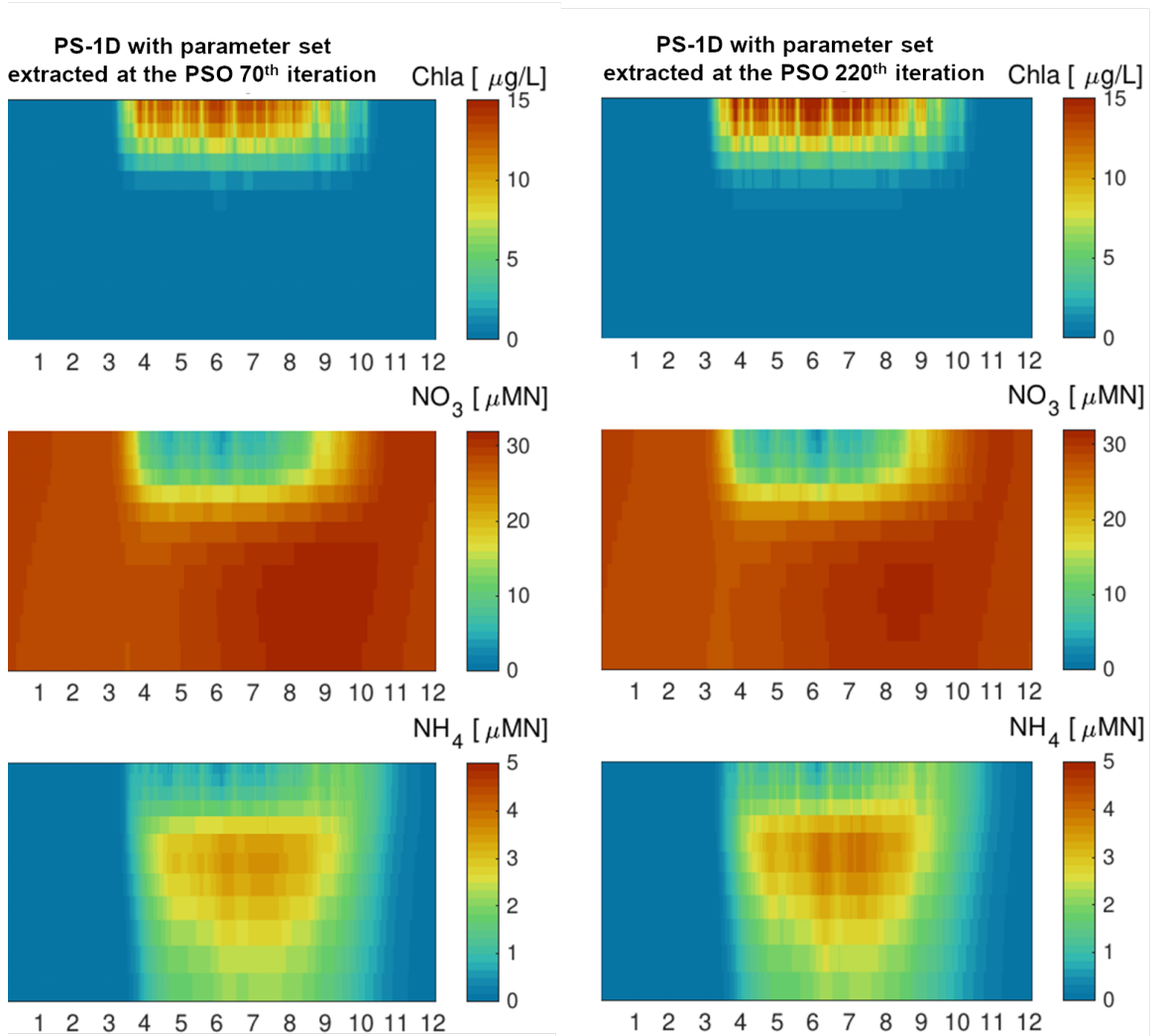


Figure 5.6: The PS-1D model run with parameters extracted at the PSO iteration of 70th (the first) and 220th (the second). Compare to figure 5.5, right-hand panels

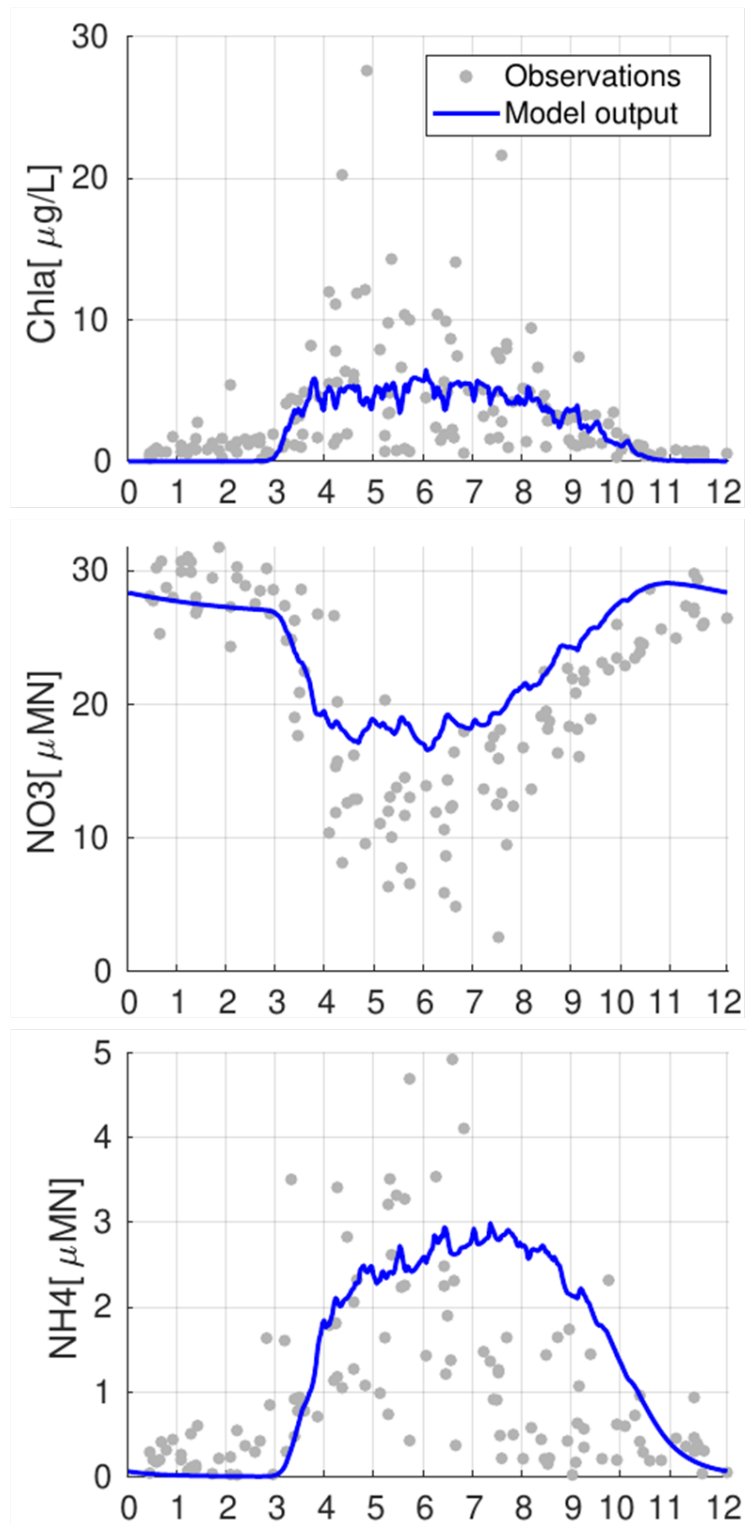


Figure 5.7: Average integral of the PS-1D model state variables over euphotic depth against time. The PS-1D outputs (blue line) in comparison to observations (grey dots. The PS-1D is run with the best PSO parameter set.)

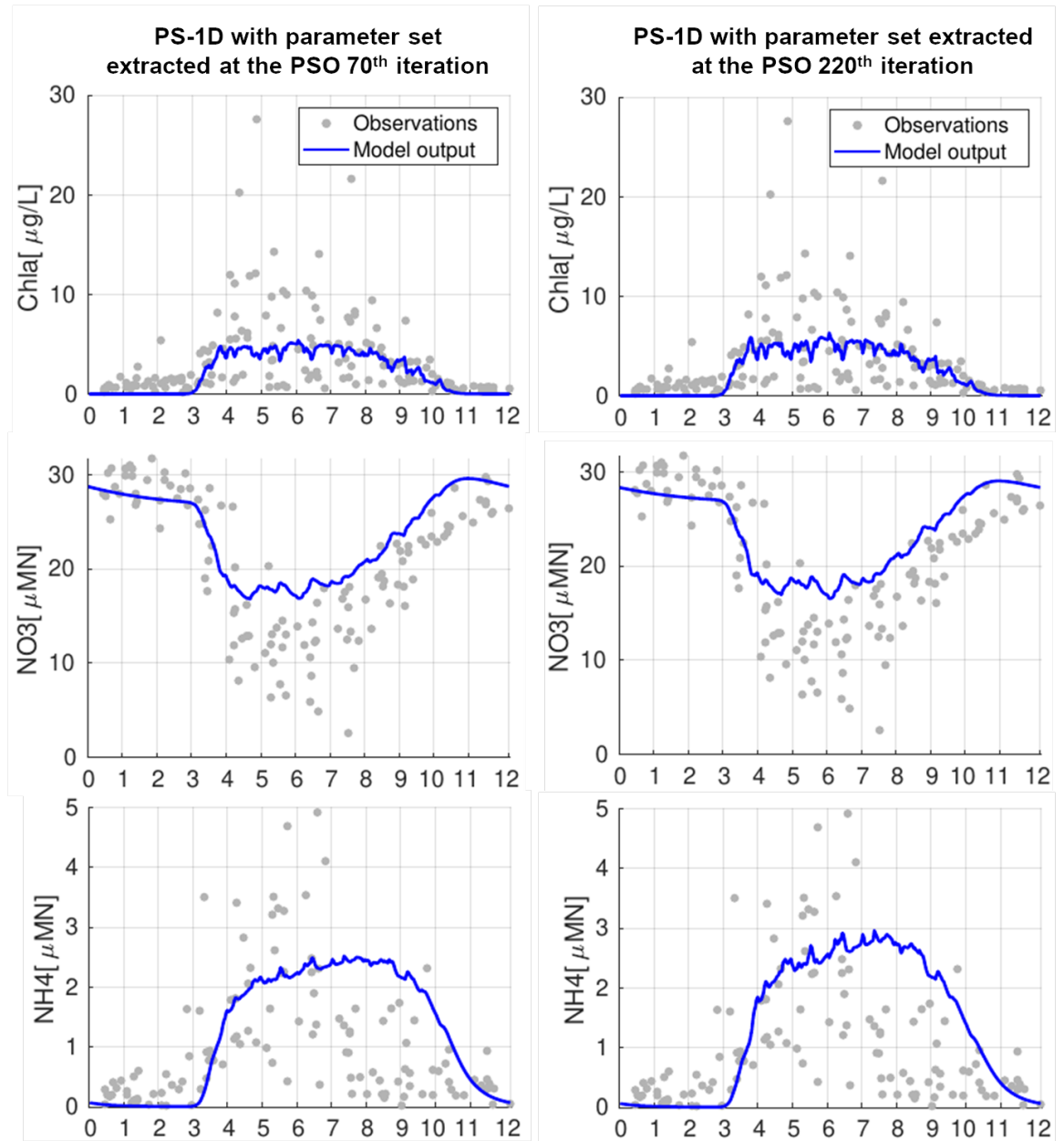


Figure 5.8: Average integral of state variables over euphotic depth from PS-1D outputs (blue line) in comparison to observations (grey dots). The PS-1D model run with parameters extracted at the PSO iteration of 70th (the first) and 220th (the second)

According to *Winter et al. (1975)*, maximum phytoplankton growth rate (μ_0) in Puget Sound was possibly in range of 2.8 d^{-1} to 6.4 d^{-1} . This range seems rather high in comparison to typically observed values from laboratory data reported by *Eppley*

(1972); *Bissinger et al.* (2008) and *Chen and Laws* (2017). However, it is worth to note that a major limitation of this laboratory data is that experimental conditions were not always replete and maximum growth rates were not always achieved (*Bissinger et al.*, 2008). *Strickland* (1983) stated that Puget Sound is considered to be a highly productive system, which was in line with high phytoplankton growth rate reported by *Winter et al.* (1975). Thus, given evidence from *Winter et al.* (1975) and *Strickland* (1983), as well as no clear difference is observed in bloom timing between parameter sets despite distinguishable system dynamics, the best PSO parameter set (global best at the last PSO iteration, in which $\mu_0 = 4 \text{ d}^{-1}$), which represents high turnover production rate is chosen for further parameter sensitivity analysis in the next section.

5.3 Sensitivity analysis

As PSO suggested numerous parameter sets that produce an equally good-fit of the model to observations, sensitivity analysis is an additional necessary step to provide further insight into the system dynamics. By doing sensitivity analysis, this study will distinguish between strong and weak constrained parameters, and hence gain added evidence to support the final parameter set selection.

The same parameter search spaces given in the optimization procedure are used to explore the parameter sensitivity. Each parameter range is divided into twenty equal spaces. One at a time, the PS-1D model is set up and run for each parameter variation. After the run, *WSS_MAEs* are calculated for each state variable (Chla, nitrate, and ammonium) and total model (by taking sum of all state variables). Finally, the index of agreement of *WSS_MAEs* are exported and plotted against the parameter range along with the base case (red line) and the *Davis et al.* (2014) value (blue line) (Figure 5.9).

Figure 5.9 shows *WSS_MAE* in response to parameter variation. The distance of red and blue line represent difference/similarity between the best PSO parameter values and the *Davis et al.* (2014) values. The sensitivity analysis again confirms that the

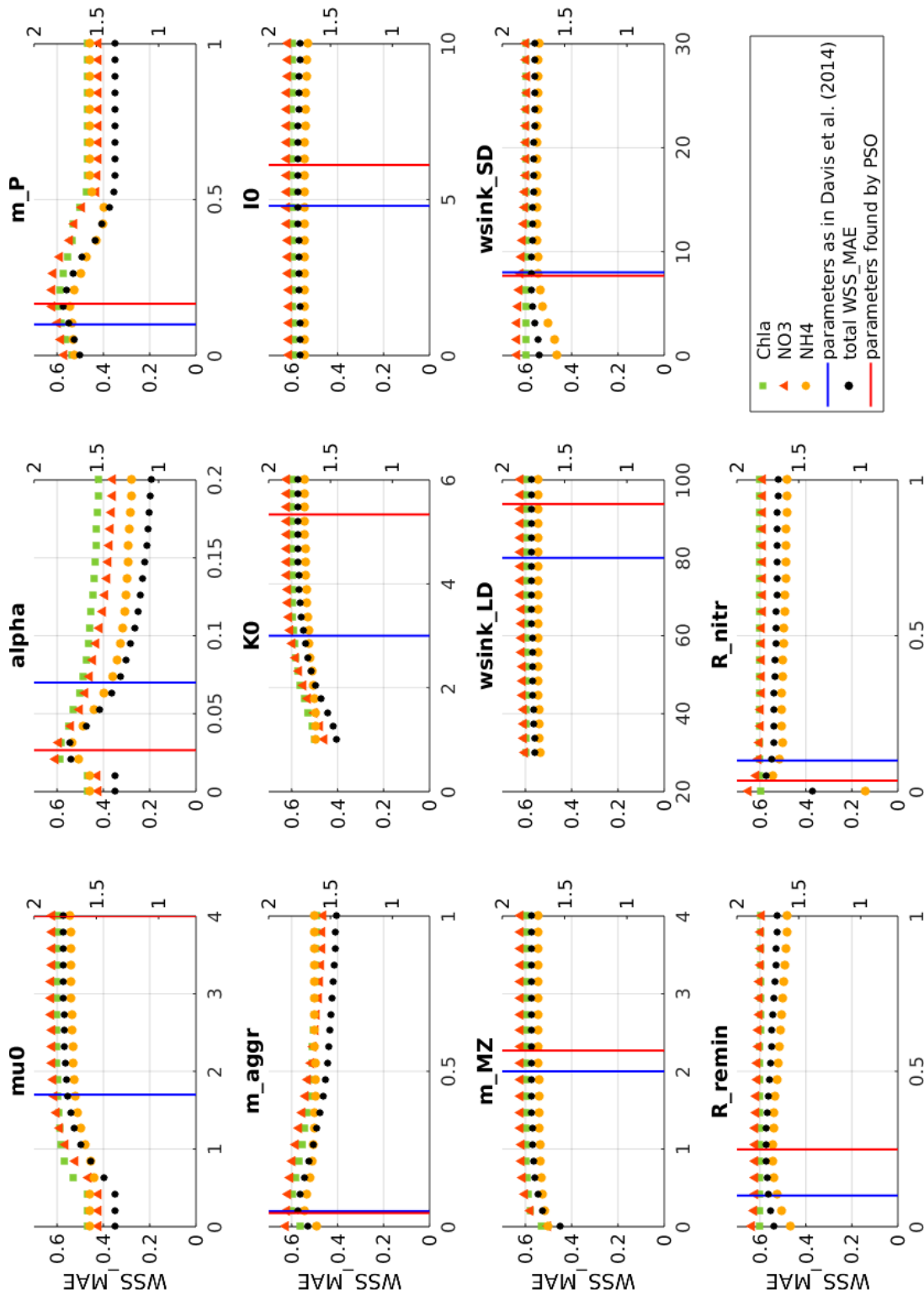


Figure 5.9: Parameters sensitivity analysis. PS-1D run with parameters found by PSO was the base case (straight red line) of the analysis. One at a time, parameter was varied in its equally-divided space range, WSS_{MAE} was calculated for variables Chla (green squares), NO_3 (red triangle), NH_4 (orange dots), and whole model (black dots). Blue line marked parameter values of the outer coast model for comparison.

PSO best parameter set is the one that yields highest model goodness-of-fit. Figure 5.9 suggests that I_0 , m_{MZ} , w_{sink_LD} do not affect the PS-1D model performance given their parameter ranges. Among all the parameters, α stands out as the most sensitive parameter that considerably influences model fitness. Indeed, table 5.1, which displays WSS_MAE difference between the PSO best and the *Davis et al.* (2014) parameter set, points out that the contribution of α to model improvement is far greater than all other parameters combined. (0.38 compare to 0.194, respectively). Given light is one of the vital factors controlling phytoplankton growth rate, and chapter 4 denoted considerable change in the main basin Puget Sound underwater light, it is understandable that initial growth-light slope (α), a light-related parameter, turns out to be highly influential.

One would expect that the parameters that vary most in PSO would turn out to be insensitive parameters. This is the case for I_0 , m_{MZ} , K_0 , but μ_0 . The reason is that I_0 , m_{MZ} , K_0 are direct parameters controlling microzooplankton (MZ) biomass, while μ_0 indirectly influences MZ biomass through phytoplankton biomass. As observations of MZ biomass are not available, MZ-direct parameters are free to move in their spaces or are insensitive. μ_0 , on the other hand, is controlled by phytoplankton biomass observations, thus compensating the model performance (or its sensitivity to the model) for its free movement.

Parameter	WSS_MAE difference
w_{sSD}	$1.3 \cdot 10^{-4}$
m_{MZ}	$5 \cdot 10^{-4}$
w_{sLD}	$5.6 \cdot 10^{-4}$
I_0	$2.4 \cdot 10^{-3}$
m_{aggr}	$4.1 \cdot 10^{-3}$
R_{remin}	0.021
R_{nitr}	0.036
μ_0	0.037
K_0	0.05
m_P	0.05
α	0.38

Table 5.1: WSS_MAE (index of model – observation agreement) difference between model runs with PSO-optimized parameters and parameters from the outer coast model

5.4 Selecting final parameters

To examine how each parameter in the best PSO parameter set influences the PS-1D model behaviour (via WSS_MAE) in comparison to corresponding *Davis et al.* (2014)'s parameter and vice versa, *Davis et al.* (2014)'s parameter values are put back in the PS-1D model in the order shown in table 5.1. Table 5.2 presents WSS_MAE of Chla, nitrate (NO_3), ammonium (NH_4) and of the whole model at each parameter replacement. As can be guessed from previous results, parameters: small detritus sinking rate (w_{sSD}), microzooplankton mortality (m_{MZ}), large detritus sinking rate (w_{sLD}), microzooplankton maximum ingestion rate (I_0), and phytoplankton loss via aggregation (m_{agg}) do not change the PS-1D model performance, thus these parameters can remain as given in *Davis et al.* (2014).

Table 5.3 again clearly restates notable model enhancement with the PSO best parameters when comparing the PS-1D performance between usage of the PSO best

parameter set and *Davis et al.* (2014) on the top layer of 20 meter and the whole water column.

In summary, table 5.4 presents the final PS-1D parameters for the main basin Puget Sound in comparison with the *Davis et al.* (2014) parameters. The parameters that potentially improve model performance are highlighted.

Substitue	WSS_MAE				% worsen
	Chla	NO_3	NH_4	Total	
parameters found by optimization	0.6	0.622	0.543	1.765	-
w_{sSD}	0.6	0.621	0.544	1.765	-
m_{MZ}	0.6	0.621	0.544	1.765	-
w_{sLD}	0.6	0.62	0.544	1.764	$5.7e^{-2}$
I_0	0.599	0.619	0.546	1.764	$5.7e^{-2}$
m_{agg}	0.6	0.619	0.545	1.764	$5.7e^{-2}$
r_{remin}	0.601	0.62	0.523	1.744	1.2
r_{nitr}	0.601	0.609	0.508	1.718	2.7
μ_0	0.597	0.611	0.504	1.712	3
K_0	0.582	0.564	0.5	1.646	6.7
m_P	0.585	0.559	0.507	1.651	6.5
α	0.513	0.501	0.438	1.47	16.7

Table 5.2: The PS-1D model performance worsens when PSO-proposed parameters are substituted one at a time with parameters from the outer coast model.

PS-1D runs with parameters	Top 20 meter			All data		
	Chla	NO_3	NH_4	Chla	NO_3	NH_4
- taken from (<i>Davis et al.</i> , 2014)	0.32	0.42	0.21	0.48	0.41	0.37
- as a result from parameterization and sensitivity analysis	0.59	0.78	0.53	0.6	0.62	0.55

Table 5.3: Comparison of PS-1D performance using PSO and sensitivity analysis proposed parameters (or final PS-1D parameters, table 5.4, figure 5.5 and 5.7) to parameters taken from *Davis et al.* (2014)'s study. The model performance is evaluated by Willmott Skill Score mean absolute error (WSS_MAE)

Parameter	Description	Unit	Davis et al.	PS-1D
att_{bg}	Light attenuation by water column	m^{-1}	0.05	0.15
att_{fw}	Light attenuation by fresh water	m^{-1}	-0.0065	0
$attp$	Light attenuation by phytoplankton	$m^{-1} \mu M N^{-1}$	0.03	0.026
μ_0	Maximum phytoplankton growth rate	d^{-1}	1.7	4
k_{min}	Minimum half-saturation for NO_3	$\mu M N$	0.1	0.1
α	Initial growth-light slope	$(W m^{-2})^{-1} d^{-1}$	0.07	0.027
φ_{NH_4}	Preference for NH_4		2	2
mp	Phytoplankton mortality	d^{-1}	0.1	0.163
m_{agg}	Phytoplankton loss via aggregation	$(\mu M N)^{-1} d^{-1}$	0.05	0.05
I_0	Microzooplankton maximum ingestion rate		4.8	4.8
K_0	Microzooplankton grazing half-saturation	$\mu M N$	3	5.3
ϵ	Microzooplankton growth efficiency		0.3	0.3
mmz	Microzooplankton mortality	d^{-1}	2	2
f_{ex}	Fraction of grazing excreted to NH_4		0.5	0.5
r_{remin}	Detrital remineralisation rate	d^{-1}	0.1	0.25
w_{sSD}	Small detritus sinking rate	$m d^{-1}$	8	8
w_{sLD}	Large detritus sinking rate	$m d^{-1}$	80	80
r_{nitr}	Nitrification rate		0.1	0.035

Table 5.4: The final PS-1D model optimized parameter set of main basin Puget Sound, compared with (Davis et al., 2014) values for the outer coast. Parameters suggested to be changed are in bold. μMN = mmol nitrogen m^{-3} .

5.5 Discussions and Conclusions

The PS-1D parameterisation restates a classical problem of parameter underdetermination in marine biogeochemical modelling. Often, there are too many parameters to be adequately constrained by the available data in marine ecosystem models, which commonly results in many parameter sets that fit chosen observations equally well (Anderson, 2010). Here, the PS-1D parameterized by the PSO produces numerous parameter sets that yield a similar index of agreement with observations (i.e., *WSS_MAEs* are almost unchanged from around the 50th iteration onwards (Figure 5.2), while fluctuation in parameters is still observed (Figure 5.4)). Among these equally good parameter sets, noticeably perhaps parameter sets obtained at iterations of 70th and 220th (Figure 5.6 and 5.8) which yield rather contrasting dynamics. The former represents a system of low turnover rate, while the later illustrates a fast turnover system (i.e., phytoplankton growth rate (μ_0), microzooplankton maximum ingestion rate (I_0) of the former are lower than the later). This is possible as standing stock (e.g., Chla biomass) is not an ideal proxy for a system's production, as a system of high input – high turnover rate – high production could produce the same standing stock as a system of low input – low turnover rate – low production. This suggests further studies are needed to constraint highly fluctuating parameters (e.g., μ_0 , I_0), and therefore to define the system dynamics.

Among fairly good parameter sets proposed by the PSO, decision on the appropriate parameter set might need to be carefully considered. For instance, despite representing opposite production dynamics, the two parameter sets discussed above do not show noticeable difference in bloom timing and nutrient, and just slight variation in bloom magnitude (Figure 5.6 and 5.8). Thus, it might not matter which of the two parameter sets outlined above should be employed in the PS-1D model given that this study selects bloom timing and bloom magnitude as major metrics to describe bloom dynamics. However, it would not be the case if this study investigated interaction between trophic levels and/or carbon export (or biological bump) as these processes

are largely influenced by the ecosystem production (Figure 5.10). Hence, extra caution is needed to apply the PS-1D to examine the trophic level dynamics and/or carbon export of the region.

Tightly coupled ecological parameters to environment need to be taken into account when examining the optimization outcomes. The ecological variables depend largely on the physical forcing conditions, while in terms of the parameter estimation procedure, prescribing the physical forcing is equivalent to the assumption that the forcing is correct. Thus, the optimized parameters are adjusted in such a way that they correct for any errors related to physical forcing conditions that influence the ecological state variables. For example, in Puget Sound, large freshwater inputs during summer potentially influence the hydrological structure of the region, which consequently affects underwater light environment and mixing. These are suggested as major drivers of Puget Sound plankton dynamics. The PS-1D model is represented by yearly vertical advection and mixing, which clearly cannot produce changes in mixing in summer, and therefore results in an overestimate of phytoplankton biomass during this season. Or in other words, the PS-1D parameterized by PSO cannot reproduce observed pattern of bloom succession (i.e., decline of first bloom in summer and formation of second bloom in autumn). The bloom succession might be captured by time-varying mixing. However, the PS-1D built upon available observations is not designed for that purpose. A more effective approach is to apply the PS-1D biological parameters to well-presented Puget Sound hydrodynamics of 2D or 3D models.

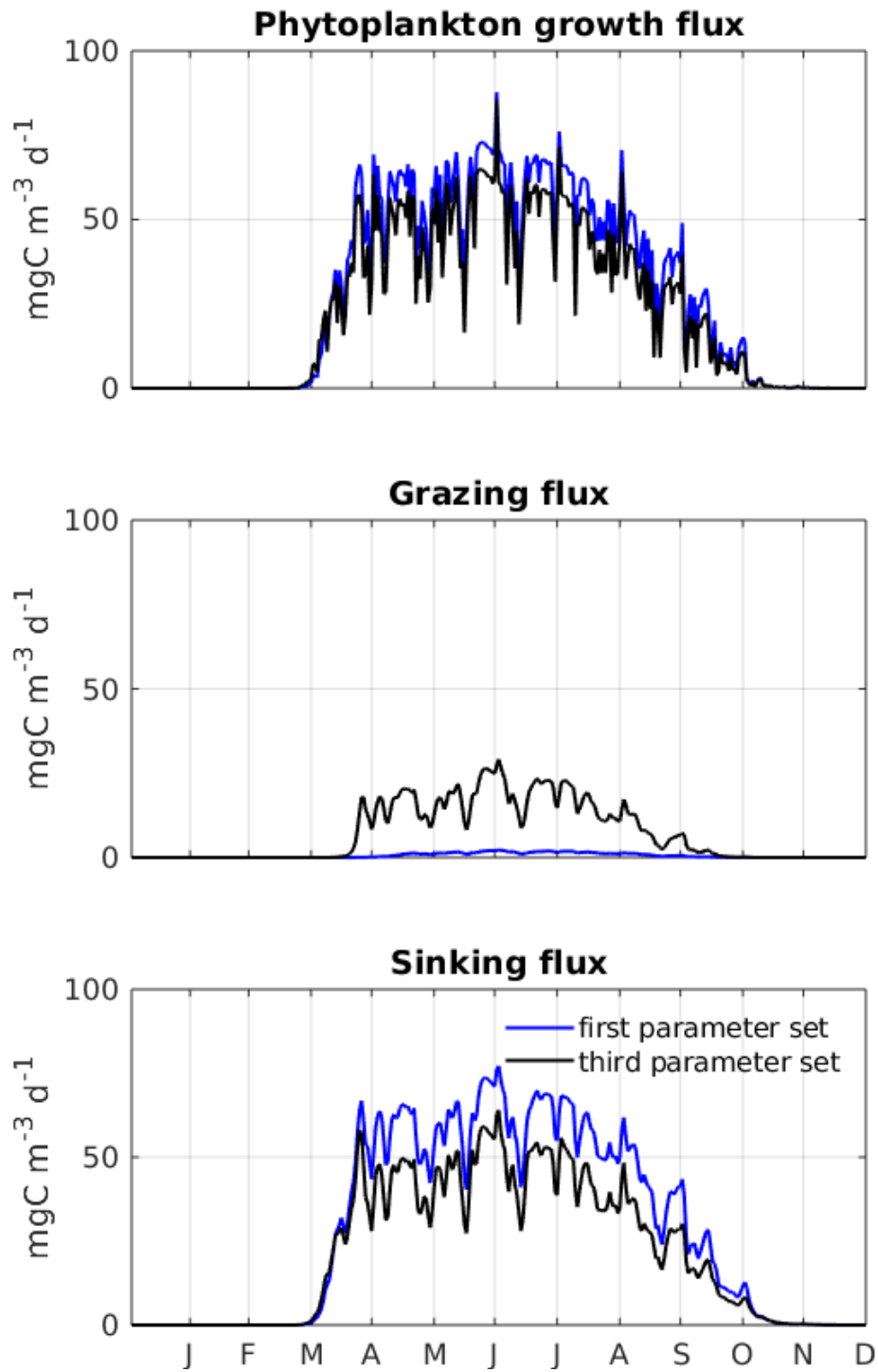


Figure 5.10: Differences in dynamics between the two parameter sets which produce similar model goodness-of-fit. The first and third parameter sets are taken at the 70th and 220th iteration of PSO. The figure shows clear difference in carbon transfer between trophic levels (via grazing) and carbon export (via sinking) between the two parameter sets.

Sensitivity analysis classifies the influence of parameters to total model performance. The ranking names initial growth-light slope (α) as the strongest constraint parameter, which might be a consequence of light environment complexity. The analysis ranks phytoplankton natural mortality (m_P) and microzooplankton half-saturation rate (K_0) as moderate constraints. Phytoplankton maximum growth rate (μ_0) and remineralization rates (r_{remin} and r_{nitr}) continue the ranking as potential influence parameters, and remaining parameters are listed as weak to non-constraint parameters. It is worth noting that weak constraint parameters might not be a robust conclusion as freedom in these parameters (e.g., I_0 , m_{MZ} , $w_{sink_{LD}}$) might again result from a lack of observations on unconstrained processes.

Our parameter sensitivity ranking differs from *Khangaonkar et al. (2012)*, whose rank listed the most sensitive as maximum photosynthetic rate (μ_0), grazing loss rate, settling rates ($w_{s_{SD}}$ and $w_{s_{LD}}$), and half saturation constants of nutrient uptake (equivalent to $k_{min} + 2\sqrt{k_{min}N_{tot}}$ in PS-1D model). The difference in ranking perhaps comes from model structures of and observations used in the two studies. First, the PS-1D employs 1-D vertical physical processes against the 3-D FVCOM model in *Khangaonkar et al. (2012)* study. Clearly, 3-D model would present the complex hydrodynamics of Puget Sound in greater details than simplified 1-D model. Second, model evaluation of the PS-1D model is based on 22-year monthly observations, while monthly observations of year 2006 is presented in *Khangaonkar et al. (2012)* study. Although the authors particularly reproduced phytoplankton succession in typical year of 2006, they might leave out the general dynamics, which emerges over long-term data and is often different from a typical year pattern. *Newton and Van Voorhis (2002)* study observed strong spatial and temporal variation in Puget Sound primary production, which suggests longer-term observations would be necessary to explain key features of the Puget Sound phytoplankton dynamics. Thirdly, a biogeochemical model (NPZD model) is described in the PS-1D, while CE-QUAL-ICM was demonstrated in *Khangaonkar et al. (2012)*. The two models deploy notably different light and nutrient functions, hence the photosynthesis. Finally, differences in model assessment skills might largely influ-

ence model goodness-of-fit estimation. The PS-1D performs Willmott Skill Score mean absolute error (WSS_MAE), whereas *Khangaonkar et al. (2012)* used root mean square error (RMSE). *Willmott et al. (2012)* pointed out a problem of RMSE is that it possibly over-weights the influence of larger errors, when squared, on the sum-of-squared error, which results in a smaller RMSE, hence mistakenly yield higher model goodness-of-fit.

While parameterisation suggests phytoplankton growth rate (μ_0), and microzooplankton maximum ingestion rate (I_0) might need to be accurately constrained to define system dynamics, sensitivity analysis highlights initial growth-light slope (α) is the most sensitive parameter to the model performance. This is consistent with findings in chapter 4, which drew significant influence of underwater light environment to the PS-1D model performance. Phytoplankton mortality (m_P) and microzooplankton grazing half-saturation (K_0) moderately affect model goodness-of-fit, while phytoplankton growth rate (μ_0), nitrification rate (r_{nit}), and remineralization rate (r_{remin}) show slight control on the model performance (Table 5.2).

Overall, parameterisation and analysis propose the parameter set that greatly improves fitness of the PS-1D model to observations (e.g., on Chla, nitrate and ammonium) in comparison to the outer coast (or *Davis et al. (2014)*) parameters (Table 5.3). The proposed parameter set captures bloom timing well along with the sharp change in nutrient (decline in nitrate, and increase in ammonium) happening in the second half of April (Figure 5.7). However the parameter set underestimates bloom magnitude as well as nutrient shortage in summer. The underestimation of bloom magnitude might be due to the lack of microzooplankton observations to constrain microzooplankton population. The shortage of nutrients in summer, on the other hand, is due to 1-D physical model limitation, whereas the yearly vertical mixing easily overestimates the summer mixed layer depth. Although the proposed parameter set undervalues bloom magnitude, it is worth noting that blooms where Chla concentration is over $15 \mu g L^{-1}$ are rarely observed (just 3 events of Chla concentration over $15 \mu g L^{-1}$ in total 160 Chla profiles over 17 year observations). Almost all blooms are at Chla concentration below

$15 \mu\text{gL}^{-1}$ which is reported by the PS-1D model (Figure 5.5 and 5.6). Turning back to question what parameters in *Davis et al.* (2014) parameter set improve the outer coast model goodness-of-fits in main basin Puget Sound, initial growth-light slope (α) evidently is the first and foremost parameter which needs to be adjusted to significantly improve the outer coast model performance in main basin Puget Sound (Table 5.2). Further parameters that should be adjusted might depend on compensation between the model performance improvement needed and processes willing to be changed.

This study has extensively explored the PS-1D parameter space and proposed the parameter set (Table 5.4) that adequately captures bloom timing, one of important metrics to describe phytoplankton bloom. This finding also answers the first question stated in this study aims (Section 1.4). The next chapter will employ this parameter set to further investigate climate-linked drivers – pathways (section 1.4) to finally answer the remaining questions.

Chapter 6

Climate-linked drivers and pathways regulate Puget Sound phytoplankton bloom

Although the Puget Sound plankton seasonal cycle is well described, quantitative estimation of the regional phytoplankton bloom timing and magnitude (or production), as well as the impact of environmental variation during the year, are not. This chapter employs the PS-1D model which was built from previous chapters to explore what controls the phytoplankton bloom onset and production in the Puget Sound, and how these are likely to be impacted by factors which are driving changes in the Puget Sound. At the same time, the exploration of phytoplankton bloom onset and magnitude also examines: potential changes in underwater light that may disrupt juvenile salmon visual search due to high phytoplankton concentration, and a period of strong nutrient limitation in summer as a proxy to *Alexandrium* HABs occurrence. Thus, the chapter begins by introducing numerical experiments which include environmental forcings range and interpretation of the experiments (Section 6.1). Outcomes of the numerical experiments are then presented in the next section (Section 6.2). Finally, discussions and conclusions are given in section 6.3.

6.1 Numerical experiments set up

As stated in section 1.4 and figure 1.2, this study investigates Puget Sound phytoplankton blooms through metrics of (1) the annual primary production, (2) spring bloom timings, (3) spring and summer phytoplankton concentrations, and (4) the occurrence or non-occurrence of strong nutrient limitation in summer. These metrics are examined through light and nutrient limitation, and temperature variation. While temperature is a direct regional climate factor, light and nutrient limitation are regulated by mixing, vertical advection, underwater light, and deep nutrient, which in turn are influenced by regional climate such as river flow, wind stress, and cloud cover.

6.1.1 Investigated forcing ranges

Variability of mixing, vertical advection, temperature, photosynthetic active radiation (PAR), nutrient and light attenuation background (att_{bg} as in equation 4.4) are defined based on the values defined in the PS-1D model in the last chapter (the base case).

Mixing. Mixing in the main basin Puget Sound is driven by tides at the bottom, and by wind and stratification at the surface. *Garnier (2020), in preparation*, proved that wind and stratification play a dominant role on mixing in comparison to tide. Indeed, figure 2.9 showed mixing changes mostly in the top 20 metres. Thus, variation of mixing is estimated through its variation in the top 20 m. Integral of mixing from MoSSea model over the top 20 m is averaged (namely κ_{0-20m}). Then, mean ($\bar{\kappa}_{0-20m}$) and standard deviation ($\hat{\kappa}_{0-20m}$) are calculated over time. The possible range of mixing is then defined $[(\bar{\kappa} - 2\hat{\kappa}), (\bar{\kappa} + 2\hat{\kappa})]$ or $[1.2 \cdot 10^{-04}, 2.6 \cdot 10^{-04} (m^2 s^{-1})]$. Upon this range, κ_{0-20m} is equally divided into 20 spaces. These values are then scaled by $\bar{\kappa}_{0-20m}$ to generate mixing profile variation (Figure 6.1).

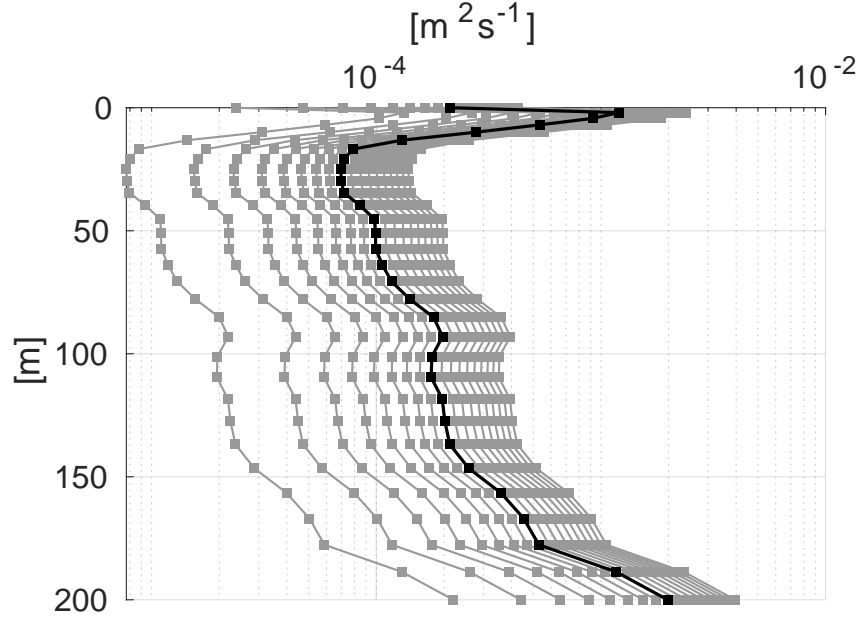


Figure 6.1: Mixing profile variation (gray) with black profile showing yearly average as given in figure 2.9

Vertical advection. Vertical advection variation is defined through water transported in and out the central Puget Sound in a similar way to determine vertical advection as given in section 2.3.1. This study estimates vertical advection variation through change of velocity at bottom of upper layer, H_{ul} (Figure 2.2). From personal communication with P. MacCready, University of Washington, average transported water ($\overline{Q_{in}}$) flowed into the main basin Puget Sound through Ad.Inlet (Figure 2.2) was 29000 ($m^3 s^{-1}$) and its standard variation (\hat{Q}_{in}) was 7000 ($m^3 s^{-1}$) (data of 2018). Assuming vertical advection variation is proportional to variation of transported water, results in

$$\widehat{\Delta Q} = \frac{\hat{Q}_{in}}{Q_{in}} \cdot \Delta Q$$

where $\Delta Q = 4000$ ($m^3 s^{-1}$) according to *Sutherland et al.* (2011) (Section 2.3.1). As a result $\widehat{\Delta Q} = 950$ ($m^3 s^{-1}$). Or variation in vertical advection at bottom of the upper layer H_{ul} is $\hat{w}_{H_{ul}} = \widehat{\Delta Q} / (B \cdot L) = 0.7 \cdot 10^{-05}$ (ms^{-1}). Thus, possible range of $w_{H_{ul}}$ was

$[w_{H_{ul}} - 2\hat{w}_{H_{ul}}, w_{H_{ul}} + 2\hat{w}_{H_{ul}}] = [1.5 \cdot 10^{-05}, 4.3 \cdot 10^{-05}] (ms^{-1})$. Over the range, $w_{H_{ul}}$ is equally divided in 20 spaces. Vertical advection variation is defined in a similar way to the mixing profile variation given above (Figure 6.2).

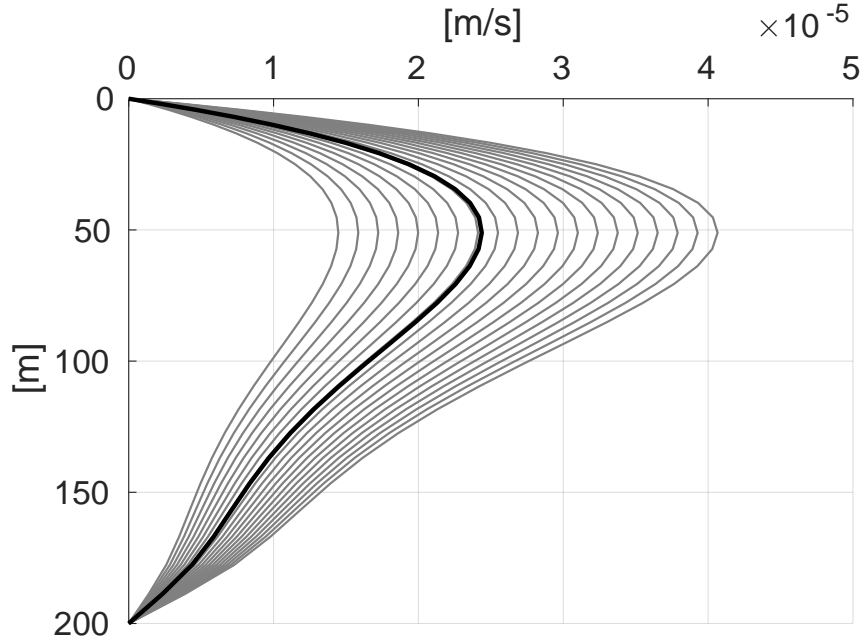


Figure 6.2: Vertical advection profile variation (gray) with black profile showing yearly average as given in figure 2.8

Temperature. As the global temperature is projected to be 3°C higher by the end of the century (*IPCC*, 2018), this study defines temperature range +3 and -3 around the mean temperature of the top 20 m. The range is then divided in to 6 equal spaces.

PAR and deep nutrient. PAR annual cycle (Figure 3.2) is varied in between half and double of its annual average, while variation of deep nutrient lies in a range of half and double a value at the bottom of nutrient profile (Figure 3.1).

One at a time, the PS-1D model is run for each driver upon its range of values given above. After a model run, metrics of (1) annual primary production P_{tot} , (2) bloom date t_{bloom} , (3) phytoplankton during outmigration (spring and summer) of two major

salmon species, Chinook $P_{outmigr}^{chinook}$ and Steelhead $P_{outmigr}^{steelhead}$, and (4) number of days that nutrient is in short supply Δt_{nut} , are calculated. Further details on the four metrics, with metric (3) subdivided, are given as follows:

1. Total annual primary production PP_{tot} , converted to units of $gCm^{-2}yr^{-1}$ assuming a C:N ratio of 106:16 mol:mol;
2. Date of the spring bloom t_{bloom} , defined as the day of the year when cumulative, vertically-integrated phytoplankton biomass reached 15% of its annual total;
3. Phytoplankton concentration during the seasonal period and depth layer associated with steelhead outmigration ($P_{outmigr}^{steelhead}$), mid April–first week of June (year-days 109–159), and 0–2 m depth;
4. Phytoplankton concentration during chinook outmigration in summer $P_{outmigr}^{chinook}$, first week of June–mid September (year-days 159–258), 0–15 m depth;
5. Incidence of strong nutrient stress in summer Δt_{nut} , defined as the count of days on which surface nutrient concentration is less than $3 \mu MNm^{-3}$ (or $mmolNm^{-3}$).

6.1.2 Experimental Interpretation

The primary timescale of analysis is interannual variation in seasonal averages. Table 6.1 presents seasonal averages (i.e. spring: April – June or summer: July – September) across a number of years (e.g. mixing, deep nutrient, temperature, surface PAR). In some cases, it is not possible to calculate interannual variation in this way. For example, variation in exchange flow (and hence vertical advection) has been calculated across one annual cycle in LiveOcean (*MacCready et al., 2020, in prep*), but never across a useful ensemble of years. In these cases, event-scale (10 day) variation is interpreted as a high upper bound on the unknown interannual variation (e.g. vertical advection, background light attenuation). Also, in some cases, it is not clear whether seasonal averages are indeed the timescale on which the environment drives variation in phytoplankton dynamics. For instance, weak to nonexistent correlations between

stratification and Chla on the monthly scale and longer were observed in a 3-year high resolution profiling buoy in Carr Inlet, South Puget Sound (*Banas et al.*, 2019). Thus, event-scale (10 day) variation for select quantities (e.g. mixing, surface PAR) are reported to support interpretation.

Relating these scales of variability in drivers to the associated variability in phytoplankton metrics is done through multiplication and the chain rule. For example, the variability in spring bloom date t_{bloom} in relation to interannual variability in spring riverflow Q_r , via the effect of riverflow on stratification and consequently on mixing (Figure 1.2), is given by

$$\Delta t_{bloom} = \Delta(\log_{10} Q_r) \cdot \frac{\partial(\log_{10} \rho)}{\partial(\log_{10} Q_r)} \cdot \frac{\partial(\log_{10} \kappa_v)}{\partial(\log_{10} \rho)} \cdot \frac{\partial t_{bloom}}{\partial(\log_{10} \kappa_v)} \quad (6.1)$$

where $\Delta(\log_{10} Q_r)$ is given in table 6.1, $\frac{\partial(\log_{10} \rho)}{\partial(\log_{10} Q_r)}$, and $\frac{\partial(\log_{10} \kappa_v)}{\partial(\log_{10} \rho)}$ as in table 6.2, while $\frac{\partial t_{bloom}}{\partial(\log_{10} \kappa_v)}$ will be calculated from the numerical experiment outputs. The variation of phytoplankton metrics (e.g., t_{bloom}) to environmental forcings (e.g., $\log_{10} \kappa_v$) will be given in the next section (section 6.2) and table 6.3.

6.2 Results

Figure 6.3 – 6.7 present variation of four phytoplankton metrics upon drivers' range around the base case (red dot is the PS-1D model run with parameters concluded in chapter 5). It can be seen that surface PAR is consistently the driver that causes the highest variation in most metrics (apart from period nutrient limitation in summer), mixing κ_v is the second most influential parameter. On other side of the variation spectrum, temperature seems to have the smallest influence, and deep nutrient produces almost unnoticeable variation in bloom date.

To obtain sensitivity of phytoplankton metrics to physical drivers (e.g., $\frac{\partial t_{bloom}}{\partial(\log_{10} \kappa_v)}$), slopes of tangents to the base case values (at red dots) on each metric and its cor-

<i>Quantity</i>	<i>Units</i>	<i>Symbol</i>	<i>Interannual</i>		<i>Event-scale</i>		<i>Comments</i>	<i>Sources</i>
			<i>variation (2 s.d.)</i>	<i>variation (2 s.d.)</i>	<i>variation (2 s.d.)</i>	<i>variation (2 s.d.)</i>		
			Δx	$\Delta(\log_{10} x)$	Δx	$\Delta(\log_{10} x)$		
Riverflow	$\text{m}^3 \text{ s}^{-1}$	Q_r	0.19		0.28		spring	
			0.22		0.38		summer	
Wind stress	Pa	τ	0.082		0.24		spring	<i>Garnier (2020)</i>
			0.078		0.22		summer	
Vertical advection	m day^{-1}	w_{adv}			0.99		derived from exchange flow Q_{ex}	<i>Garnier (2020)</i>
Main Basin deep nutrients	mmol m^{-3}	N_{deep}	2.8					
Temperature	$^{\circ}\text{C}$	T_{20}	1.2				0–20 m, spring	
			0.8				summer	
Surface PAR	W m^{-2}	E_0	8.6		34		spring	
			8.6		43		summer	
Background light attenuation	m^{-1}	att_{bg}			0.03		confidence limits on regression	<i>Chapter 4</i>

Table 6.1: Estimates of environmental variability used in the scaling analysis. Scales of variation denoted by Δ are defined throughout as 2 standard deviations

Sensitivity of mixing to stratification	$\frac{\partial(\log_{10} \kappa_v)}{\partial(\log_{10} \delta\rho)}$	-0.89 ± 0.37		<i>Garnier (2020)</i>
Sensitivity of mixing to wind stress	$\frac{\partial(\log_{10} \kappa_v)}{\partial(\log_{10} \tau)}$	0.67 ± 0.29		
Sensitivity of stratification to riverflow	$\frac{\partial(\delta\rho)}{\partial Q_r}$	1.87	spring	<i>Garnier (2020)</i>
		1.14	summer	

Table 6.2: Sensitivity of mixing to stratification and wind stress, and of stratification to riverflow

responding physical driver are calculated (Table 6.3). The signs present direction of phytoplankton metrics' changes in relation to variability in physical drivers.

Table 6.4 presents variability in phytoplankton metrics associated to scales of variability in drivers given in table 6.1 and followed equation 6.1. The mark ** indicates the most influential process for each metric, while * denotes other potentially important (second order of importance) mechanisms. Table 6.4 allows this study to reduce all possible climate-induced drivers – pathways given in figure 1.2 into a focused diagram, figure 6.8, of leading and potentially important mechanisms (marked with ** and * respectively in table 6.4). At a first look, the table 6.4 and figure 6.8 again confirm the important role of PAR on interannual variation across most metrics. Further discussions on the role of drivers on each metric will be provided in the next section.

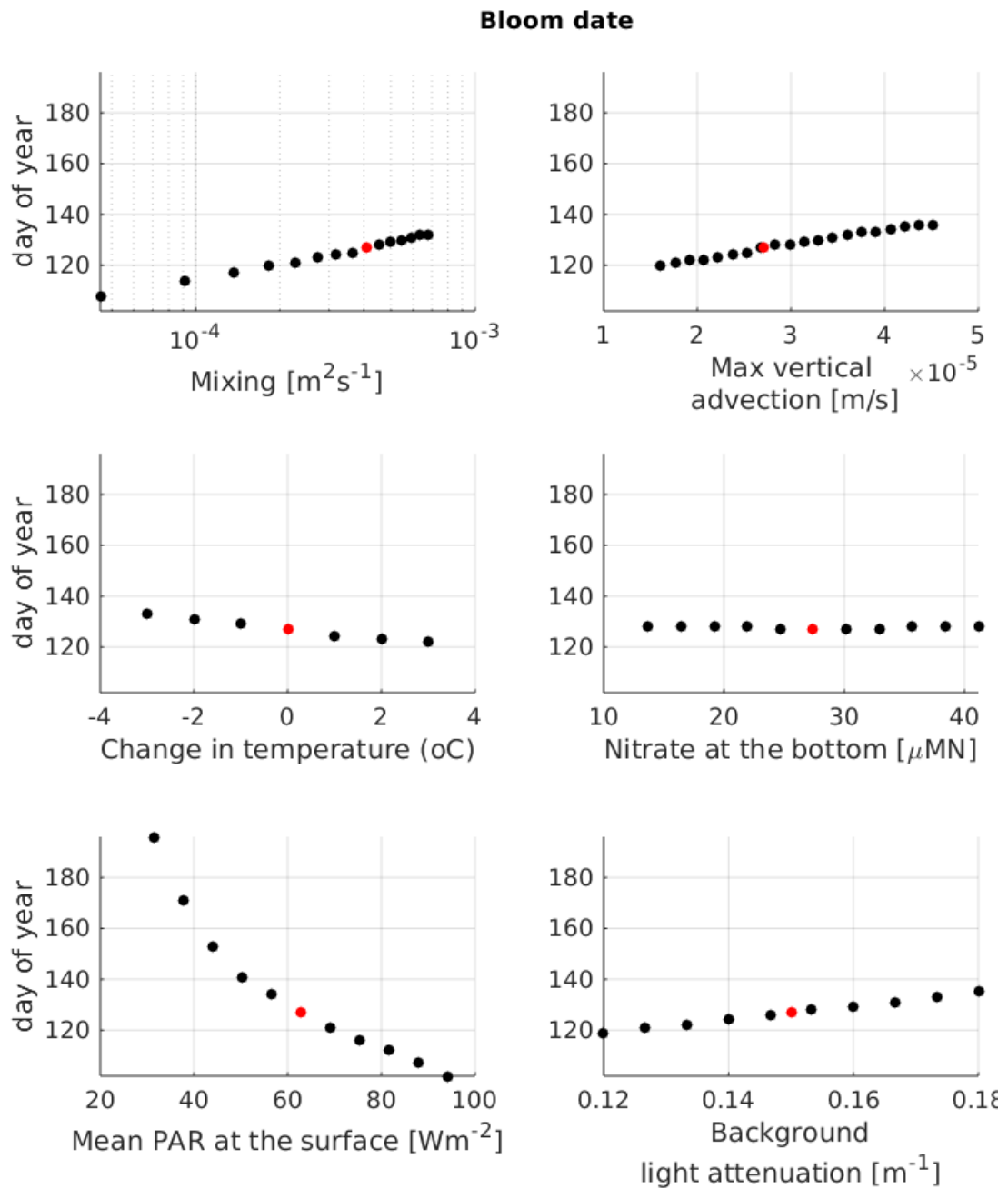


Figure 6.3: Responses of bloom date (metric i) to environmental forcings, where the red dot represents the base case (PS-1D runs with parameters concluded in chapter 5)

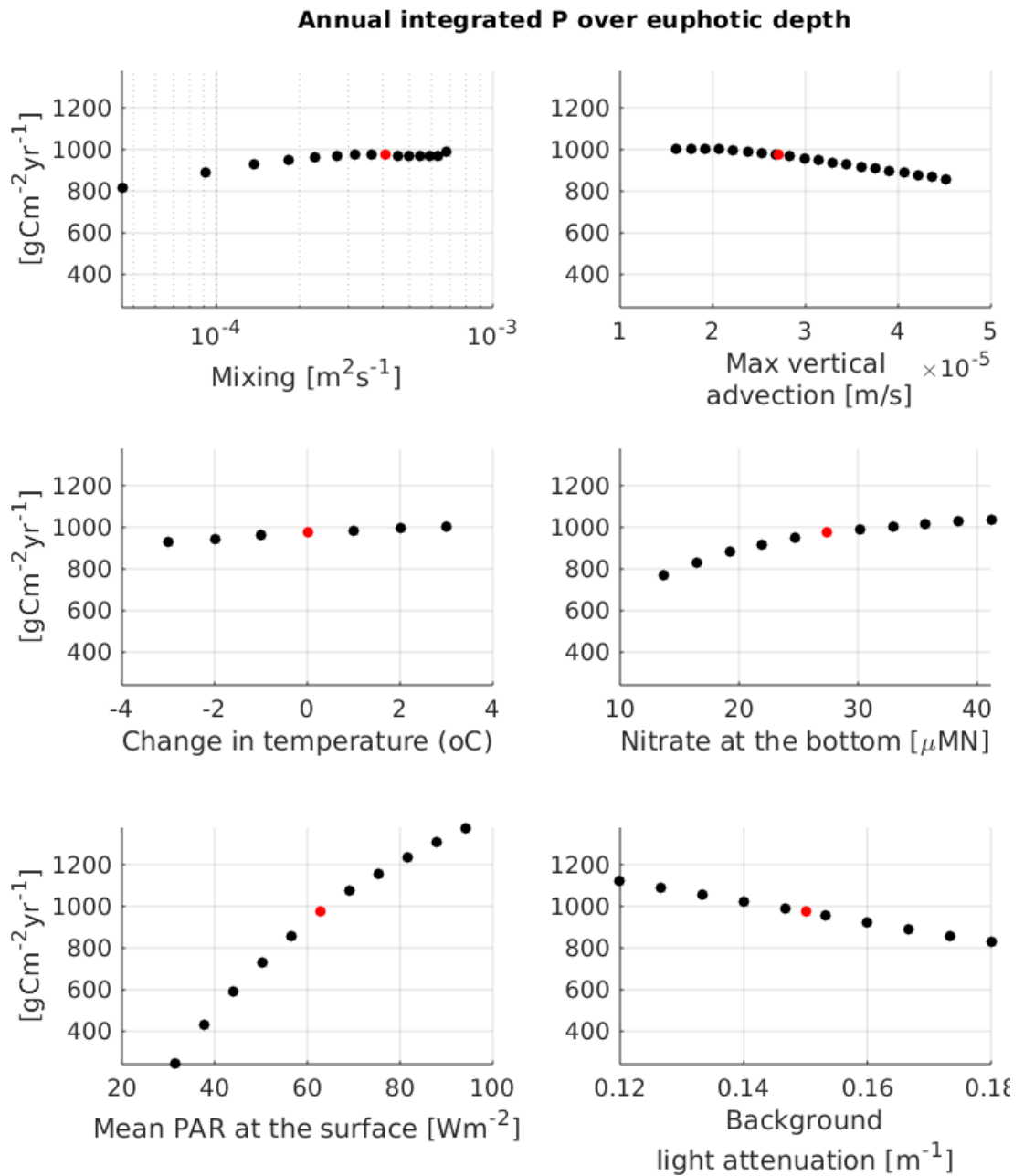


Figure 6.4: Responses of primary production (metric *ii*) to environmental forcings, where the red dot represents the base case (PS-1D runs with parameters concluded in chapter 5)

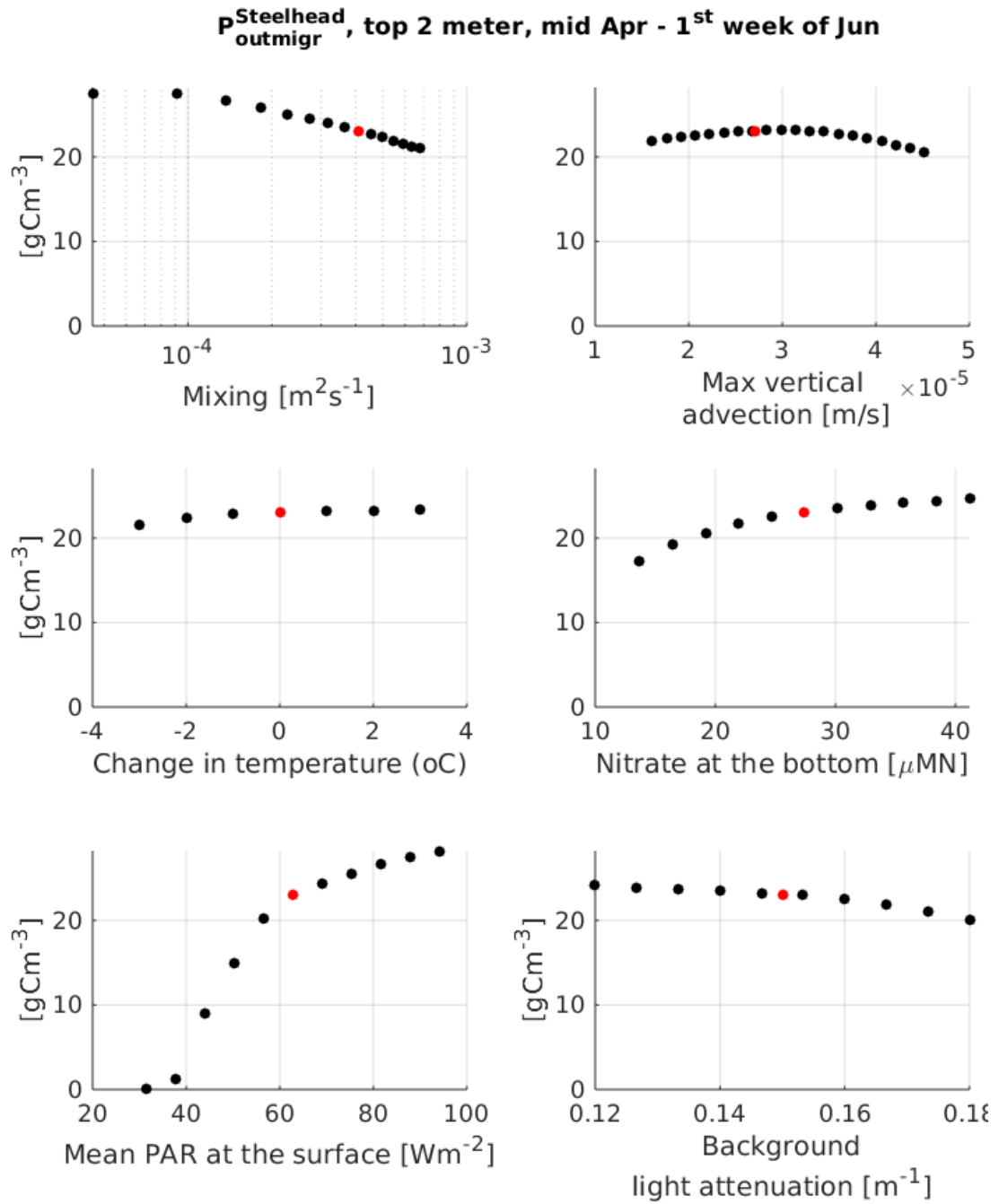


Figure 6.5: Responses of phytoplankton concentration at Steelhead outmigration (metric (iii)) to environmental forcings, where the red dot represents the base case (PS-1D runs with parameters concluded in chapter 5)

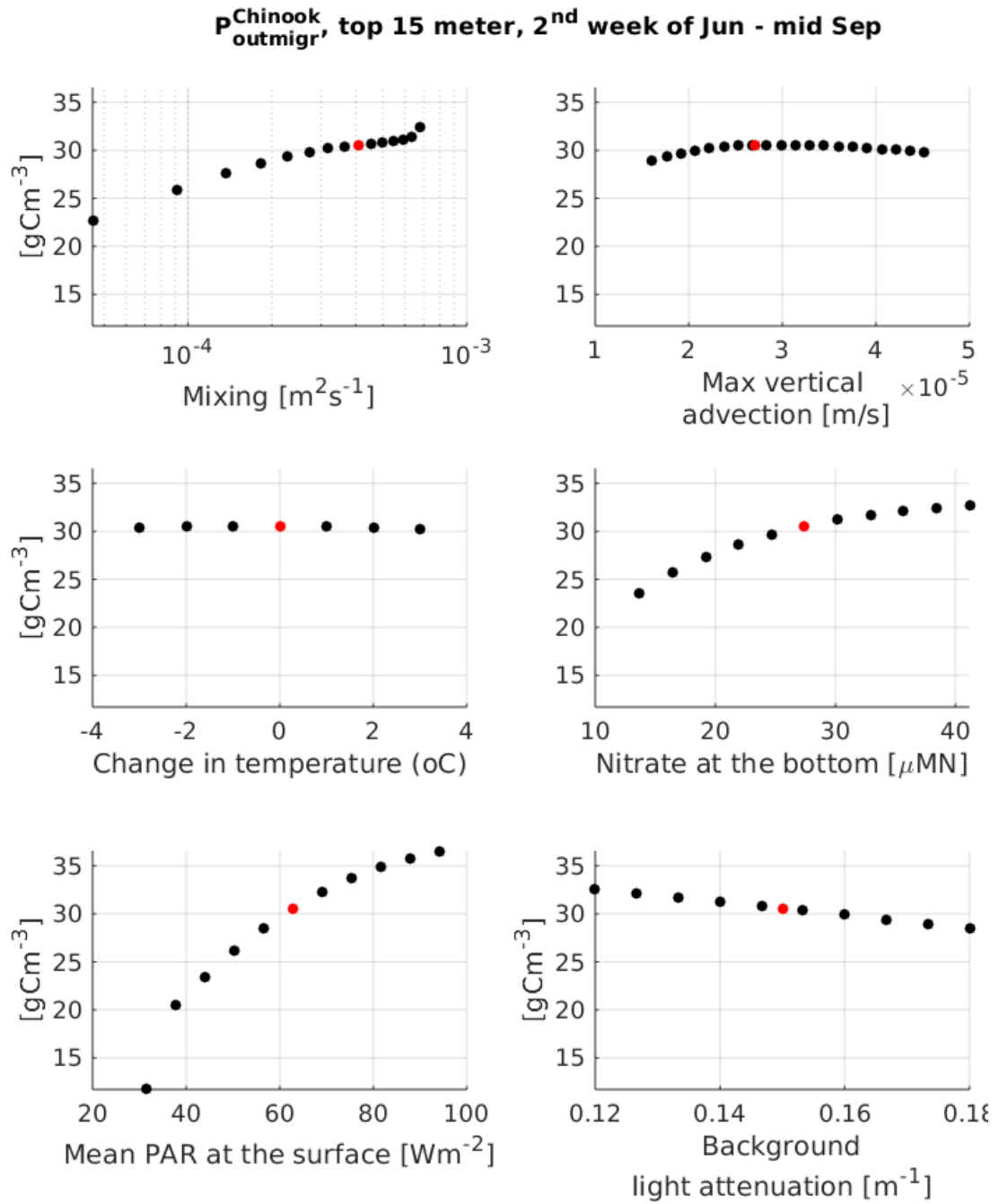


Figure 6.6: Responses of phytoplankton concentration at Chinook outmigration (metric (iii)) to environmental forcings, where the red dot represents the base case (PS-1D runs with parameters concluded in chapter 5)

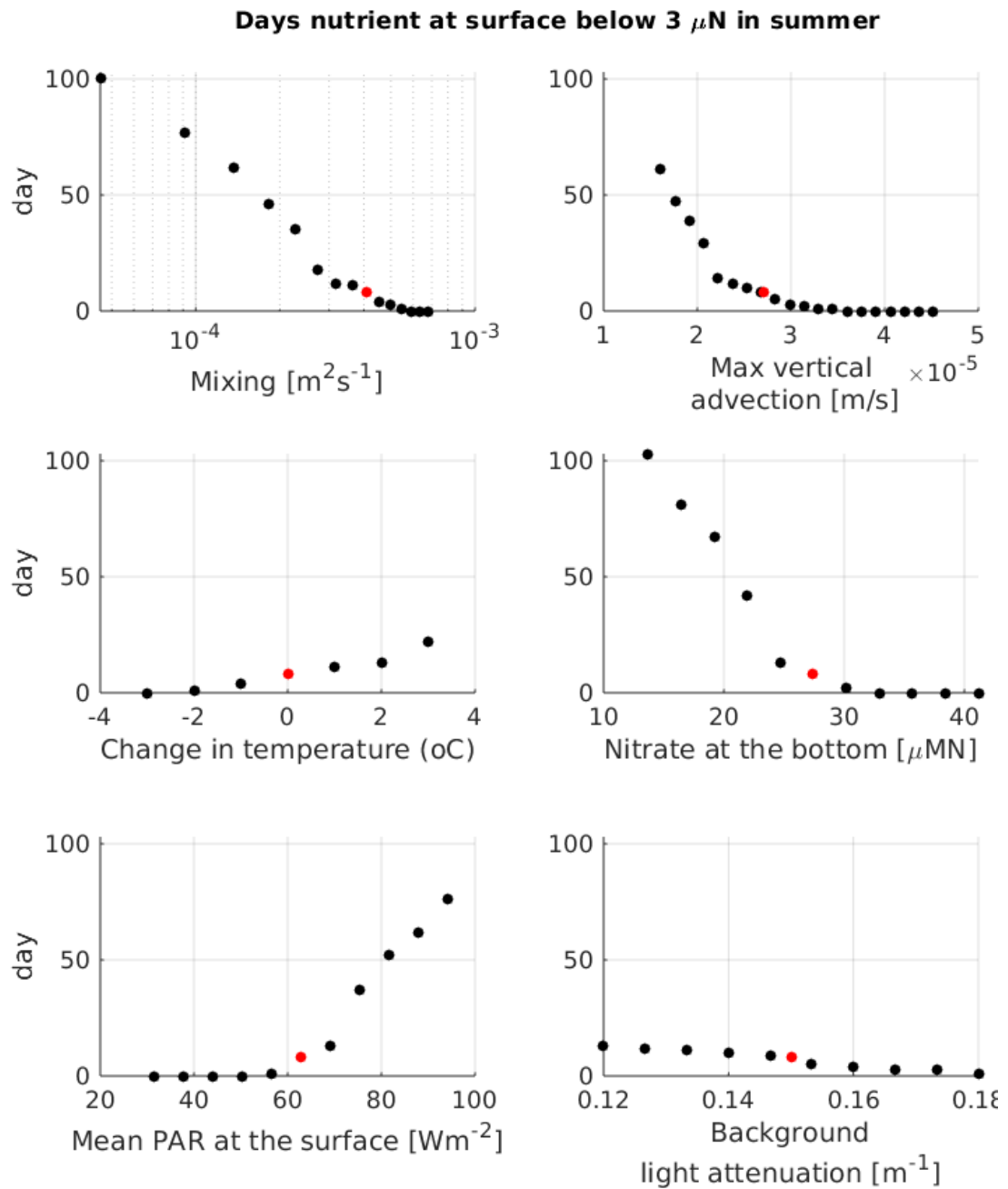


Figure 6.7: Responses of duration nutrient limitation in summer (metric (*iv*)) to environmental forcings, where the red dot represents the base case (PS-1D runs with parameters concluded in chapter 5)

Response of phytoplankton metrics (\rightarrow) to variability in physical drivers (\downarrow)	Annual primary production PP_{tot}	Date of spring bloom t_{bloom}	Phyto conc. during steelhead outmigration (spring, 0–2 m) $P_{steelhead}^{outmigr}$	Phyto conc. during chinook outmigration (summer, 0–15 m) $P_{chinook}^{outmigr}$	Duration of strong nutrient stress δt_{nut}
<i>Base-case value</i>	973 ($gC\ m^{-2}\ yr^{-1}$)	127 (year day)	23 ($g\ C\ m^{-3}$)	31 ($g\ C\ m^{-3}$)	8 (day)
Mixing $log_{10}(k_v)$	-28 ($log_{10}\ m^2\ s^{-1}$)	31	-9	3	-72
Vertical advection w_{adv}	-67 ($m\ d^{-1}$)	8	0.4	0.3	-23
Near-surface temperature T_{20}	13 ($^{\circ}C$)	-3	0.2	-0.02	3.5
Deep nutrient concentration N_{deep}	8 (μMN)	0	0.2	0.3	-2
Surface PAR E_0	17 ($W\ m^{-2}$)	-1	0.3	0.3	1
Background light attenuation att_{bg}	-4900 (m^{-1})	300	-41	-67	-600

Table 6.3: Response of phytoplankton metrics (PP_{tot} , etc.) to variability in physical drivers (*mixing*, etc). Each value is a sensitivity defined as $\frac{\partial(Phytoplankton\ metric)}{\partial(physical\ driver)}$ (slope of the tangent at the red dot in figure 6.3 – 6.7), for example, the sensitivity of PP_{tot} to mixing has unit of $gC\ m^{-2}\ yr^{-1}\ (log_{10}\ m^2\ s^{-1})^{-1}$

	Annual primary production	Date of spring bloom	Phyto conc. during steelhead outmigration (spring, 0–2 m)	Phyto conc. during chinook outmigration (summer, 0–15 m)	Duration of strong nutrient stress
<i>Base-case value</i>	PP_{tot} 973 $\text{gC m}^{-2} \text{yr}^{-1}$	t_{bloom} 127 yearday	$P_{steelhead}^{outmigr}$ 23 mg C m^{-3}	$P_{chinook}^{outmigr}$ 31 mg C m^{-3}	δt_{nut} 8 d
<i>Scale of variability in \rightarrow via \downarrow</i>	<i>Interann.</i>	<i>Interann. Event</i>	<i>Interann.</i>	<i>Interann.</i>	<i>Interann.</i>
Wind stress τ (via mixing)	1.5	1.7	0.5	0.16	3.8
Riverflow Q_r (via stratification and mixing)	10	9.8**	2.8**	0.7	16**
Exchange flow Q_{ex} (via vertical advection)	$\ll 66$	$\ll 7.9^*$	$\ll 0.4$	$\ll 0.3$	$\ll 23^*$
Deep nutrient concentration N_{deep}	22.4	0	0.56	0.84	5.6
Near-surface temperature T_{20}	15.6	3.6	0.24	0.02	2.8
Surface PAR E_0	146**	8.6**	2.6**	2.6**	8.6*
Background light attenuation att_{bg}	$\ll 147^*$	$\ll 9^*$	$\ll 1.2^*$	$\ll 2^*$	$\ll 18^*$

Table 6.4: Scales of variation in five metrics of phytoplankton production (PP_{tot} , etc.) associated with seven climate-linked drivers (τ , etc.). *Interann.* and *Event* indicate interannual variation in seasonal averages, and variation among 10 day averages within one season, respectively, and are given as an absolute value corresponding to 2 s.d. of variation in the driver (table 6.1). ** indicates the most influential process for each metric, and * denotes other potentially important (second order of importance) mechanisms

6.3 Discussions and Conclusions

6.3.1 Primary production

Annual primary production shows the clearest results, the strongest separation between major and minor effects. Variation in light limitation overrides variation in nutrient limitation. Seasonally-averaged incoming PAR appears to be sufficient to drive around 15% variation in annual primary production (table 6.4). Variation in background light attenuation, i.e. all effects of water-mass variation and freshwater influence, excluding self-shading by phytoplankton, is on the same scale ($att_{bg} = 0.15 \pm 0.03 \text{ m}^{-1}$, table 6.1) and varying att_{bg} on this scale in the PS-1D model also leads to 15% changes in PP_{tot} , however much of this variability in att_{bg} might average out on seasonal timescales.

It's worth noting that the PS-1D model does not include photoacclimation by individual cells, or succession of phytoplankton populations as environmental conditions change, and either mechanism would be expected to level out the response to variations in light conditions. Thus, the sensitivity of PP_{tot} in the analysis is likely to be a high estimate.

Strikingly, variations in mixing and circulation have very small effects on PP_{tot} on interannual timescales. This may be due to changes in mixing have opposite effects in spring (via light) and summer (via nutrient supply), or because while turbulent mixing shows intense variation on short time and spatial scales, it is almost constant in seasonal averages.

6.3.2 Spring bloom timing

Variation in surface PAR (via variation in cloud cover) again appears as a crucial influence on variation in spring bloom timing in the main basin Puget Sound. Historical variation in seasonally-averaged E_0 is sufficient to explain perhaps a 15 day range of spring bloom date ($\pm 2s.d.$), while event scale (10 day) variation in E_0 is several times

larger (table 6.4) and leads to more than 2-month variation in t_{bloom} in PS-1D ($\pm 2s.d.$). It is unclear about the actual historical variation in t_{bloom} in the Main Basin, since monthly DOE sampling could easily miss the bloom entirely and high-time-resolution ORCA chlorophyll time series are only available for a couple of years. However, the assessment is close to the longer model-based estimates by *Newton and Van Voorhis* (2002) (spring bloom March - May, 1999 - 2001) and also close to observed spring-bloom variability over 60 years in the southern Strait of Georgia (*Collins et al.*, 2009; *Allen and Wolfe*, 2013).

Accordingly, this study finds that wind mixing may have measurable effects on bloom date but appears to play a minor role compared with E_0 , whereas river flow-driven variation in stratification and mixing has the same scale of effect as E_0 in seasonal averages. This ranking is consistent with the finding that in the Main Basin, river flow variability has stronger effects on mixing in spring than does wind stress.

Deep nutrient appears not to influence bloom date (figure 6.3, and table 6.4), which is clear evidence to support the fact that spring bloom onset in the Main Basin is controlled by light limitation (*Newton and Van Voorhis*, 2002).

6.3.3 Conditions during salmon outmigration

The subsurface light environment is a major determinant of feeding behaviour and vertical distribution of visual predators (*Dupont and Aksnes*, 2011; *Wilson and Heath*, 2019). Here, this study considered variability in phytoplankton standing stock during the presumed period of juvenile steelhead and chinook outmigration, as an indication of possible changes in the light environment during a critical life stage for these fish. This study speculates that the effect of a dense phytoplankton bloom on visual refuge and predation during this period would come through light scattering, not through light attenuation. Thus, this study can not directly compare the changes in the underwater light field that would result from the phytoplankton changes to the changes in light that drive the phytoplankton dynamics; however, this comparison would have to be

made by studies that attempted to follow on from the results here. Overall, this study finds predicted changes in phytoplankton concentration, $P_{outmigr}^{steelhead}$ and $P_{outmigr}^{chinook}$, to be quite small, on the order of 10%. This might suggest that variation in $P_{outmigr}^{steelhead}$ and $P_{outmigr}^{chinook}$ is not attributable to physical drivers in seasonal as well as event scale. The variation perhaps is due to biological processes (i.e., phytoplankton grow rapidly when light and nutrient are sufficient). Thus, if phytoplankton blooms have an effect on visual predation by and on juvenile salmonid, it is mainly through intense, localised blooms, not through seasonal-average conditions. Surface PAR and underwater light are again major drivers of phytoplankton concentration during salmon outmigration.

6.3.4 Nutrient stress in summer

Although the PS-1D model does not resolve phytoplankton succession, the incidence of days in which nutrients become severely limiting can provide a clue to likely compositional changes during summer. The metric Δt_{nut} counts the days in which surface NO_3 and NH_4 is less than 3 mmolm^{-3} in the PS-1D model a threshold that identifies an extreme but regularly occurring level of nutrient stress: its base-case value is 8 days per year.

Historical variation in seasonally-averaged surface PAR and in riverflow effects on stratification and mixing are both sufficient to drive variation in Δt_{nut} between approximately 2 - 3 times its base-case value (Table 6.4). Near-surface temperature and wind mixing do not appear likely to explain year-to-year variability but may well drive dramatic long-term trends (towards more frequent or sustained nutrient stress in the case of temperature, and also toward higher nutrient stress if the prevailing northerly summer winds increase in strength: table 6.4 and *Moore et al. (2015)*). Changes in the exchange flow and background light attenuation could potentially also drive nutrient-stress changes of the same magnitude as the other mechanisms mentioned, but without a better quantification of seasonal-average patterns in these processes this study can not be sure.

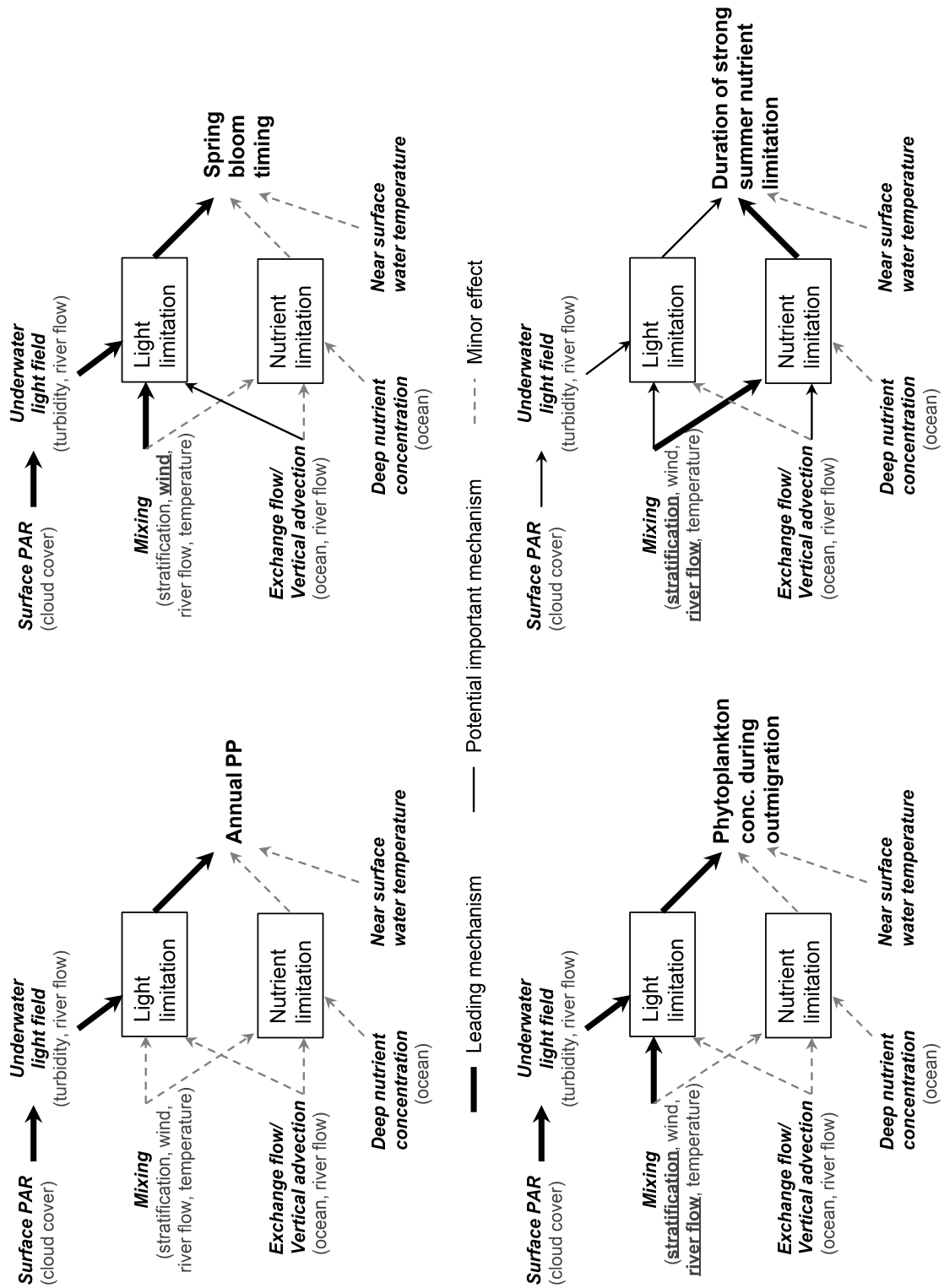


Figure 6.8: Final ranking of pathways of climate influence on four metrics of phytoplankton dynamics

For Δt_{nut} and to a lesser extent t_{bloom} , new temperature effects beyond the range of historical variability seem likely to emerge over the next few decades, if they have not already. It is worth noting that the effect of warming on nutrient stress in general, as discussed here, is likely to be accompanied by an independent effect of warming on *Alexandrium* growth rate and seasonal window of opportunity (Moore *et al.*, 2015).

The numerical experiment was repeated with the PSO 70th iteration parameter set (see Chapter 5), which has lower phytoplankton maximum growth rate ($\mu_0 = 1.71 \text{ d}^{-1}$). To this experiment, when the same nutrient limitation threshold (at $3 \mu MN$) was used, it resulted in no nutrient shortage in summer (or number of days nutrient fall below the threshold is 0), which is contradict to observations in Puget Sound. Apart from the difference in nutrient limitation threshold, the numerical experiment on parameter set with lower growth rate (not shown in details) resulted in the same conclusions as the one with higher growth rate shown above. This meant that the growth rate did not change the dynamics of the system represented by chosen metrics. The difference in nutrient limitation level observed between the two growth rates probably lay in the simple 1-D model that could not resolve complexity of the Puget Sound fjord estuarine circulation, and/or chlorophyll might not be a good constraint in parameterisation to determine growth rate.

Overall, the numerical experiments result in relatively simple pictures of interannual variation in bloom timing and primary production in the Main Basin Puget Sound (Figure 6.8). Light intensity (via cloud cover) is the dominant driver of all metrics (primary production, phytoplankton bloom timing, biomass, and duration nutrient limitation in summer). Riverflow (via stratification and mixing, and via turbidity and light attenuation) and vertical advection (via exchange flow) are both of the second order of importance. The results show more complex pictures for changes in duration of strong nutrient stress in summer (Δt_{nut}), in which a large number of mechanistic pathways all seem capable of producing variations in phytoplankton dynamics on the same scale. This process complexity, in addition to the incompleteness of available

observations, may explain why simple correlative approaches to Puget Sound spring bloom have never resulted in a clear picture (*MacCready and Banas, 2016*).

The μ_0 satisfies Eppley and Bissinger resulted in no nutrient limitation, which is contradicting with observations. Experiment to run with the lower growth rate, the mechanism observed the same, but the nutrient limitation increase to 9 otherwise no nutrient limitation. Probably physical processes, or lacking data to constraint free parameters. Contradict to decide.

Chapter 7

Summary and Conclusions

7.1 Summary

Exploration of the PS-1D model (Chapter 3 – 5), which was built upon an existing model used in Puget Sound (LiveOcean with *Davis et al. (2014)* biological model) (Chapter 2), shows that changes should be made on light attenuation (caused by phytoplankton att_P , by water background att_{bg}) and initial growth-light slope (α) to significantly improve model performance. Changes in other parameters (e.g., m_P , K_0 , μ_0 , r_{nitr} , r_{remin}) depends on trade-off between model performance of the Puget Sound and other regions as well as the entire Salish Sea. The exploration also shows evidence that model skill assessment of WSS_MSE might overestimate model fitness, and suggests WSS_MAE may be a better model skill assessment. The study came to this conclusion as follows

Investigation into underwater light field (Chapter 4) revealed unexpected complexity in the light environment. Statistical regressions between light attenuation and salinity-represented freshwater strikingly resulted in a weak correlation. However, the weak correlation does not mean there is no effect of freshwater on light attenuation, but rather that salinity is not a good proxy to represent freshwater influence on light environment. This is possible as Puget Sound basin receives freshwater from numerous rivers, which originate from a real diversity of watershed types and therefore sediment

load type (Cuo *et al.*, 2009, 2011). The diversity of river inputs, with the most dominant effects from distant rivers (e.g. Fraser and Skagit) (Banas *et al.*, 2015), complicates optical water properties in Puget Sound, which could not be predicted by salinity only. In addition, the analysis on underwater light field shows a significant difference between light attenuation coefficients (caused by phytoplankton, particulates, and CDOM) in Puget Sound and the outer coast environment. Puget Sound light attenuation coefficients deduced from observations measured by different techniques (Secchi disk and beam transmissometer) resulted in consistent values, hence these coefficients are considered to closely reflect Puget Sound light environments. Adjustment of underwater light field to these coefficients improves PS-1D model goodness-of-fit over 20% at the top 20m layer for Chla and nutrients (nitrate and ammonium).

The particle swarm optimizer (PSO), one of parameterisation algorithms, was used to determine undefined parameters of the PS-1D model (Chapter 5). The PSO outcome proposes numerous parameter sets that significantly improve model goodness-of-fit (over 46% improvement on index of agreement WSS_MAE for Chla and nutrients at the top 20 meter layer) as well as capturing spring bloom onset and nitrate pattern. Notably, this study recognized parameter sets with opposite dynamics (high turn-over rate against low turn-over rate) resulted in similar model goodness of fit. However, the contrasting dynamics do not result in clear differences in bloom onset and magnitude – major metrics that this study chooses to examine phytoplankton bloom in Puget Sound. Thus, these parameter sets would adequately and equally suit the purpose of this study. However, it would not be the case when other phytoplankton dynamics are investigated (e.g., trophic levels, carbon export). It is also worth noting that the optimization process could produce inappropriate results. One possible explanation is that the optimizer might adjust parameters in such a way that they correct for any errors related to physical forcing conditions that influence the biological state variables (Fennel *et al.*, 2001). This study is also aware that PS-1D model is 1-dimensional with yearly average of mixing and advection profiles, which is clearly a simplification of the partial mixed fjord of Puget Sound. Further, incompleteness of available obser-

vations on several processes (e.g. grazing, sinking) might result in the free movement of parameters in those unconstrained processes.

In general, the numerical exploration on response of phytoplankton growth to environmental changes suggests that light limitation outweighs nutrient limitation on most metrics (except the count of days nutrient limitation in summer, Δt_{nut}). Cloud cover (via light intensity E_0) and riverflow (via background water light attenuation (att_{bg}), and mixing (κ_v) mediated by stratification) are the first and second order climate factors regulating light limitation. The underlying mechanisms of duration nutrient limitation in summer (Δt_{nut}), or the window of opportunity for *Alexandrium* HAB to develop, however, is more complex. The complexity in Δt_{nut} variation is due to a large number of possible climate-induced drivers – pathways that produce impact in similar scale.

7.2 Conclusions

In summary, this study proposes a parameter set for the biogeochemical model of Puget Sound (the PS-1D) and key drivers – pathways influencing phytoplankton bloom dynamics in Puget Sound. This study finds that the complexity of underwater light field can not be simply explained in term of salinity. Among biological parameters, initial growth-light slope (α) has the greatest impact on the model performance. Some parameters (e.g., sinking rate, microzooplankton mortality) are insensitive, which might be due to incompleteness of available observations (e.g., lack of data on microzooplankton). This study indicates variation in incoming light, i.e. variation in cloud cover and riverflow (via light attenuation and mixing), as key climate-induced drivers on phytoplankton dynamics in Puget Sound.

The merits of this study is to quantify the response of phytoplankton bloom, namely timing and annual primary production, to changes in environment. This study draws a clear simple picture of drivers (light limitation outweighs nutrient limitation) and pathways (via cloud cover and riverflow-driven mixing) influencing phytoplankton spring

bloom date (t_{bloom}) and annual primary production (P_{tot}). A large number of potential climate-linked drivers and pathways can be classified as minor effects in comparison to others (e.g., cloud cover – underwater light field – light limitation) (Figure 6.8). However, climate-induced drivers and pathways for the count of days of strong nutrient stress in summer, Δt_{nut} , is rather complex. There are a large number of mechanistic pathways which all seem capable of producing variations in Δt_{nut} on the same scale.

The limitations of this study lie in the simplification of 1-dimensional model with yearly profile of mixing and advection, which clearly does not fully resolve the complexity of partial mixed fjord properties of Puget Sound. The simplification of hydrodynamic properties might also partly be a cause of numerous equally good parameter sets, and the co-existence of two opposite system dynamics observed in parameterisation due to parameterisation (e.g., PSO) works in such a way that it corrects errors occurring in physical processes. Also, standing stock (e.g., Chla biomass) probably is not an ideal proxy for a system's production, which resulted in a wide range of value for maximum growth rate. Although, the PS-1D could capture spring bloom, and nitrate pattern, it could not produce succession of phytoplankton bloom. This again might be due to yearly profiles of mixing and advection in the PS-1D model, which result in overestimation of light and nutrient availability in summer. Or, it might be due to the fact that a single phytoplankton group described in the PS-1D is not satisfactory to resolve the bloom dynamics that involve large contribution of nanoplankton to the phytoplankton community during late August (90%) and early September (92%) (*Feely et al.*, 2012). This study also suspects that the complexity of the light environment could lead to different strategies phytoplankton use for adaptation, for which a single growth – light response function in the PS-1D could not explain.

For future work, this study suggests further investigation into underwater light field. Although this study found an underwater light model that satisfactorily produces underwater light observations, it could not resolve the complexity of the Puget Sound underwater light field (e.g., differentiate light attenuation caused by riverflow from the

background water). This study pointed out that light significantly improves the phytoplankton model performance (Chapter 4), and is the largest driver of variability in primary production timing, magnitude, and nutrient limitation in Puget Sound (Chapter 6). Thus, a detailed study of what watershed characteristics link hydrology to the marine underwater light environment, and hence to effects on primary production, is needed to advance understanding of Puget Sound phytoplankton dynamics.

Bibliography

- Ackleh, A. S., B. G. Fitzpatrick, and T. G. Hallam (1994), Approximation and parameter estimation problems for algal aggregation models, *Mathematical Models and Methods in Applied Sciences*, 4(03), 291–311.
- Alexander J. Chester, David M. Damkaer, Douglas B. Dey, Gayle A. Heron, and Jerry D. Larrance (1980), Plankton of the Strait of Juan de Fuca, 1976 - 1977, *Tech. rep.*, National Oceanic and Atmospheric Administration.
- Allen, S. E., and M. A. Wolfe (2013), Hindcast of the timing of the spring phytoplankton bloom in the Strait of Georgia, 1968–2010, *Progress in Oceanography*, 115(C), 6–13, doi:10.1016/j.pocean.2013.05.026.
- Anderson, T., W. Gentleman, and A. Yool (2015), Empower-1.0: an efficient model of planktonic ecosystems written in r, *Geoscientific Model Development*, 8(7), 2231–2262.
- Anderson, T. R. (1993), A spectrally averaged model of light penetration and photosynthesis, *Limnology and Oceanography*, 38(7), 1403–1419.
- Anderson, T. R. (2010), Progress in marine ecosystem modelling and the “unreasonable effectiveness of mathematics”, *Journal of Marine Systems*, 81(1-2), 4–11.
- Araujo, H. A., C. Holt, J. M. Curtis, R. Perry, J. R. Irvine, and C. G. Michielsens (2013), Building an ecosystem model using mismatched and fragmented data: a probabilistic network of early marine survival for coho salmon *Oncorhynchus kisutch* in the strait of georgia, *Progress in Oceanography*, 115, 41–52.

- Armstrong, R. A. (2006), Optimality-based modeling of nitrogen allocation and photoacclimation in photosynthesis, *Deep Sea Research Part II: Topical Studies in Oceanography*, 53(5), 513 – 531, doi:<https://doi.org/10.1016/j.dsr2.2006.01.020>, the US JGOFS Synthesis and Modeling Project: Phase III.
- Babson, A. L., M. Kawase, and P. Maccready (2006), Seasonal and Interannual Variability in the Circulation of Puget Sound , Washington : A Box Model Study, *Atmosphere-Ocean*, 44(1), 29–45.
- Banas, N. S., L. Conway-Cranos, D. A. Sutherland, P. MacCready, P. Kiffney, and M. Plummer (2015), Patterns of River Influence and Connectivity Among Subbasins of Puget Sound, with Application to Bacterial and Nutrient Loading, *Estuaries and Coasts*, 38(3), 735–753, doi:10.1007/s12237-014-9853-y.
- Banas, N. S., J. Zhang, R. G. Campbell, R. N. Sambrotto, M. W. Lomas, E. Sherr, B. Sherr, C. Ashjian, D. Stoecker, and E. J. Lessard (2016), Spring plankton dynamics in the eastern bering sea, 1971–2050: Mechanisms of interannual variability diagnosed with a numerical model, *Journal of Geophysical Research: Oceans*, 121(2), 1476–1501.
- Banas, N. S., H. T. Nguyen, S. Garnier, and P. MacCready (2019), Climate impacts on patterns of phytoplankton production in puget sound, usa: A model synthesis and narrowing of hypotheses, *marinesurvivalproject.com*.
- Barange, M., G. Merino, J. L. Blanchard, J. Scholtens, J. Harle, E. H. Allison, J. I. Allen, J. Holt, and S. Jennings (2014), Impacts of climate change on marine ecosystem production in societies dependent on fisheries, *Nature Climate Change*, 4(3), 211–216, doi:10.1038/nclimate2119.
- Beamish, R. J., and C. Mahnken (2001), A critical size and period hypothesis to explain natural regulation of salmon abundance and the linkage to climate and climate change, *Progress in Oceanography*, 49(1-4), 423–437.

- Beamish, R. J., C. Neville, R. Sweeting, and K. Lange (2012), The synchronous failure of juvenile pacific salmon and herring production in the strait of georgia in 2007 and the poor return of sockeye salmon to the fraser river in 2009, *Marine and Coastal Fisheries*, 4(1), 403–414, doi:10.1080/19425120.2012.676607.
- Beauchamp, D., J. Keister, N. Mantua, and M. Zimmerman (2012), Marine Survival of Salmon & Steelhead in the Salish Sea HYPOTHESES AND PRELIMINARY RESEARCH RECOMMENDATIONS FOR PUGET SOUND Marine Survival of Salmon and Steelhead in the Salish Sea – Puget Sound Component: Hypotheses and Preliminary Research Recommendati, *Tech. rep.*, US Salish Sea Technical Team.
- Bernhard, A. E., and E. R. Peele (1997), Nitrogen Limitation of Phytoplankton in a Shallow Embayment in Northern Puget Sound, *Estuaries*, 20(4), 759, doi:10.2307/1352249.
- Beven, K., and A. Binley (1992), The future of distributed models: model calibration and uncertainty prediction, *Hydrological processes*, 6(3), 279–298.
- Bissinger, J. E., D. J. Montagnes, J. harples, and D. Atkinson (2008), Predicting marine phytoplankton maximum growth rates from temperature: Improving on the eppley curve using quantile regression, *Limnology and Oceanography*, 53(2), 487–493.
- Blackman, F. F. (1905), Optima and limiting factors, *Annals of botany*, 19(74), 281–295.
- Bonachela, J. A., M. Raghil, and S. A. Levin (2011), Dynamic model of flexible phytoplankton nutrient uptake, *Proceedings of the National Academy of Sciences*, 108(51), 20,633–20,638, doi:10.1073/pnas.1118012108.
- Boss, E., M. J. Perry, and M. C. Talbot (1998), Observation of an Intense Deep-Water Intrusion in Puget Sound, *Tech. rep.*, Observation of an Intense Deep-Water Intrusion in Puget Sound.
- Bottom, D. L., G. Anderson, A. Baptista, J. Burke, M. Burla, M. Bhuthimethee, L. Campbell, E. Casillas, S. Hinton, K. Jacobson, et al. (2008), Salmon life histories,

- habitat, and food webs in the columbia river estuary: an overview of research results, 2002–2006, *Report of Research by Northwest Fisheries Science Center, National Marine Fisheries Service, Seattle, WA.*
- Brandenburg, K. M., L. N. de Senerpont Domis, S. Wohlrab, B. Krock, U. John, Y. van Scheppingen, E. van Donk, and D. B. Van de Waal (2017), Combined physical, chemical and biological factors shape alexandrium ostenfeldii blooms in the netherlands, *Harmful Algae*, 63, 146–153.
- Brussaard, C. P. D. (2004), Viral control of phytoplankton populations—a review 1, *Journal of Eukaryotic Microbiology*, 51(2), 125–138, doi:10.1111/j.1550-7408.2004.tb00537.x.
- Burchard, H., E. Deleersnijder, and A. Meister (2005), Application of modified patankar schemes to stiff biogeochemical models for the water column, *Ocean Dynamics*, 55(3-4), 326–337.
- Burd, A. B., and G. A. Jackson (2009), Particle aggregation, *Annual review of marine science*, 1, 65–90.
- Cannon, G., and N. Laird (1978), Variability of currents and water properties from year-long observations in a fjord estuary, in *Hydrodynamics of Estuaries and Fjords, Elsevier Oceanography Series*, vol. 23, edited by J. C. Nihoul, pp. 515 – 535, Elsevier, doi:https://doi.org/10.1016/S0422-9894(08)71296-0.
- Cannon, G., and N. Laird (1980), Characteristics of flow over a sill during deep water renewal, in *Fjord Oceanography*, edited by L. C. Freeland H.J., Farmer D.M., Springer, Boston, MA, doi:10.1007/978-1-4613-3105-6_51.
- Cannon, G. A., M. Baldrige, J. V. Byrne Administrator, and G. H. Ludwig Director (1983), NOAA Technical Memorandum ERL PMEL-48 An Overview of Circulation in the Puget Sound Estuarine System, *Tech. rep.*, Pacific Marine Environmental Laboratory, Seattle, Washington.

- Chassot, E., S. Bonhommeau, N. K. Dulvy, F. Mélin, R. Watson, D. Gascuel, and O. Le Pape (2010), Global marine primary production constrains fisheries catches, *Ecology Letters*, *13*(4), 495–505, doi:10.1111/j.1461-0248.2010.01443.x.
- Chen, B., and E. A. Laws (2017), Is there a difference of temperature sensitivity between marine phytoplankton and heterotrophs?, *Limnology and Oceanography*, *62*(2), 806–817.
- Cloern, J. E. (1996), Phytoplankton bloom dynamics in coastal ecosystems: A review with some general lessons from sustained investigation of san francisco bay, california, *Reviews of Geophysics*, *34*(2), 127–168, doi:10.1029/96RG00986.
- Cokelet, E., R. J. Stewart, and C. C. Ebbesmeyer (1990), The annual mean transport in puget sound, *Tech. rep.*, Pacific Marine Environmental Laboratory, Seattle, Washington.
- Collias, E. E., and J. H. Lincoln (1977), A study of the nutrient in the main basin of Puget Sound, *Tech. rep.*, Department of Oceanography, University of Washington.
- Collins, a. K., S. E. Allen, and R. Pawlowicz (2009), The role of wind in determining the timing of the spring bloom in the Strait of Georgia, *Canadian Journal of Fisheries and Aquatic Sciences*, *66*(9), 1597–1616, doi:10.1139/F09-071.
- Côté, B., and T. Platt (1983), Day-to-day variations in the spring-summer photosynthetic parameters of coastal marine phytoplankton, *Limnology and Oceanography*, *28*(2), 320–344.
- Cuo, L., D. P. Lettenmaier, M. Alberti, and J. E. Richey (2009), Effects of a century of land cover and climate change on the hydrology of the Puget Sound basin, *Hydrological Processes*, *23*(6), 907–933, doi:10.1002/hyp.7228.
- Cuo, L., T. K. Beyene, N. Voisin, F. Su, D. P. Lettenmaier, M. Alberti, and J. E. Richey (2011), Effects of mid-twenty-first century climate and land cover change on the hydrology of the Puget Sound basin, Washington, *Hydrological Processes*, *25*(11), 1729–1753, doi:10.1002/hyp.7932.

- Cushing, D. (1990), Plankton production and year-class strength in fish populations: an update of the match/mismatch hypothesis, in *Advances in marine biology*, vol. 26, pp. 249–293, Elsevier.
- Cushing, D. H. (1982), *Climate and fisheries*, Academic press.
- Cushing, D. H., and J. J. Walsh (1976), *The Ecology of the seas*, 467 pp., Philadelphia: W.B Saunders Co.
- Davis, K. A., N. S. Banas, S. N. Giddings, S. A. Siedlecki, P. MacCready, E. J. Lessard, R. M. Kudela, and B. M. Hickey (2014), Estuary-enhanced upwelling of marine nutrients fuels coastal productivity in the u.s. pacific northwest, *Journal of Geophysical Research: Oceans*, 119(12), 8778–8799, doi:10.1002/2014JC010248.
- Doney, S. C., D. M. Glover, and R. G. Najjar (1996), A new coupled, one-dimensional biological-physical model for the upper ocean: Applications to the jgofs bermuda atlantic time-series study (bats) site, *Deep Sea Research Part II: Topical Studies in Oceanography*, 43(2-3), 591–624.
- Dortch, Q. (1982), Effect of growth conditions on accumulation of internal nitrate, ammonium, amino acids, and protein in three marine diatoms, *Journal of Experimental Marine Biology and Ecology*, 61(3), 243–264, doi:https://doi.org/10.1016/0022-0981(82)90072-7.
- Dortch, Q. (1990), The interaction between ammonium and nitrate uptake in phytoplankton, *Marine Ecology Progress Series*, 61, 183–201, doi:10.3354/meps061183.
- Dortch, Q., J. R. Clayton, S. S. Thoresen, and S. I. Ahmed (1984), Species differences in accumulation of nitrogen pools in phytoplankton, *Marine Biology*, 81(3), 237–250, doi:10.1007/BF00393218.
- Dowd, M. (2011), Estimating parameters for a stochastic dynamic marine ecological system, *Environmetrics*, 22(4), 501–515.

- Dupont, N., and D. L. Aksnes (2011), Effects of bottom depth and water clarity on the vertical distribution of calanus spp, *Journal of plankton research*, 34(3), 263–266.
- Ebbesmeyer, C., J. Helseth, C. Barnes, J. Lincoln, and W. Bendiner (1977), On nearshore trapping of pollutants by tidal eddies downstream from points in puget sound, washington 134-145, *Proceedings of The Use, Study and Management of Puget Sound, University of Washington WSG-W077-1*.
- El Saadi, N., and O. Arino (2006), A stochastic modelling of phytoplankton aggregation, *Revue Africaine de la Recherche en Informatique et Mathématiques Appliquées*, 5, 80–94.
- Eppley, R. W. (1972), Temperature and phytoplankton growth in the sea, *Fish. bull*, 70(4), 1063–1085.
- Evans, G. T., and J. S. Parslow (1985), A model of annual plankton cycles, *Biological oceanography*, 3(3), 327–347.
- Eyes over Puget Sound, C. K. (), Eyes over Puget Sound, <https://ecology.wa.gov/Research-Data/Monitoring-assessment/Puget-Sound-and-marine-monitoring/Eyes-over-Puget-Sound>, accessed: 03-07-2020.
- Fasham, M. J. R., H. W. Ducklow, and S. M. McKelvie (1990), A nitrogen-based model of plankton dynamics in the ocean mixed layer, *Journal of Marine Research*, 48(3), 591–639, doi:10.1357/002224090784984678.
- Feely, R. A., T. Klinger, J. A. Newton, M. Chadsey, C. S. Friedman, J. Ruesink, G. Waldbusser, S. R. Alin, C. Krembs, and M. Roberts (2012), Scientific Summary of Ocean Acidification in Washington State Marine Waters NOAA OAR Special Report, *Tech. rep.*, National Oceanic and Atmospheric Administration.
- Fennel, K., M. Losch, J. Schröter, and M. Wenzel (2001), Testing a marine ecosystem model: sensitivity analysis and parameter optimization, *Journal of Marine Systems*, 28(1-2), 45–63, doi:10.1016/S0924-7963(00)00083-X.

- Flynn, K. J. (2003), Modelling multi-nutrient interactions in phytoplankton; balancing simplicity and realism, *Progress in Oceanography*, 56(2), 249 – 279, doi:[https://doi.org/10.1016/S0079-6611\(03\)00006-5](https://doi.org/10.1016/S0079-6611(03)00006-5).
- Franks, P. J. S. (2009), Planktonic ecosystem models: perplexing parameterizations and a failure to fail, *Journal of Plankton Research*, 31(11), 1299–1306, doi:10.1093/plankt/fbp069, n/a.
- Friebertshauser, M. A., and A. C. Duxbury (1972), A water budget study of puget sound and its subregions1, *Limnology and Oceanography*, 17(2), 237–247, doi:10.4319/lo.1972.17.2.0237.
- Gallegos, C. L., D. L. Correll, and J. W. Pierce (1990), Modeling spectral diffuse attenuation, absorption, and scattering coefficients in a turbid estuary, *Limnology and Oceanography*, 35(7), 1486–1502.
- Gallegos, C. L., P. J. Werdell, and C. R. McClain (2011), Long-term changes in light scattering in chesapeake bay inferred from secchi depth, light attenuation, and remote sensing measurements, *Journal of Geophysical Research: Oceans*, 116(C7).
- Garcia-Gonzalo, E., and J. L. Fernandez-Martinez (2012), A brief historical review of particle swarm optimization (pso), *Journal of Bioinformatics and Intelligent Control*, 1(1), 3–16.
- Garnier, S. (2020), A box model of fjords and sea lochs, Ph.D. thesis, University of Strathclyde, in preparation.
- Geider, R. J., H. L. MacIntyre, and T. M. Kana (1998), A dynamic regulatory model of phytoplanktonic acclimation to light, nutrients, and temperature, *Limnology and oceanography*, 43(4), 679–694.
- Gentleman, W., A. Leising, B. Frost, S. Strom, and J. Murray (2003), Functional responses for zooplankton feeding on multiple resources: a review of assumptions and biological dynamics, *Deep Sea Research Part II: Topical Studies in Oceanography*, 50(22-26), 2847–2875.

- Gentleman, W. C., and A. B. Neuheimer (2008), Functional responses and ecosystem dynamics: how clearance rates explain the influence of satiation, food-limitation and acclimation, *Journal of Plankton Research*, 30(11), 1215–1231, doi:10.1093/plankt/fbn078.
- Geyer, W. R., and P. MacCready (2014), The estuarine circulation, *Annual review of fluid mechanics*, 46, 175–197.
- Gregg, W. W., M. A. Friedrichs, A. R. Robinson, K. A. Rose, R. Schlitzer, K. R. Thompson, and S. C. Doney (2009), Skill assessment in ocean biological data assimilation, *Journal of Marine Systems*, 76(1-2), 16–33.
- Groot, C., and T. Quinn (1987), Homing migration of sockeye salmon, *Oncorhynchus nerka*, *Fishery Bulletin*, 85(3), 455.
- Gunson, J., A. Oschlies, and V. Garçon (1999), Sensitivity of ecosystem parameters to simulated satellite ocean color data using a coupled physical-biological model of the north atlantic, *Journal of Marine Research*, 57(4), 613–639.
- Hamilton, P., J. T. Gunn, and G. A. Cannon (1985), A box model of puget sound, *Estuarine, Coastal and Shelf Science*, 20(6), 673 – 692, doi:[https://doi.org/10.1016/0272-7714\(85\)90025-3](https://doi.org/10.1016/0272-7714(85)90025-3).
- Harris, G. (2012), *Phytoplankton ecology: structure, function and fluctuation*, Springer Science & Business Media.
- Heinz, H. J. (2008), *The state of the nation's ecosystems 2008: measuring the lands, waters, and living resources of the United States*, Island Pr.
- Holling, C. S. (1959), Some characteristics of simple types of predation and parasitism, *The Canadian Entomologist*, 91(7), 385–398.
- Holling, C. S. (1965), The functional response of predators to prey density and its role in mimicry and population regulation, *The Memoirs of the Entomological Society of Canada*, 97(S45), 5–60.

- Holmes, R. W. (1970), The secchi disk in turbid coastal waters 1, *Limnology and oceanography*, 15(5), 688–694.
- Houska, T. (2017), Uncertainty analysis of complex hydro-biogeochemical models, Ph.D. thesis, Justus-Liebig University Gießen.
- Hunter, J. R. (1968), Effects of light on schooling and feeding of jack mackerel, *trachurus symmetricus*, *Journal of the Fisheries Board of Canada*, 25(2), 393–407.
- Hurtt, G. C., and R. A. Armstrong (1996), A pelagic ecosystem model calibrated with bats data, *Deep Sea Research Part II: Topical Studies in Oceanography*, 43(2-3), 653–683.
- Idso, S. B., and R. G. Gilbert (1974), On the universality of the poole and atkins secchi disk-light extinction equation, *Journal of Applied Ecology*, pp. 399–401.
- IPCC, X. (2018), Global Warming of 1.5°C. An IPCC Special Report on the impacts of global warming of 1.5°C above pre-industrial levels and related global greenhouse gas emission pathways, in the context of strengthening the global response to the threat of climate change, sustainable development, and efforts to eradicate poverty, *Tech. rep.*, IPCC.
- Ivlev, V. (1955), *Experimental ecology of the feeding of fishes*, Pischepromizdat, Moscow, 302pp. (Translated from Russian by D. Scott, Yale University Press, New Haven, 1961).
- Jones, E., J. Parslow, and L. Murray (2010), A bayesian approach to state and parameter estimation in a phytoplankton-zooplankton model, *Australian Meteorological and Oceanographic Journal*, 59(SP), 7–16.
- Kawamiya, M. (2002), Numerical model approaches to address recent problems on pelagic ecosystems, *Journal of oceanography*, 58(2), 365–378.
- Khangaonkar, T., Z. Yang, T. Kim, and M. Roberts (2011), Tidally averaged circulation in Puget Sound sub-basins: Comparison of historical data, analytical model, and

- numerical model, *Estuarine, Coastal and Shelf Science*, 93, 305–319, doi:10.1016/j.ecss.2011.04.016.
- Khangaonkar, T., B. Sackmann, W. Long, T. Mohamedali, and M. Roberts (2012), Simulation of annual biogeochemical cycles of nutrient balance, phytoplankton bloom(s), and DO in Puget Sound using an unstructured grid model, *Ocean Dynamics*, 62(9), 1353–1379, doi:10.1007/s10236-012-0562-4.
- Kirk, J. T. (1994), *Light and photosynthesis in aquatic ecosystems*, Cambridge university press.
- Kirkpatrick, S., C. D. Gelatt, and M. P. Vecchi (1983), Optimization by simulated annealing, *science*, 220(4598), 671–680.
- Klausmeier, C. A., and E. Litchman (2001), Algal games: The vertical distribution of phytoplankton in poorly mixed water columns, *Limnology and Oceanography*, 46(8), 1998–2007.
- Koenings, J., and J. Edmundson (1991), Secchi disk and photometer estimates of light regimes in alaskan lakes: effects of yellow color and turbidity, *Limnology and Oceanography*, 36(1), 91–105.
- Kruckeberg, A. R. (1995), *The natural history of Puget Sound country*, University of Washington Press.
- Kudela, R., S. Seeyave, and W. Cochlan (2010), The role of nutrients in regulation and promotion of harmful algal blooms in upwelling systems, *Progress in Oceanography*, 85(1-2), 122–135.
- Larkin, P., and T. Northcote (1969), Fish as indices of eutrophication, in *Eutrophication: causes, consequences, correctives. Proceedings of a symposium. National Academy of Sciences. Washington, DC*, pp. 256–273.
- Lavelle, J. W., E. D. Cokelet, and G. A. Cannon (1991), A model study of density

- intrusions into and circulation within a deep, silled estuary: Puget sound, *Journal of Geophysical Research: Oceans*, 96(C9), 16,779–16,800, doi:10.1029/91JC01450.
- Laws, E. A. (2013), Evaluation of in situ phytoplankton growth rates: A synthesis of data from varied approaches, *Annual Review of Marine Science*, 5(1), 247–268, doi:10.1146/annurev-marine-121211-172258, PMID: 22809184.
- Lee, Z., S. Shang, K. Du, and J. Wei (2018), Resolving the long-standing puzzles about the observed secchi depth relationships, *Limnology and Oceanography*, 63(6), 2321–2336.
- Lehtiniemi, M., J. Engström-Öst, and M. Viitasalo (2005), Turbidity decreases anti-predator behaviour in pike larvae, *esox lucius*, *Environmental Biology of Fishes*, 73(1), 1–8.
- Lombard, J. (2006), *Saving Puget Sound: a conservation strategy for the 21st century*, vol. 6, Published with American Fisheries Society.
- Loos, E., M. Costa, and S. Johannessen (2017), Underwater optical environment in the coastal waters of british columbia, canada, *FACETS*, 2(2), 872–891, doi:10.1139/facets-2017-0074.
- MacCready, P., and N. Banas (2016), Linking Puget Sound Primary Production to Stratification and Atmospheric Drivers on Seasonal to Inter-decadal Scales, *Tech. rep.*, School of Oceanography, University of Washington.
- Mackas, D., M. Galbraith, D. Faust, D. Masson, K. Young, W. Shaw, S. Romaine, M. Trudel, J. Dower, R. Campbell, et al. (2013), Zooplankton time series from the strait of georgia: Results from year-round sampling at deep water locations, 1990–2010, *Progress in Oceanography*, 115, 129–159.
- Matsushita, B., W. Yang, P. Chang, F. Yang, and T. Fukushima (2012), A simple method for distinguishing global case-1 and case-2 waters using seawifs measurements, *ISPRS journal of photogrammetry and remote sensing*, 69, 74–87.

- Mayzaud, P., and S. A. Poulet (1978), The importance of the time factor in the response of zooplankton to varying concentrations of naturally occurring particulate matter 1, *Limnology and Oceanography*, 23(6), 1144–1154.
- Metropolis, N., A. W. Rosenbluth, M. N. Rosenbluth, A. H. Teller, and E. Teller (1953), Equation of state calculations by fast computing machines, *The journal of chemical physics*, 21(6), 1087–1092.
- Miller, C. B. (2009), *Biological oceanography*, John Wiley & Sons.
- Moffione, R. A. (2001), Evolution and revolution in measuring ocean optical properties, *Oceanography*, 14(3), 9–14.
- Moore, C. (2001), Transmissometry and nephelometry*, in *Encyclopedia of Ocean Sciences (Second Edition)*, edited by J. H. Steele, second edition ed., pp. 109 – 118, Academic Press, Oxford, doi:<https://doi.org/10.1016/B978-012374473-9.00323-4>.
- Moore, S. K., N. J. Mantua, J. A. Newton, M. Kawase, M. J. Warner, and J. P. Kellogg (2008), A descriptive analysis of temporal and spatial patterns of variability in puget sound oceanographic properties, *Estuarine, Coastal and Shelf Science*, 80(4), 545 – 554, doi:<https://doi.org/10.1016/j.ecss.2008.09.016>.
- Moore, S. K., N. J. Mantua, and E. P. Salathé (2011), Past trends and future scenarios for environmental conditions favoring the accumulation of paralytic shellfish toxins in puget sound shellfish, *Harmful Algae*, 10(5), 521 – 529, doi:<https://doi.org/10.1016/j.hal.2011.04.004>.
- Moore, S. K., J. A. Johnstone, N. S. Banas, and E. P. Salathé Jr (2015), Present-day and future climate pathways affecting Alexandrium blooms in Puget Sound, WA, USA, *Harmful Algae*, 48, 1–11, doi:[10.1016/j.hal.2015.06.008](https://doi.org/10.1016/j.hal.2015.06.008).
- Morel, A. (1988), Optical modeling of the upper ocean in relation to its biogenous matter content (case i waters), *Journal of geophysical research: oceans*, 93(C9), 10,749–10,768.

- Mote, P. W., E. A. Parson, A. F. Hamlet, W. S. Keeton, D. Lettenmaier, N. Mantua, E. L. Miles, D. W. Peterson, D. L. Peterson, R. Slaughter, et al. (2003), Preparing for climatic change: the water, salmon, and forests of the pacific northwest, *Climatic change*, 61(1-2), 45–88.
- Nairn, B. J., and M. Kawase (2002), Comparison of observed circulation patterns and numerical model predictions in puget sound, wa, in *Proceedings 2001 Puget Sound Research Conference. Puget Sound Water Quality Action Team, Olympia*, vol. 9.
- Newton, J. A., and K. Van Voorhis (2002), Seasonal Patterns and Controlling Factors of Primary Production in Puget Sound’s Central Basin and Possession Sound, *Tech. rep.*, Washington State Department of Ecology.
- Newton, J. A., E. Siegel, and S. L. Albertson (2003), Oceanographic changes in puget sound and the strait of juan de fuca during the 2000–01 drought, *Canadian Water Resources Journal / Revue canadienne des ressources hydriques*, 28(4), 715–728, doi:10.4296/cwrj2804715.
- Ocean Policy, C. o. (2004), *An ocean blueprint for the 21st century*, vol. 1, Commission, United States.
- Opdal, A. F., C. Lindemann, and D. L. Aksnes (2019), Centennial decline in north sea water clarity causes strong delay in phytoplankton bloom timing, *Global Change Biology*, 25(11), 3946–3953, doi:10.1111/gcb.14810.
- Oschlies, A., and V. Garçon (1999), An eddy-permitting coupled physical-biological model of the north atlantic: 1. sensitivity to advection numerics and mixed layer physics, *Global Biogeochemical Cycles*, 13(1), 135–160.
- Pahlow, M. (2005), Linking chlorophyll-nutrient dynamics to the redfield n: C ratio with a model of optimal phytoplankton growth, *Marine Ecology Progress Series*, 287, 33–43.
- Papaioannou, G., N. Papanikolaou, and D. Retalis (1993), Relationships of photosyn-

- thetically active radiation and shortwave irradiance, *Theoretical and Applied Climatology*, 48(1), 23–27.
- Pauly, D., and V. Christensen (1995), Primary production required to sustain global fisheries, *Nature*, 374(6519), 255–257, doi:10.1038/374255a0.
- Peterson, D., M. Perry, K. Bencala, and M. Talbot (1987), Phytoplankton productivity in relation to light intensity: a simple equation, *Estuarine, coastal and shelf science*, 24(6), 813–832.
- Phillips, S. R. (2015), Bio-optical characterization of the Salish Sea, Canada, towards improved chlorophyll algorithms for MODIS and Sentinel-3, Ph.D. thesis, Department of Geography, University of Victoria.
- Platt, T., and A. D. Jassby (1976), The relationship between photosynthesis and light for natural assemblages of coastal marine phytoplankton1, *Journal of Phycology*, 12(4), 421–430, doi:10.1111/j.1529-8817.1976.tb02866.x.
- Platt, T., S. Sathyendranath, O. Ulloa, W. G. Harrison, N. Hoepffner, and J. Goes (1992), Nutrient control of phytoplankton photosynthesis in the western north atlantic, *Nature*, 356(6366), 229–231.
- Poli, R., J. Kennedy, and T. Blackwell (2007), Particle swarm optimization, *Swarm Intelligence*, 1(1), 33–57, doi:10.1007/s11721-007-0002-0.
- Poole, H., and W. Atkins (1929), Photo-electric measurements of submarine illumination throughout the year, *Journal of the Marine Biological Association of the United Kingdom*, 16(1), 297–324.
- Preikshot, D., R. J. Beamish, R. M. Sweeting, C. M. Neville, and T. D. Beacham (2012), The Residence Time of Juvenile Fraser River Sockeye Salmon in the Strait of Georgia, *Marine and Coastal Fisheries*, 4(1), 438–449, doi:10.1080/19425120.2012.683235.
- Quinn, T. (2010), An environmental and historical overview of the puget sound ecosys-

- tem, Shipman, H., Dethier, MN, Gelfenbaum, G., Fresh, KL, and Dinicola, RS, eds, pp. 11–18.
- Roberts, M., J. Bos, and S. Albertson (2008), *South Puget Sound Dissolved Oxygen Study: Interim Data Report*, Washington State Department of Ecology.
- Ruckelshaus, M., and M. McClure (2007), *Sound science: synthesizing ecological and socioeconomic information about the Puget Sound ecosystem*, NOAA.
- Sarmiento, J. L., R. Slater, M. Fasham, H. Ducklow, J. Toggweiler, and G. Evans (1993), A seasonal three-dimensional ecosystem model of nitrogen cycling in the north atlantic euphotic zone, *Global biogeochemical cycles*, 7(2), 417–450.
- Sayer, M. D. (2019), Fishery manipulation through stock enhancement or restoration, in *Encyclopedia of Ocean Sciences (Third Edition)*, edited by J. K. Cochran, H. J. Bokuniewicz, and P. L. Yager, third edition ed., pp. 385 – 392, Academic Press, Oxford, doi:<https://doi.org/10.1016/B978-0-12-409548-9.04115-4>.
- Schartau, M., P. Wallhead, J. Hemmings, U. L optien, I. Kriest, S. Krishna, B. A. Ward, T. Slawig, and A. Oschlies (2017), Reviews and syntheses: parameter identification in marine planktonic ecosystem modelling, *Biogeosciences*, 14(6), 1647–1701, doi: 10.5194/bg-14-1647-2017.
- Sengupta, S., S. Basak, and R. A. Peters (2019), Particle swarm optimization: A survey of historical and recent developments with hybridization perspectives, *Machine Learning and Knowledge Extraction*, 1(1), 157–191.
- Shannon, J. G. (1975), Correlation Of Beam And Diffuse Attenuation Coefficients Measured In Selected Ocean Waters, in *Ocean Optics IV*, vol. 0064, pp. 3 – 11, International Society for Optics and Photonics, SPIE, doi:10.1117/12.954489.
- Sheldon, R., A. Prakash, and W. Sutcliffe Jr (1972), The size distribution of particles in the ocean 1, *Limnology and oceanography*, 17(3), 327–340.

- Sinclair, M. (1978), Summer Phytoplankton Variability in the Lower St. Lawrence Estuary, *Journal of the Fisheries Research Board of Canada*, *35*(9), 1171–1185, doi:10.1139/f78-188.
- Sloughter, T., N. Banas, and R. Sambrotto (2019), Seasonal variation in light response of polar phytoplankton, *Journal of Marine Systems*, *191*, 64–75.
- Smith, R. C., and C. D. Mobley (2008), Underwater light, in *Photobiology*, pp. 131–138, Springer.
- Smith, S., Y. Yamanaka, M. Pahlow, and A. Oschlies (2009), Optimal uptake kinetics: physiological acclimation explains the pattern of nitrate uptake by phytoplankton in the ocean, *Marine Ecology Progress Series*, *384*, 1–12, doi:10.3354/meps08022.
- Smith, S. L., A. Merico, K. W. Wirtz, and M. Pahlow (2014), Leaving misleading legacies behind in plankton ecosystem modelling, *Journal of Plankton Research*, *36*(3), 613–620, doi:10.1093/plankt/fbu011.
- Smith, S. L., M. Pahlow, A. Merico, E. Acevedo-Trejos, Y. Sasai, C. Yoshikawa, K. Sasaoka, T. Fujiki, K. Matsumoto, and M. C. Honda (2015), Flexible phytoplankton functional type (flexpft) model: size-scaling of traits and optimal growth, *Journal of Plankton Research*, *38*(4), 977–992, doi:10.1093/plankt/fbv038.
- Sommer, U. (1994), The impact of light intensity and daylength on silicate and nitrate competition among marine phytoplankton, *Limnology and Oceanography*, *39*(7), 1680–1688, doi:10.4319/lo.1994.39.7.1680.
- Stow, C. A., J. Jolliff, D. J. McGillicuddy Jr, S. C. Doney, J. I. Allen, M. A. Friedrichs, K. A. Rose, and P. Wallhead (2009), Skill assessment for coupled biological/physical models of marine systems, *Journal of Marine Systems*, *76*(1-2), 4–15.
- Strickland, D. R. (1983), *The fertile fjord - Plankton in Puget Sound*, Puget Sound books, Washington Sea Grant Program, University of Washington.

- Sutherland, D. a., P. MacCready, N. S. Banas, and L. F. Smedstad (2011), A Model Study of the Salish Sea Estuarine Circulation, *Journal Of Physical Oceanography*, *41*(6), 1125–1143, doi:10.1175/2011JPO4540.1.
- Thomson, R. E., R. J. Beamish, T. D. Beacham, M. Trudel, P. H. Whitfield, and R. A. Hourston (2012), Anomalous ocean conditions may explain the recent extreme variability in fraser river sockeye salmon production, *Marine and Coastal Fisheries*, *4*(1), 415–437.
- Tilman, D., M. Mattson, and S. Langer (1981), Competition and nutrient kinetics along a temperature gradient: An experimental test of a mechanistic approach to niche theory¹, *Limnology and Oceanography*, *26*(6), 1020–1033, doi:10.4319/lo.1981.26.6.1020.
- Transmissometer Manual, X. (), *Transmissometer Manual*, Sea Tech Inc.
- Watson, R., D. Zeller, and D. Pauly (2014), Primary productivity demands of global fishing fleets, *Fish and Fisheries*, *15*(2), 231–241, doi:10.1111/faf.12013.
- Watson, R. A., G. B. Nowara, K. Hartmann, B. S. Green, S. R. Tracey, and C. G. Carter (2015), Marine foods sourced from farther as their use of global ocean primary production increases, *Nature Communications*, *6*(May 2014), 1–6, doi:10.1038/ncomms8365.
- Willmott, C. J. (1981), On the validation of models, *Physical geography*, *2*(2), 184–194.
- Willmott, C. J., M. Robeson, and K. Matsuura (2012), Short Communication A refined index of model performance, *International Journal of Climatology*, *2094*(September 2011), 2088–2094, doi:10.1002/joc.2419.
- Wilson, R. J., and M. R. Heath (2019), Increasing turbidity in the north sea during the 20th century due to changing wave climate, *Ocean Science*, *15*(6), 1615–1625, doi:10.5194/os-15-1615-2019.

- Winter, D. F., K. Banse, and G. C. Anderson (1975), The dynamics of phytoplankton blooms in puget sound a fjord in the Northwestern United States, *Marine Biology*, 29(2), 139–176, doi:10.1007/BF00388986.
- Wirtz, K. W., and M. Pahlow (2010), Dynamic chlorophyll and nitrogen: carbon regulation in algae optimizes instantaneous growth rate, *Marine Ecology Progress Series*, 402, 81–96.
- Yang, Z., and T. Khangaonkar (2010), Multi-scale modeling of puget sound using an unstructured-grid coastal ocean model: from tide flats to estuaries and coastal waters, *Ocean Dynamics*, 60(6), 1621–1637.
- Ye, Y., and K. Cochrane (2011), Global overview of marine fishery resources, *Review of the state of world marine fishery resources*, p. 3.
- Yentsch, C. S., and R. F. Vaccaro (1958), Phytoplankton nitrogen in the oceans 1, *Limnology and Oceanography*, 3(4), 443–448.
- Zhang, Y., X. Liu, Y. Yin, M. Wang, and B. Qin (2012), Predicting the light attenuation coefficient through secchi disk depth and beam attenuation coefficient in a large, shallow, freshwater lake, *Hydrobiologia*, 693(1), 29–37.